Applied Materials Today 48 (2026) 103030

Contents lists available at ScienceDirect

Applied Materials Today

journal homepage: www.elsevier.com/locate/apmt

A review of acoustic metamaterials for electrical devices reliability: A reliability-oriented design perspective

Lingfeng Huang [a,*], Mostafa Ranjbar [b,*], Mohammad Samie [a]

[a] Integrated Vehicle Health Management Centre (IVHM), Cranfield University, College Rd, Wharley End, Bedford, MK43 0AL, United Kingdom
[b] Centre for Energy Decarbonization and Recovery, Cranfield University, College Rd, Wharley End, Bedford, MK43 0AL, United Kingdom

ARTICLE INFO

Keywords:
Acoustic metamaterials
Multifucntion materials
Electrical reliability

ABSTRACT

Modern electronic systems increasingly operate in harsh environments where vibration, thermal cycling, and electromagnetic interference (EMI) jointly threaten their long-term reliability. Acoustic metamaterials (AMMs), with their ability to manipulate wave propagation through engineered subwavelength structures, offer a promising pathway toward mitigating these reliability risks. This review provides a comprehensive overview of AMMs from a reliability-oriented design (ROD) perspective. The proposed ROD framework systematically maps environmental stressors to failure mechanisms and corresponding AMM strategies, thereby bridging the gap between material innovation and reliability assurance. Core AMM mechanisms—including local resonance, Bragg scattering, and cavity absorption—are analyzed alongside emerging multifunctional designs that integrate mechanical, thermal, and electromagnetic functions. Representative applications in MEMS, RF resonators, vehicular electronics, and data-center cooling systems demonstrate the practical benefits of AMMs in suppressing failure-inducing stressors, while emerging applications such as voice security and wearable devices are also introduced. The discussion section addresses persistent challenges in multifunctional coupling, scale incompatibility, manufacturing constraints, and the need for reliable integration across multiple physical domains, while also highlighting emerging trends in intelligent design facilitated by artificial intelligent (AI) integration. This review links material-level innovation and system-level reliability, offering a new paradigm for embedding AMMs into next-generation resilient electronic systems.

1. Introduction

The growing deployment of electronic systems in transportation, healthcare, aerospace, and other intelligent infrastructures has raised critical concerns around long-term device reliability [1]. As functionality becomes increasingly complex and densely integrated, these systems operate under multi-stress environments—where vibration, temperature cycling, and electromagnetic interference (EMI) often act in concert to accelerate failure [2].

Field data confirms the scale of this problem. For instance, 52 % of failures in airborne electronics stem from environmental stressors, with temperature variations (42 %), vibration (27 %), and humidity (19 %) leading the causes [3]. The automotive sector sees similar trends, where 60 % of contact failures result from fretting corrosion under combined thermal and vibrational loads [4]. These coupled effects can trigger severe degradation: vibration accelerates thermal fatigue, and temperature swings amplify wear, often initiating EMI issues due to crack formation in shielding layers [3–8].

The economic impact is substantial. Reliability-related warranty costs exceed $12 billion annually in the automotive industry, while the aviation sector spends over $100,000 per aircraft annually investigating "no-fault-found" (NFF) events [9,10]. The U.S. Department of Defence allocates more than $2 billion per year addressing similar reliability issues [11].

Acoustic metamaterials (AMMs)—artificially structured materials that exhibit unusual acoustic behaviour—offer a promising path forward [12,13]. Their ability to provide lightweight, tuneable, and frequency-selective control over acoustic waves makes them ideal for enhancing reliability in compact, high-performance electronic devices. Unlike traditional vibration-absorbing or thermal-insulating materials, whose performance depends primarily on intrinsic material properties, AMMs achieve controllable wave manipulation through structural design, enabling tuneable responses across a wide frequency range (from subsonic to ultrasonic) and offering new strategies for mitigating

* Corresponding authors.
E-mail addresses: lingfeng.huang@cranfield.ac.uk (L. Huang), mostafa.ranjbar@cranfield.ac.uk (M. Ranjbar).

https://doi.org/10.1016/j.apmt.2025.103030
Received 13 July 2025; Received in revised form 18 November 2025; Accepted 1 December 2025
Available online 9 December 2025
2352-9407/© 2025 The Author(s). Published by Elsevier Ltd. This is an open access article under the CC BY license (http://creativecommons.org/licenses/by/4.0/).

coupled failure mechanisms [14–20].

However, the current design of AMMs remains largely materials-performance-centric, often overlooking their potential to address complex reliability scenarios. Most designs optimize for peak performance under isolated stressors rather than addressing the multifactorial nature of real-world failure [21]. Furthermore, over-engineering for worst-case conditions results in unnecessary cost and material complexity.

To address these gaps, we introduce a Reliability-Oriented Design (ROD) framework to improve the practicability of AMM. As shown on Fig. 1, this approach repositions reliability as a design input rather than a post-verification only metric. It evaluates specific stressors for reliability in application scene, mapping them to dominant failure mechanisms and providing solution of AMM, facilitating material choices based on specific reliability goals rather than generic performance metrics.

This review article aims to provide a comprehensive overview of the recent advances of AMMs and build a practical design framework to bridge real life application. The remainder of this paper is organized as follows: Section 2 introduces AMM types and their core mechanisms. Section 3 explores multifunctional AMMs tailored for multi-stressor environments. Section 4 provides a mapping method from material performance to electronic reliability. Section 5 presents case applications in microelectronics, RF devices, and vehicular systems and estimated by the ROD framework. Section 6 discusses key challenges and emerging research opportunities, and Section 7 concludes with a summary.

2. Types of acoustic metamaterials

Under the ROD approach, various acoustic metamaterials can be viewed as functional modules for suppressing specific failure mechanisms. In this section, they will be classified according to their structural characteristics and action mechanism, and the action characteristics of these structures will be expounded, which will lay the foundation for the subsequent application deployment based on failure mode.

Acoustic metamaterials primarily operate based on three mechanisms: local resonance (LR), cavity resonance, and scattering sound absorption. Utilizing these mechanisms, researchers have developed various structural designs for vibration control. In this review, these designs can be classified into six types: mechanical LR, phononic crystals, cavity-based structures, acoustic black hole, meta porous and active control. Given that multiple mechanisms may coexist within a single structure, this classification is based solely on the design approach and the most prominent structural characteristics.

2.1. Mechanical LR

Acoustic metamaterials utilize LR to generate sub-Bragg scattering bandgaps, which arise from the resonant scattering interactions between propagating waves and periodically arranged resonators [22]. The wave behavior of these metamaterials results from the collective interaction of their locally resonant constituent units. As the resonance frequency of each unit is determined solely by its inertia and restoring force, the corresponding wavelength at resonance can be several orders of magnitude larger than the physical dimensions of the resonant unit [23]. Study of modulating acoustic waves using LR can be categorized into membrane-type and non-membrane-type systems according to their structures.

2.1.1. Membrane-type

Membrane-type acoustic metamaterials (MAMs) are one of AMMs based on the principle of LR. These metamaterials typically consist of thin membranes, attached masses, and a supporting frame structure, where the interaction between inertia and restoring forces enables the formation of negative dynamic mass density [24]. Due to their simple structure, small volume, and lightweight characteristics, membrane-type acoustic metamaterials have attracted significant attention. The working mechanism of membrane-based acoustic metamaterials involves increasing the resonance modes to enhance the energy density of low-frequency acoustic waves within the metamaterial. When a metallic sheet is subjected to external vibration, the contact boundary with the membrane contains enhanced elastic curvature energy, counteracting the coupling effect with acoustic waves and achieving sound absorption [25] .

The concept of membrane-based structures for acoustic insulation derives from 1991, when Hashimoto et al. [26] proposed a mass-attached membrane that significantly enhanced low-frequency sound insulation. This early work laid the foundation for the development of MAMs. In 2008, Yang et al. [24] formally introduced the term “membrane-type acoustic metamaterials” and demonstrated the existence of an acoustic bandgap, associated with the generation of negative dynamic mass. Subsequent research by Naify et al. [27] in 2010 further explored the sound transmission loss (STL) and modal behavior of MAMs, revealing that in the narrowband low-frequency range (100–1000 Hz), these materials exhibited greater STL than predicted by the traditional mass law (Fig. 2a). These early breakthroughs initiated widespread research interest in MAMs and encouraged further exploration into their optimization and application.

To enhance the performance of MAMs, researchers have investigated

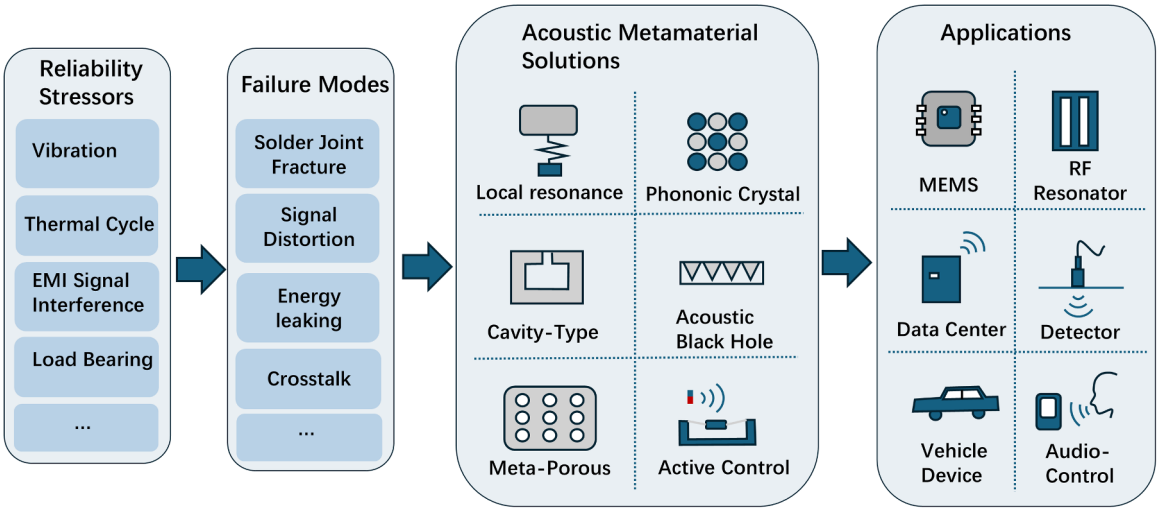


Fig. 1. The ROD framework in AMM design.

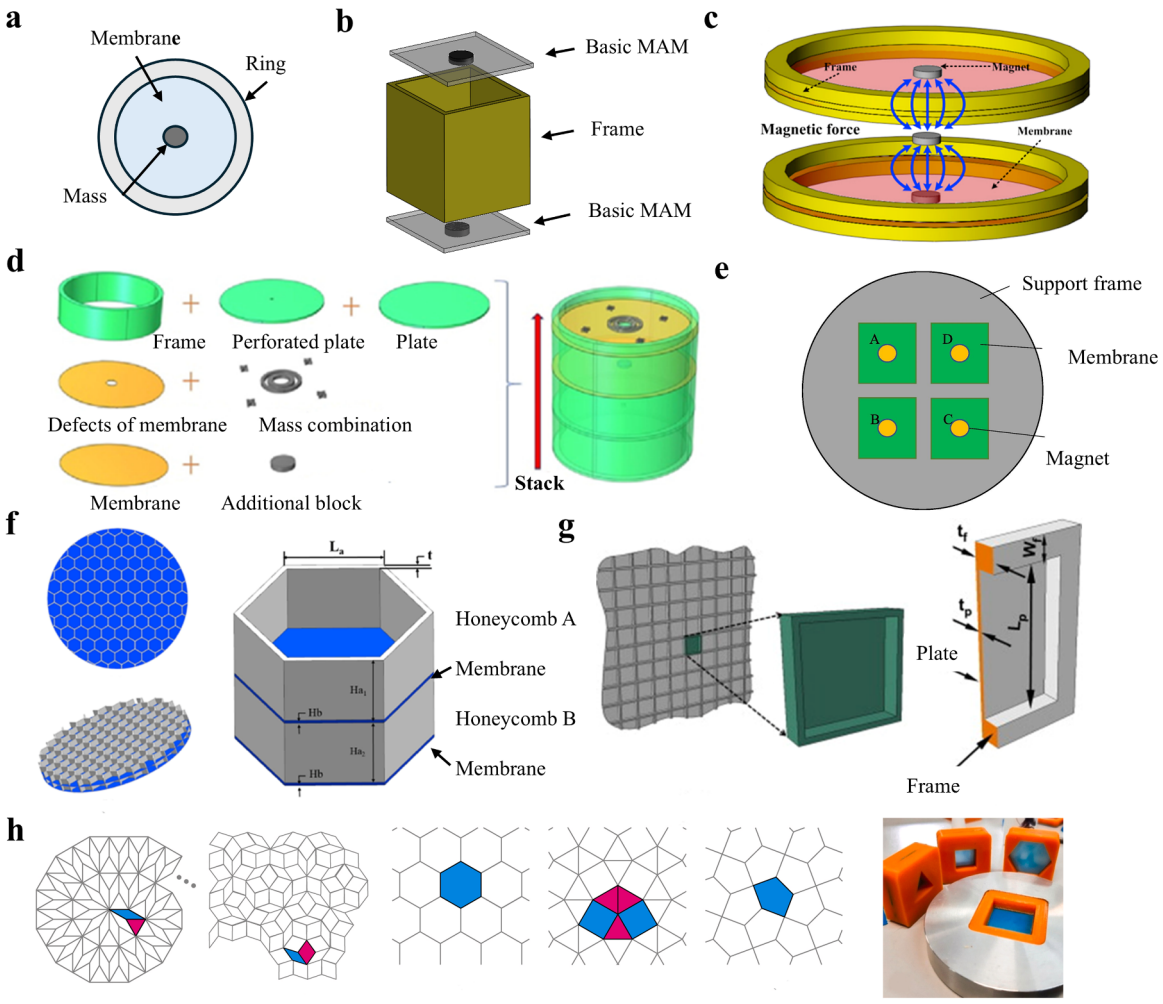


Fig. 2. Schematic diagram of MAM structure: (a) Basic membrane-mass-ring unit cell schematic. Figure redrawn based on [27]. (b) Double-layer membrane-type AMM unit cell. Figure redrawn based on [28]. (c) Bilayer MAM with magnetic oscillator. Reproduced from [29], under the Creative Commons CC-BY-NC—ND license. (d) Combined HR membrane structure. Reprinted from [30], Copyright 2023, with permission from Elsevier. (e) A compact MAM array with centered magnets. Reprinted from [31], Copyright 2022, with permission from Elsevier. (f) Multilayer honeycomb MAM. Reprinted from [32], Copyright 2020, with permission from Elsevier. (g) Plate-mass-frame structure. Reprinted from [33], Copyright 2013, with permission from Elsevier. (h) MAM supercell configurations. Reprinted from [34], Copyright 2022, with permission from Elsevier.

various structural optimizations. One approach involves modifying the unit cell's geometric shape and material properties to achieve more effective wave manipulation. For example, Bucciarelli et al. [35] optimized the shape and density distribution of membranes, achieving precise eigenfrequencies tuning. Another method to improve MAM efficiency involves using multi-layered structures. Nguyen et al. [28] developed a dual-layer membrane-based acoustic panel that demonstrated significant wider bandgaps than single layer MAMs, achieving an overall STL exceeding 20 dB with much wider stopband (Fig. 2b). In addition, the researchers have also tried to adjust the position and shape of the additional mass to optimize the noise attenuation and have achieved effective results in expanding the operational bandwidth of MAMs [36,37].

In addition to geometric and multi-layer optimizations, researchers have also explored alternative framework structures, particularly honeycomb-based configurations. Honeycomb structures offer improved skeletal stiffness and mechanical stability while maintaining lightweight characteristics, making them ideal for MAM applications. Lu et al. [38] proposed a honeycomb-based MAM composed of a rubber membrane sandwiched between two honeycomb unit panels. This design demonstrated exceptional low-frequency STL, maintaining values of at least 20 dB at frequencies below 100 Hz. Similarly, Li et al. [32] developed a lightweight multilayer honeycomb MAM, achieving an average STL of 15.07 dB in the 63–1600 Hz range (Fig. 2f). Gao et al. [39] reported a deformable honeycomb acoustic metamaterial design composed of a honeycomb structure and copolymer membranes, demonstrating that different deformation states exhibit varying STL. Zhong et al. [40] investigated composite underwater honeycomb acoustic metamaterial panels, demonstrating an average sound insulation performance of 10 dB under a 3 MPa hydrostatic pressure. Li et al. [30] integrated membrane structure with Helmholtz cavity resonance by employing a dual-layer membrane combined with an HR design, thereby achieving an average transmission loss of 72.29 dB over the 50–1600 Hz range—with low-frequency attenuation of up to 80 dB on average in the 50–200 Hz range (Fig. 2d). These studies highlighted the potential of honeycomb acoustic metamaterials in high-compression environments, making them suitable for engineering applications requiring high structural rigidity.

Despite their promising performance, membrane-based acoustic metamaterials face several limitations. One of the major challenges is their sensitivity to prestress tension. Because MAMs rely on membrane elasticity for their resonance behavior, variations in tension due to environmental changes can shift resonance frequencies, potentially reducing their effectiveness. Additionally, membrane structures are

prone to mechanical damage under excessive stress or contaminated conditions, limiting their long-term durability. Another significant challenge is the difficulty in ensuring consistent membrane assembly and structural alignment, which can affect the uniformity of acoustic performance across large-scale applications.

To address these limitations, researchers have proposed the use of plate-type acoustic metamaterials as an alternative to MAMs. Unlike membranes, thin plates offer higher mechanical stiffness and do not require prestress tension, reducing susceptibility to environmental fluctuations. Early developments in this area were reported by Varanasi et al. [33], who introduced a plate-mass-frame structure that exhibited similar negative dynamic mass properties to membrane-based designs but with improved durability and mechanical stability (Fig. 2g). Further advancements were made by Ma et al. [41], who replaced conventional low-modulus membranes with high-modulus nylon sheets to achieve an ultra-thin and lightweight design that not only guarantees significant sound insulation, but also improves mechanical stability and durability. More recently, Wang et al. [42,43], Belle et al. [44], Filho et al. [45] and Langfeldt et al. [46], by optimizing mass block distribution, introducing cantilever resonators and multi-layer integration, the problem of STL trough caused by the coupling between cells and air is effectively solved, and the performance of plate metamaterials in low frequency band is better. Compared to membrane-based metamaterials, plate-type designs offer more reliable sound insulation performance, greater durability, and easier fabrication, making them a promising alternative for long-term engineering applications.

Beyond the development of plate-based alternatives, recent research has also focused on tunable MAMs, which allow for dynamic control over resonance frequencies. Gao et al. [29] proposed a dual-layer membrane-type acoustic metamaterial incorporating magnetic oscillators (Fig. 2c). Frequency tuning can be implemented by controlling the magnetic mass block through the external magnetic field to adjust the film preload force. Zhao et al. [47] introduced a membrane structure with rigid blocks and compact magnets, where the nonlinear magnetic attraction led to frequency shifts in the 100–800 Hz range with an average attenuation of over 10 dB. Similarly, a compact MAM array (with a centered magnet in the cell) designed by Li et al. [31] achieved an average attenuation of >15 dB over 100–1000 Hz (Fig. 2e). These tunable designs provide increased flexibility for applications requiring adaptive noise control, although they typically result in narrower bandgaps and slightly lower absorption efficiency compared to fixed-frequency MAMs.

An additional innovative direction in MAM design involves the concept of supercell configurations. Sampaio et al. [34] proposed assembling membranes of different shapes and sizes into tessellated supercells, which enhanced geometric compatibility and periodicity (Fig. 2h). Unlike traditional single-plane membrane structures, these supercell configurations allow for multi-directional noise mitigation and geometric compatibility, making them particularly suitable for real-world applications in irregular structure and complex acoustic environments. The ability to construct customized, high-performance acoustic insulation panels using this approach expands the potential applications of MAMs in industrial noise reduction and precision acoustic control.

Although MAMs demonstrate promising potential, they are still predominantly in the experimental stage, with limited practical testing on relevant devices. To advance the commercialization and real-world application of MAMs, further engineering tests and practical validations are essential in future research. Table 1 concludes the characters and parameters of typical types of MAM.

2.1.2. Non-membrane-type

In recent years, research on non-membrane-type LR structures has increasingly focused on achieving ultra-wide bandgaps, tunability, flexible designs, and low-frequency vibration attenuation. Due to its larger stiffness, it is easier to achieve a higher frequency band than MAM. Because a single LR mechanism responds only at its intrinsic resonance frequency, it is challenging to realize a broad stopband. Consequently, incorporating the Bragg scattering (BG) mechanism has emerged as an effective method to broaden the stopband. BG exploits the phase difference between the incident and radiated waves to generate destructive interference, thereby producing a broadband isolation effect [48]. By coupling LR and BG mechanisms, the synergistic effects of low-frequency resonance and mid-to-high-frequency scattering can be utilized to achieve broadband bandgap characteristics spanning from low to mid-to-high frequencies.

This research direction can be traced back to Hsu [49] in 2011, who demonstrated that LR and BG mechanisms can coexist using simple neck-shaped resonators (Fig. 3a). Their work revealed the synergistic interaction between the two mechanisms, providing new insights for bandgap optimization. Subsequently, Coffy et al. [50] investigated an acoustic metamaterial composed of tungsten stubs periodically arranged on a silicon substrate. By optimizing the original square base into a thin straight-beam structure, they significantly enhanced the low-frequency bandgap performance, underscoring the critical role of substrate structure optimization in achieving wide bandgaps.

In terms of structural design and multi-mechanism integration, researchers have continuously explored novel geometric parameters and lattice-tuning methods. Zhang et al. [52] proposed a perforated plate AMM with diagonally arranged short columns that achieved a broad bandgap ranging from 247.996 Hz to 979.1 Hz, confirming the effectiveness of geometric arrangement and lattice parameter tuning in expanding the bandgap (Fig. 3c). Dong et al. [53] designed a miniaturized multi-band locally resonant elastic unit, exhibiting low-frequency multi-bandgap characteristics spanning 399 Hz to 2753 Hz with exceeding 95 % coverage below 3000 Hz (Fig. 3d). Meanwhile, Xu et al. [54] constructed a three-dimensional LR unit using a multi-holes silicone rubber matrix and high-density lead scatterers,

Table 1
The literature comparison of typical MAMs has been presented.

Approach	Stopband Range (Hz)	Average Transmission loss (dB)	Strengths	Limitations	Study/year
Basic MAM	270–490	About 4	Accurate narrow bandgap control	Membrane degradation, not supportive	Bucciarelli et al. [35] (2018)
Dual layer MAM	320–2500	>20	Supportive design, wide bandgap	Membrane degradation, sensitive to prestress tension	Nguyen et al. [28] (2021)
Honeycomb structure MAM	63–1600	15.07	Supportive design, wide bandgap	Membrane degradation, sensitive to prestress tension	Li et al. [32] (2020)
Dual layer with HR design	50–1600	72.29	Ultra-high Transmission loss rate	Membrane degradation, sensitive to prestress tension	Li et al. [30] (2023)
Plate type MAM	200–1000	About 25	Low susceptibility to environmental fluctuations	Fabrication difficulty	Ma et al. [41] (2017)
Tunable MAM	Frequency shift in about 700 Hz under 2000 Hz	About 15	Changeable target frequency	Extra weight, narrow bandgap	Gao et al. [29] (2017), Li et al. [31] (2022)

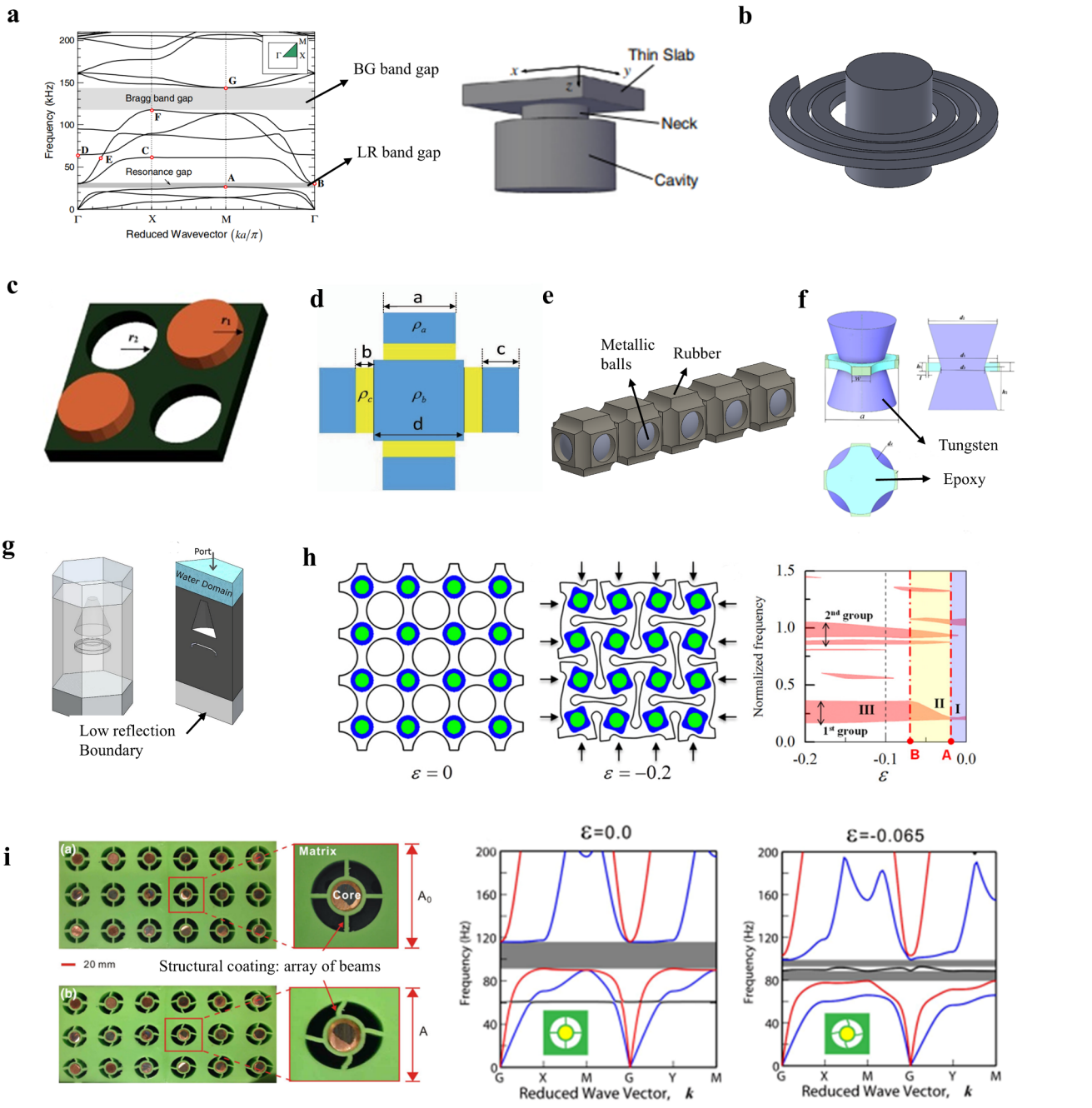


Fig. 3. Mechanical local resonant structures: (a) Coexist of LR and BG in neck-shape resonators. Reproduced from [49] © IOP Publishing. Reproduced with permission. All rights reserved. (b) A chiral spiral elastic LR metamaterial. Figure redrawn based on [51]. (c) Diagonally arranged short columns AMM. Reprinted from [52], Copyright 2016, with permission from Elsevier. (d) Elastic AMM unit. Reprinted from [53], Copyright 2019, with permission from Elsevier. (e) Three-dimensional muti-holes AMM. Figure redrawn based on [54]. (f) Symmetric conical scatterer structure AMM. Reproduced from [55], under the terms of the Creative Commons CC BY license. (g) Air cavities in locally resonant underwater anechoic coating structure. Reproduced from [56], under the terms of the Creative Commons CC BY license. (h) Deformable tunable AMM. Reprinted from [57], Copyright 2020, with permission from Elsevier. (i) Elastic strain controlled tunable AMM. Reprinted with permission from [58] Copyright (2014) by the American Physical Society.

which achieved an average attenuation of over 200 dB in the 177–850 Hz range (Fig. 3e). Later, Wen et al. [59] were the first to experimentally verify the existence of hybrid bandgaps in beam structures, the LR, coupled bandgap, and BG bandgap. This finding further confirmed the importance of the coupling of different mechanisms in optimizing broadband bandgaps and providing specific instruction for further development. More recent advances include Tang et al. [55], who proposed a symmetric conical scatterer structure that achieved an ultra-wide bandgap of 122.47–4360.2 Hz with a lattice constant of 8.5 mm, underscoring the role of silicone rubber-based LR in low-frequency bandgap formation; providing robust theoretical and practical support for low-frequency broadband vibration attenuation (Fig. 3f). These studies show that mechanical local resonators have achieved outstanding acoustic absorption within compact design and have huge potential to implement into low frequency applications.

At the same time, to meet the demands for tunability and flexible structures in practical engineering applications, the adaptive and self-tuning capabilities of LR AMMs have received significant attention. Wang et al. [58] introduced an adaptive AMM that replaced the surrounding plate with flexible beams, thereby enabling tuning of the

resonance frequency via the application of an out-of-plane compressive strain (Fig. 3i). Ning et al. [57] further developed a multi-mode deformable tunable metamaterial by embedding resonant elements into an elastic matrix (Fig. 3h). Through different deformation modes, the LR bandgap could be expanded by up to 7.76 times.

To further optimize low-frequency bandgaps, Liu et al. [51] investigated a chiral spiral elastic LR metamaterial (Fig. 3b), achieving ultra-low-frequency vibration attenuation in the 96.9–124 Hz range. Moreover, Yu et al. [60] employed a flexible cantilever beam resonator design that achieved a bandwidth of 504–621 Hz, thereby enhancing system flexibility and providing potential for lightweight design. Ranjbar et al. [56] introduced air cavities into locally resonant underwater anechoic coatings and, by adjusting the cavity parameters (Fig. 3g), effectively improved low-frequency absorption, offering a novel approach for developing lightweight, high-performance underwater metamaterials.

Non-membrane-type LR structures have shown outstanding performance for target frequency. Although these designs generally require more space and weight compared to membrane-type configurations, they offer significant advantages in low-frequency vibration control and broadband isolation. In general, the size of the LR type AMM is relatively smaller compared with other type AMMs in same working frequency, and the specific vibration frequency regulation is flexible. From ROD's point of view, the mechanical LR type structure is especially suitable for fatigue failure scenarios caused by narrow frequency vibration and have requirements for material design size, such as on-board electronics, PCB modules, etc. By adjusting the resonance quality and the parameters of the flexible connection elements, the stop bandwidth can be precisely adjusted to achieve the suppression of the specific frequency failure source. It is worth noting that LR-based AMMs exhibit a high degree of tunability in the frequency domain. Their resonance frequencies can be tailored by adjusting material properties, while the absorption bandwidth and peak absorption efficiency can be engineered through various arrangement strategies, including periodic, aperiodic, and graded configurations. Only LR AMMs that are precisely designed according to the specific working conditions can achieve optimal performance in practical applications.

In the research of mechanical local resonator AMMs, a comprehensive analysis was conducted on of each study. The literature review of typical types of LR AMM is detailed in Table 2.

2.2. Phononic crystals (PnCs)

Phononic crystals (PnCs) are artificially engineered periodic composite materials composed of periodically distributed individual acoustic functional scatterers. These individual scatters exhibit high impedance contrast in terms of mass density and/or elastic modulus. Due to the periodic BG and local Mie scattering effects, phononic crystals generate novel acoustic scattering phenomena and band structures [61]. Due to the mismatched mechanical properties of different materials within the unit cell, phonons propagating in the reciprocal lattice exhibit dispersion phenomena, and this dispersion is closely related to the shape of the scatterers and the lattice configuration of the matrix (e.g., square, hexagonal, honeycomb) [62]. Therefore, by adjusting the geometric shape and arrangement of the scatterers, it is possible to effectively block the propagation of acoustic waves within a specific frequency range.

Early research laid the theoretical foundation for phononic crystals. In 1998, Kushwaha and Djafari-Rouhani [63] first proposed a serial structure that achieved bandgaps in the kilohertz range under low filling ratios, laying the theoretical foundation for phononic crystal research. Thereafter, researchers progressively improved the bandgap characteristics in two-dimensional structures by introducing air inclusions, altering the shapes of the scatterers, and adjusting the periodic configuration. For instance, in 2003, Lai and Zhang [64] designed a two-dimensional phononic crystal that incorporated air inclusions, achieving a bandgap-to-midgap ratio of approximately 0.53, thereby demonstrating the critical role of local defects in bandgap formation. Susa [65] modified the scatterer shape from cylindrical to elliptical, increasing the bandgap width by 40 %, while Li and colleagues [66] employed the plane wave expansion method to investigate phononic crystals with elliptical inclusions, finding that tungsten elliptical rods embedded in a silicon matrix produced wider bandgaps than conventional cylindrical structures. Moreover, other researchers achieved significant optimization by introducing cracks into the structure, adjusting the filling ratio, and tuning geometric parameters—for example, Cui et al. [67] proposed a parallel steel tube array structure that achieved a broadband bandgap of 5000 Hz within the 1000–8000 Hz range (Fig. 4a), and Yu et al. [68] enhanced acoustic attenuation in the 2000–11,000 Hz range by increasing the filling ratio.

Although design methods based on BG perform well in the high-frequency domain, the inverse relationship between bandgap frequency and lattice constant inherently limits their application in the low-frequency range. Consequently, to achieve control over mid-to-low frequency bandgaps, researchers have begun to explore alternative strategies such as LR, hierarchical structures, and novel geometric designs. For example, Wang et al. [69] employed spindle-shaped lead inclusions to achieve an attenuation exceeding 100 dB in the 163–222 Hz range (Fig. 4b), while Sun et al. [75] succeeded in designing a broadband bandgap in the 153–196 Hz range through simple modifications of conventional phononic crystals. These studies utilized LR to adjust bandgaps and achieve lower stopband. Moreover, Ranjbar et al. [70] used finite element analysis to study the vibroacoustic behavior of anti-tetrachiral and auxetic hexagonal gradient sandwich plates (Fig. 4c), minimizing the radiation sound power level within the 0–1000 Hz frequency range. In addition, hierarchical and fractal designs have

Table 2
The literature comparison of typical mechanical locally resonant AMMs has been presented.

Approach	Stopband Range (Hz)	Average Transmission loss (dB)	Strengths	Limitations	Study/year
Diagonally arranged short columns AMM	248–979	About 50	Easy manufacturing	Narrow bandgap	Zhang et al. [52] (2016)
Miniaturized multi-band elastic AMM	399–2753	13	Wide bandgap	Manufacturing difficulty, relatively weak transmission loss efficiency	Dong et al. [53] (2019)
Three-dimensional muti-holes AMM	177–850	>200	Effective transmission loss	Manufacturing difficulty	Xu et al. [54] (2021)
Symmetric conical scatterer structure AMM	122.5–4360	380	Effective transmission loss, wide bandgap	Manufacturing difficulty, expensive material	Tang et al. [55] (2023)
Deformable Tunable AMM	Change according to deformation	N/A	Multi-mode tunable design	Easy to degrade	Ning et al. [57] (2020)
Chiral spiral elastic AMM	96.9–123	About 60	Low frequency design	Narrow bandgap	Liu et al. [51] (2024)
Under water air cavities in locally resonant	500–10,000	About 7	Wide bandgap, Underwater application	Relatively weak transmission loss efficiency, Manufacturing difficulty	Ranjbar et al. [56] (2024)

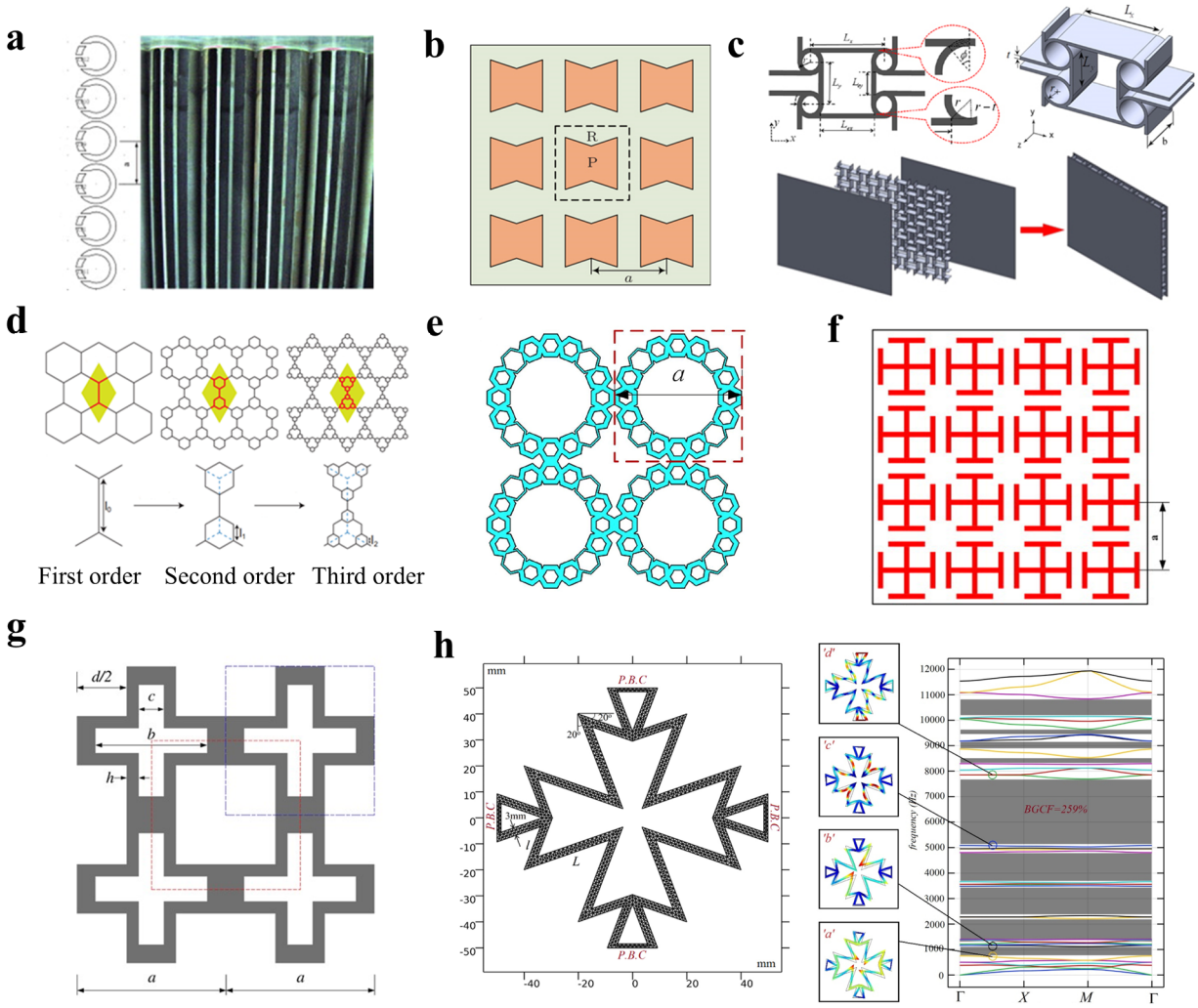


Fig. 4. Schematic diagram of PnCs structures: (a) Parallel steel tube array. Reprinted from [67], Copyright 2009, with permission from Elsevier. (b) Periodic spindle-shaped inclusions. Reprinted from [69]. Reproduced with permission. (c) Anti-tetrachiral and auxetic hexagonal gradient sandwich plates. Reproduced from [70] © IOP Publishing. Reproduced with permission. All rights reserved. (d) Fractal honeycombs. Reprinted with permission from [71] Copyright (2015) by the American Physical Society. (e) Hoberman-sphere-like structure. Reprinted from [72], Copyright 2020, with permission from Elsevier. (f) Jerusalem cross slots. Reprinted from [73], Copyright 2015, with permission from Elsevier. (g) Four square protrusions with cross holes Reproduced from [74] © Wiley. Reproduced with permission. All rights reserved. (h) Maltese cross. Reprinted from[75], Copyright 2021, with permission from Elsevier.

been shown to effectively extend low-frequency bandgaps. Mousanezhad et al. [71] transformed conventional honeycomb structures into first- and second-order fractal honeycombs (Fig. 4d), thereby reducing the starting frequency of the bandgap to half that of the original structure and expanding the overall bandwidth sixfold. Thereafter, Wen et al. [72] proposed a two-dimensional phonon crystal like the Hoberman sphere (Fig. 4e). Simulation shows that the first band gap range is 244.6–2543.9 Hz, and the band gap ratio is as high as 164.9 %. Similarly, studies by Wang [76] and Liu [77] have further confirmed the advantages of multilayer self-similar structures in broadening low-frequency bandgaps. Moreover, some novel shape designs achieved high effective sound insulation. Li et al. [73] designed a two-dimensional photonic crystal composed of a Jerusalem cross slot and a square lattice air matrix (Fig. 4f). Under infinite periodic conditions, simulations formed a total bandgap of 5523 Hz, with a significantly lower starting frequency. Jiang et al. [74] proposed a photonic crystal composed of four square protrusions or square plates with cross holes, achieving an ultra-wide bandgap with a bandgap ratio of 156.0 % (Fig. 4g). Panahi et al. [78] introduced a novel phononic crystal with a Maltese cross structure achieving a 150 dB attenuation rate in the 750–10,000 Hz frequency range and a Bandgap Coverage Factor of 259 % (Fig. 4h). Similarly, some novel geometric unit designs, such as star, cross, convex, and concave holes shapes, have also provided new approaches for achieving low-frequency bandgaps [76,77,79,80]. Although significant progress has been made in these studies, research on the development of efficient optimization for investigating phononic crystals remains limited. For this solution, Ranjbar et al. [81] systematically compared seven optimization methods using FEA to evaluate their effectiveness, stability, and computational efficiency in optimizing the local geometric shape of a steel square plate to minimize the RMS level of structure-borne noise. Later, Ranjbar et al. [82] proposed a tabu search (TS) approach for minimizing RMS noise in a steel quadratic plate, demonstrating its ability to escape local optima and improve structural performance. However, TS exhibited slow convergence in later iterations. To address computational cost and efficiency, they further introduced an ANN-based optimization method, replacing costly FEA evaluations with a trained neural network [83]. By integrating ANN with simulated annealing (SA), this approach significantly reduced optimization time while maintaining accuracy, marking a transition toward AI-assisted structural acoustic optimization. In recent years, many researchers have used topology optimization, finite element methods, genetic algorithms, and other optimization techniques to

expand bandgaps by adjusting parameters such as filling ratio, symmetry, aggregation degree, and material properties, achieving notable results [84–90].

In ultra-high-frequency acoustics research, some studies achieved meaningful development. Cheng et al. [91] first observed hypersonic bandgaps in face-centered cubic colloidal crystals. Gorisse et al. [92] reported elastic wave propagation in two-dimensional aluminum nitride (AlN) phononic crystals, while Kuo and Piazza [62] experimentally demonstrated ultra-high-frequency PnC resonant cavities in AlN sputtered thin films. Later, Baboly et al. [93] implemented a square-lattice cross-shaped air-void PnC structure in AlN thin-film substrates, identifying a bandgap between 1110 and 1175 MHz. These results confirmed both the presence of acoustic bandgaps and the ability of AMM to support high-frequency resonance modes suitable for RF communication devices. In surface acoustic wave (SAW) applications, Dehghannasiri et al. [94] introduced a novel CMOS-compatible PnC platform based on AlN pillar arrays. This all-dielectric structure demonstrated a low-loss acoustic bandgap between 1.6 and 1.75 GHz, significantly broadening its application scope.

Despite the notable successes of phononic crystals in high-frequency vibration isolation, directly integrating them into electronic devices remains a challenge. Due to size constraints, the application of phononic crystals has been mostly concentrated in the mid-to-high frequency range, particularly in the vibration isolation of electronic devices, where they are primarily applied to external structures. However, integrating phononic crystals directly into electronic devices remains a challenge.

In the ROD frame, their extra wide stopband is suitable for the application of working in multi-frequency like aircraft cabin. Moreover, their structural support and stability are key advantages, making them highly promising for integration with mechanical metamaterials. That can expand their application into supportive parts like device housing. The comparison of typical PnCs study is shown in Table 3.

2.3. Cavity type: Helmholtz cavity resonator and space coiling type

The Helmholtz resonator is a fundamental acoustic concept widely employed for sound absorption and noise reduction. Its typical design, comprising a neck and an enclosed air cavity within a rigid container, functions as a resonant absorber analogous to a mass-spring system. Under sound pressure excitation, the oscillating mass element dissipates energy through its interaction with the "spring," thereby producing damping effects [95]. Space coiling type structure is realized by extending the propagation path of sound wave to delay the transmission phase, leading to construct a fluid medium with a very slow equivalent speed [96]. Although they have different working mechanisms, they have similar working environments and may have common applications. Thus, they are discussed in this section.

In 2006, Fang et al. [97] laid the theoretical foundation for the application of Helmholtz resonators in acoustic metamaterials. They proposed an anisotropic metamaterial design using a one-dimensional Helmholtz resonator array and calculated the bandgap and transmission coefficient using the effective medium theory (Fig. 5a). This study revealed the negative effective modulus phenomenon in metamaterials incorporating Helmholtz resonators, providing a theoretical basis for wave propagation in the subwavelength range. However, this research was limited to one-dimensional structures and did not explore the complexity of multi-dimensional arrays or their potential engineering applications.

The exploration of multi-band and broadband sound absorption has been a popular research topic. Ding et al. [98] designed a multi-band negative modulus AMM composed of separate hollow spheres (SHS) of different sizes (Fig. 5b). This design demonstrated the multi-frequency characteristics of LR, achieving a negative modulus in the 900–1500 Hz frequency range and validating the feasibility of tuning geometric parameters to achieve multi-band sound absorption. However, its exploration of broadband performance and practical engineering applications was limited. Romero-Garcia et al. [104] developed both perfect subwavelength narrowband and broadband absorbers based on acoustic Helmholtz resonators. In a subwavelength multi-resonant scatterer system with a thickness of $\lambda/12$, several perfect absorption peaks overlapped, achieving an absorption rate of over 93 % for frequencies spanning more than twice the audible range. In 2019, Huang et al. [105] further optimized the structural design of Helmholtz resonators, proposing a neck-embedded Helmholtz resonator. Experimental results showed that when the thickness was only 1/50 of the working wavelength, a high average absorption coefficient of 0.957 was achieved in the 870–3224 Hz range. Additionally, tunable resonance frequencies (137–300 Hz) and adjustable absorption bandwidths (22 %–46 %) were

Table 3
The literature comparison of typical PnCs AMMs has been presented.

Approach	Stopband Range (Hz)	Average Transmission loss (dB)	Strengths	Limitations	Study/year
Parallel steel tube array	1000–8000	About 13	Wide bandgap	Heavy and bulky	Cui et al. [67] (2009)
Periodic spindle-shaped inclusions	163–222	100	Effective transmission loss	Narrow bandgap	Wang et al. [69] (2016)
Anti-tetrachiral and auxetic hexagonal gradient sandwich plates	0–1000	About 140	Effective transmission loss, supportive structure, light weight	Manufacturing difficulty	Ranjbar et al. [70] (2016)
Hoberman sphere like structure	244.6–2543.9	N/A	Low start frequency	Manufacturing difficulty	Wen et al. [72] (2020)
Jerusalem cross slot structure	1825–2968 3029–4998 6128–7668 6128–7668 10,414–11,294	N/A	Large bandgap coverage rate, light weight	Incontiguous stopband, lack of low frequency transmission loss	Li et al. [73] (2015)
Maltese cross structure	751–1165 1400–2273 2273–3500 3600–4900 5088–8000 8200–9000 10,090–11,080	About 50	Large bandgap coverage rate, light weight	Large size	Panahi et al. [78] (2021)
Square-lattice cross-shaped air-void PnC structure, novel CMOS-compatible PnC platform	MHz, GHz	N/A	Ultra-high frequency manipulation	Fabricating difficulty	Baboly et al. [93] (2016), Dehghannasiri et al. [94] (2018)

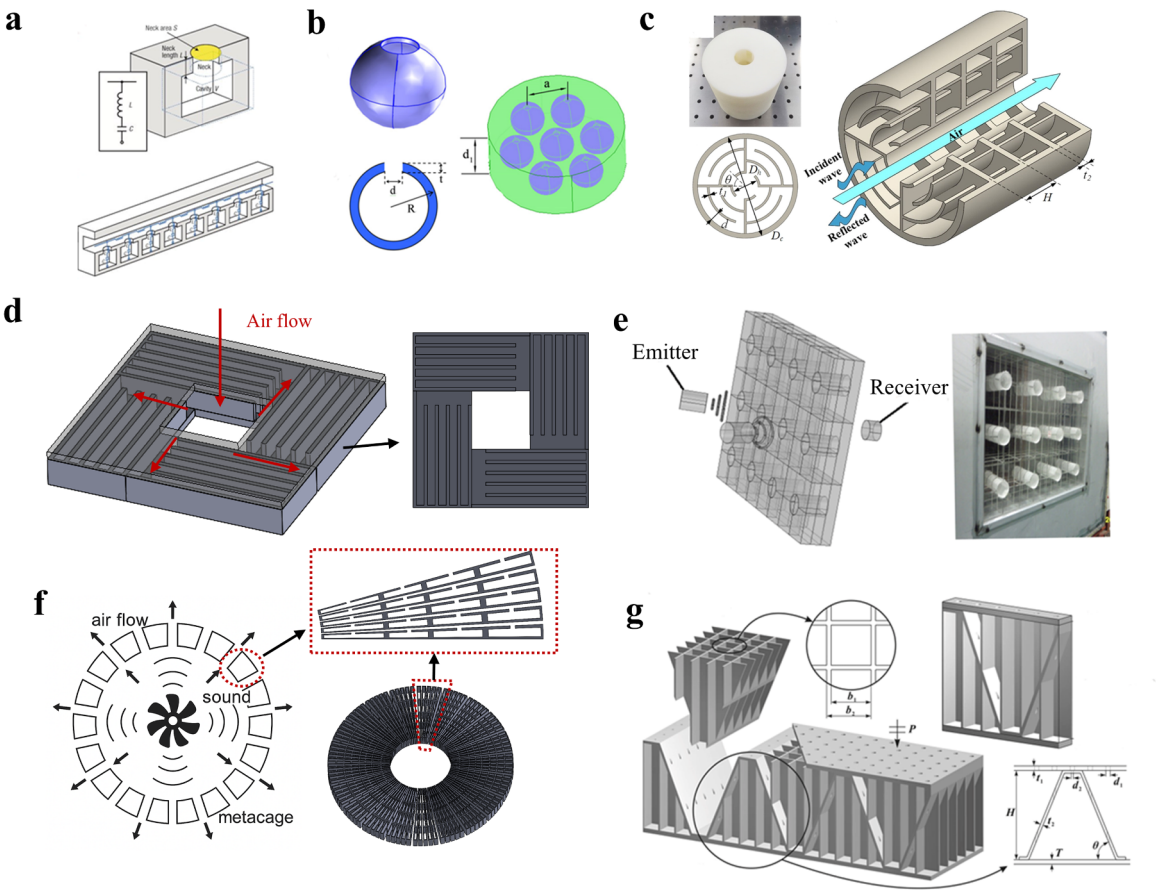


Fig. 5. Schematic diagram of Cavity type structures: (a) One-dimensional Helmholtz resonator array Reproduced from [97], with permission from Springer Nature. (b) SHS AM. Reproduced from [98] © IOP Publishing. Reproduced with permission. All rights reserved. (c) A coiled ventilation metamaterial. Reprinted from [99], Copyright 2021, with permission from Elsevier. (d) A metamaterial sandwich structure with a central hollow channel. Figure redrawn based on [100]. (e) Double-layer soundproof window. Reproduced from [101], under the terms of the Creative Commons CC BY license. (f) Meta-cage. Figure redrawn based on [102]. (g) Perforated corrugated honeycomb hybrid absorber. Reproduced from [103], under the terms of the Creative Commons CC BY license.

realized, demonstrating the structure's potential for broadband sound absorption.

Additionally, progress has been made in space-coiled metamaterials. Xiao et al. [99] proposed a coiled ventilation AMM (Fig. 5c), which achieved nearly 30 dB sound transmission loss in the 660–1200 Hz frequency range and solved airflow blocking problem. Furthermore, Yang et al. [100] developed a metamaterial sandwich structure with a central hollow channel (Fig. 5d). By utilizing transmission loss interference of sound waves in a labyrinth structure, the quarter-module panel exhibited broadband transmission loss in the 1400–2500 Hz range, with a peak transmission loss of approximately 30 dB. These studies have greatly advanced the development of cavity type metamaterial and laid fundamental for later diversified development.

In addition to purely acoustic performance, recent studies have focused on integrating ventilation with noise insulation—a combination crucial for practical applications. Kim and Lee [101] pioneered this integration by developing a double-layer soundproof window that merged cavities with a negative effective bulk modulus and macroscopic ventilation holes, thereby achieving 30–35 dB attenuation over 400–5000 Hz while maintaining natural airflow (Fig. 5e). This design is well suited for applications where both noise reduction and heat convection are required and sets a precedent for metamaterial integration. Building on this concept, Shen et al. [102] designed an acoustic meta-cage that blocked sound waves from all directions yet permitted stable fluid flow (Fig. 5f), recording average attenuations above 10 dB in the 2.2–2.6 kHz band. Other works, such as those by Nguyen et al. [106] and Kumar et al. [107], have demonstrated the feasibility of compact, ventilated silencers and Helmholtz cavity structures with high absorption coefficients and significant sound transmission loss, further highlighting the practical potential of these designs in confined spaces. Moreover, innovative configurations like subwavelength-thickness spiral acoustic barriers and ventilated spiral acoustic meta surfaces have been shown to enhance broadband sound insulation while maintaining airflow [108,109].

Further optimization efforts have targeted low-frequency sound absorption, an area traditionally challenged by the size constraints of conventional Helmholtz resonators. Cai et al. [110] proposed a coplanar Helmholtz resonator that theoretically achieved near-perfect deep subwavelength absorption, the transmission coefficient at 250 Hz is dropped to 0.15, with a thickness-to-wavelength ratio of approximately 1/102. The reduction in size is attributed to the more efficient utilization of the disk's internal space by the cavity of the Helmholtz resonator, while the long neck continues to effectively dissipate acoustic energy through intense flow-induced friction. Moreover, Tang et al. [103] developed a perforated corrugated honeycomb hybrid absorber that achieved perfect absorption near 580 Hz and demonstrated broadband low-frequency absorption over a range exceeding 1000 Hz (Fig. 5g). Later, Huang et al. [111] created a compact broadband acoustic absorber achieving quasi-perfect absorption of broadband incident sound waves through coherently coupled "weak resonances" and attaining an average absorption coefficient of 0.957 over the 870–3224 Hz frequency range with a thickness of only 3.5 m. These optimizations greatly reduced the size and improved performance in low frequency, broadening the cavity type AMMs application potential in compact

environments.

Notable, a major advantage of Helmholtz resonator-based structures lies in their ability to concurrently provide ventilation and noise insulation, which is especially valuable for electronic devices that require thermal management. In fact, ROD provides a new aspect to rethink these AMM technologies. Although Helmholtz resonators are generally less suited for low-frequency applications compared to local resonators from a technical standpoint due to larger unit size, the ROD framework highlights their significantly lower cost in large-scale manufacturing. Therefore, HRs can be considered as chassis materials when space constraints are not critical. Moreover, unlike LRs—whose resonant frequencies are governed by intrinsic material properties such as mass and elastic modulus—the resonant frequency of HRs is determined by the cavity and neck dimensions. As a result, HR performance is more sensitive to manufacturing precision in high-frequency applications. Therefore, from ROD view, HR's application will be more suitable for the application on a large scale or specifically requiring airflow. Table 4 compare characteristics and parameters of typical cavity type AMMs.

2.4. Acoustic black hole

The emergence of the acoustic black hole (ABH) phenomenon offers a new perspective for acoustic manipulation. The ABH effect allows for the manipulation of bending wave propagation within thin-walled structures by adjusting the thickness according to a power-law variation [112]. In an idealized ABH structure, the phase and group velocity of bending waves gradually reduce to zero at the tapered tip, effectively eliminating wave reflections. When this occurs, the tapered ABH structure serves as an ideal energy absorber due to its high energy concentration and trapping effects. Although, in practice, the structural thickness is inevitably truncated (referred to as the residual thickness), significant energy focusing associated with the ABH effect can still be observed. In plates embedded with conventional ABH units, the unique energy-focusing characteristics of ABH have been shown to produce distinct dispersion properties [113].

The concept of the acoustic black hole was first named by Krylov [114] in 2001. In recent years, with the advancement of metamaterials, ABH has provided novel solutions for acoustic control. Numerous studies have demonstrated that ABH can effectively control bending waves, showing great potential in noise insulation and vibration reduction applications. Conlon et al. [115] applied the ABH concept to noise control in thin metal plates and found that panels with periodic ABH structures reduced radiated sound power by 6 to 30 dB while decreasing the total structural mass by 17 % compared to a baseline uniform panel. Subsequently, Tang and Cheng [113] proposed a beam with double-leaf ABH indentations, integrating LR and BG effects to achieve an ultra-wide bandgap structure (Fig. 6a). Using only three units, this beam achieved nearly 90 % bandwidth coverage within the 0–20 kHz range, demonstrating significant vibration attenuation. They further investigated the low-frequency acoustic radiation of periodic tunnel double-leaf ABH plates (Fig. 6b), demonstrating that it was possible to reduce acoustic radiation within the LR bandgap without additional damping. By enhancing the interaction between bending structures and ABH, low-frequency control performance was significantly improved [116]. Gao et al. [117] introduced a double-leaf ABH beam embedded with mass vibrators, combining the double-leaf ABH structure with a LR design (Fig. 6c). The study revealed that the mass vibrators could either enhance or weaken wave trapping effects in finite periodic structures, expanding research in low-frequency wave manipulation and vibration control.

In terms of structural optimization, Zhao [118] developed a modeling technique that combined ABH with sandwich plates (Fig. 6d). By embedding ABH within a viscoelastic layer, the study demonstrated improved low-frequency vibration and noise control capabilities. Results indicated that the loss factor of the tapered viscoelastic layer was 50 % higher than that of a planar viscoelastic layer, with particularly significant improvements in the 400–900 Hz range.

Two-dimensional ABH plates also exhibited excellent acoustic radiation performance. For instance, Du et al. [119] proposed a circular plate embedded with two-dimensional ABH structures (Fig. 6e). When the ABH diameter was 30 mm, transmission loss improvements of 8–20 dB were observed below the first resonance frequency and within certain damping-controlled frequency ranges. However, the average transmission loss across the full frequency range remained similar to that of a uniform circular plate, highlighting the need to balance performance across different frequency bands during design. Bowyer and Krylov [126] were the first to integrate two-dimensional ABH structures into automotive engine covers, experimentally demonstrating significant reductions in engine noise. Additionally, applying ABH structures to vehicle flooring significantly suppressed in-cabin low-frequency noise [127].

Most studies have implemented ABH on planar structures; however, in many critical applications, such as aerospace and submarines, primary structures are curved. Deng et al. [120] applied ABH to a cylindrical shell (Fig. 6f), where the annular ABH structure achieved broadband noise reduction, reducing the sound power level by approximately 10–15 dB above the critical frequency. This expanded the applicability of ABH in complex structural designs.

Table 4
The literature comparison of typical Cavity type resonator acoustic metamaterials has been presented.

Approach	Stopband Range (Hz)	Average Transmission loss (dB)	Strengths	Limitations	Study/year
SHS	900–1500	About 16	Small size, light weight	Narrow bandgap, relatively weak transmission loss	Ding et al. [98] (2011)
Perfect subwavelength absorbers	100 % absorption rate in 484.5 Hz, about 10 Hz stopband		Effective transmission loss	Narrow bandgap	Romero-Garcia et al. [104] (2016)
A coiled ventilation metamaterial	660–1200	30	Light weight, effective transmission loss, supportive structure, ventilation,	Narrow bandgap	Xiao et al. [99] (2021)
Labyrinth structure	1400–2500	30	Effective transmission loss, Supportive structure, ventilation	Lack of low frequency transmission loss	Yang et al. [100] (2018)
Double-layer soundproof	400–5000	30–35	Supportive structure, wide bandgap, effective transmission loss, ventilation	Large size	Kim and Lee [101] (2014)
Meta-cage	2200–2600	10	Ventilation, all direction block	Narrow bandgap, relatively weak transmission loss, large size	Shen et al. [102] (2018)
Compact absorber	870–3224	13.7	Wide bandgap, supportive structure	Relatively weak transmission loss	Huang et al. [111] (2020)

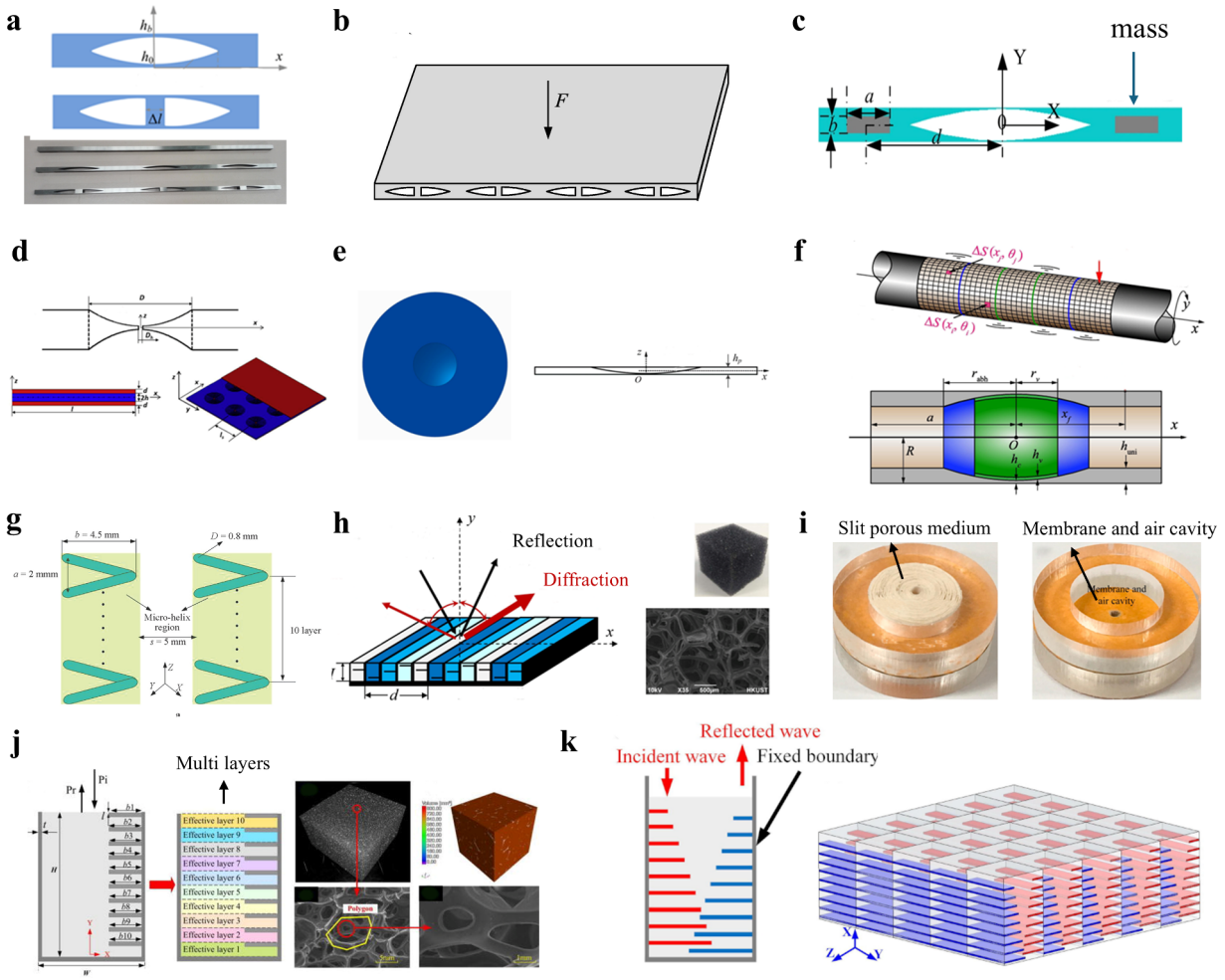


Fig. 6. Schematic diagram of ABH and meta porous structures: (a) A beam with two double-leaf ABH indentations. Reprinted with permission from [113], Copyright 2017, Acoustical Society of America. (b) Double-leaf ABH plates. Reprinted from [116], Copyright 2020, with permission from Elsevier. (c) A double-leaf ABH beam embedded with mass vibrators. Reprinted from [117], Copyright 2021, with permission from Elsevier. (d) Combined ABH with sandwich plates. Reprinted from [118], Copyright 2019, with permission from Elsevier. (e) a circular plate embedded with two-dimensional ABH structures. Reproduced from [119], under the terms of the Creative Commons CC BY license. (f) ABH cylindrical shell. Reprinted from [120], Copyright 2021, with permission from Elsevier. (g) Micro-helical AMM. Reproduced from [121], under the terms of the Creative Commons CC-BY-NC—ND license. (h) Periodic partition structures embedded in porous materials. Reprinted from [122], Copyright 2019, with permission from Elsevier. (i) A dual-resonant porous structure. Reprinted from [123], Copyright 2018, with permission from Elsevier. (j) Embedded ribs in porous materials. Reproduced from [124], under the terms of the Creative Commons CC BY license. (k) Optimized meta porous structure. Reprinted from [125], Copyright 2021, with permission from Elsevier.

These studies demonstrate that acoustic black holes and acoustic metamaterials exhibit significant potential in single direction or spot vibration control and sound absorption. Therefore, in ROD logic, this kind of wave energy trap for precise and efficient control of position is very suitable for accurate wave control in a single direction/region, such as the application of structural fatigue failure caused by stress concentration or sensor misjudgment caused by complex background noise. However, due to the highly anisotropic nature of the ABH design, it is

Table 5
The literature comparison of typical ABH AMMs has been presented.

Approach	Stopband Range (Hz)	Average Transmission loss (dB)	Strengths	Limitations	Study/year
Double-leaf ABH indentations beam	About 2500–5700 6200–8700 9000–11,500 11,700–16,600 17,000–20,000	About 40	Wide bandgap, Effective transmission loss	Lack low frequency transmission loss, one dimension model	Tang and Cheng [113] (2017)
Circular plate embedded with two-dimensional ABH structures	About 100–400 500–1000 2000–10,000	About 35	Wide bandgap, Effective transmission loss, Improved low-frequency transmission loss	Relatively large size and heavy	Du et al. [119] (2019)
ABH cylindrical shell	About 120–1000	10–15	Cylindrical application, low-frequency transmission loss	Relatively weak transmission loss	Deng et al. [120] (2021)

not suitable for multi-dimensional applications. Table 5 list the details of ABH AMMs parameters and analyze their characteristics.

2.5. Meta porous

In recent years, highly porous structures have also made substantial progress in optimizing sound absorption performance. The mechanism of that relies on the viscous damping and heat dissipation mechanism of the porous structure to absorb medium and high-frequency sound waves. Gao and Hou [121] utilized 3D printing to fabricate micro-helical metamaterials (Fig. 6g), where friction and viscosity effects within the helical structure significantly enhanced sound absorption. In the 200–1600 Hz range, the peak absorption coefficient exceeded 0.9. Fang et al. [122] investigated the sound absorption performance of periodic partition structures embedded in porous materials (Fig. 6h). The study found that controlling the phase of reflected waves effectively enhanced absorption, particularly under oblique incidence at specific frequencies.

Additionally, incorporating resonant structures into porous materials can broaden the low-to-mid frequency absorption bandwidth. For example, embedding periodically arranged slotted cylinders in a porous matrix leverages viscous dissipation and energy trapping effects to improve sound absorption. The viscosity and thermal losses within the pores, along with low-frequency resonances of the inclusions and energy trapping between the inclusions and the rigid backing, enhanced acoustic energy dissipation within the porous material [128]. Kim and Park [123] proposed a dual-resonant porous structure utilizing a slit porous medium, where the structure consisted of a helical slit absorber connected to a porous membrane supported by an air chamber (Fig. 6i). The structure exhibited a similar absorption coefficient of over 0.9 above 4000 Hz as traditional porous media but also doubled the absorption coefficient below 4000 Hz, reaching a first absorption peak of approximately 0.75 near 1000 Hz. Zhu et al. [129] further investigated the sound absorption performance of periodic acoustic metamaterial resonators embedded in porous materials. The composite structure exhibited an absorption rate exceeding 80 % in the 180–550 Hz range and an average absorption coefficient of approximately 0.75 in the 800–10,000 Hz range. Additionally, Feng [130] placed a rigid thin plate on a porous material, shifting the absorption peak from 1200 Hz to 850 Hz, significantly improving low-frequency absorption while slightly reducing high-frequency absorption. Yang et al. [131] was the first to study the effect of rigid side panels on the sound absorption of porous materials. Compared to homogeneous plates, ultra-porous layered panels exhibited more resonance peaks and a lower effective absorption cutoff frequency, increasing the average absorption coefficient by approximately 0.15 within the 0–10,000 Hz range.

To broaden the absorption bandwidth, Gao et al. [124] proposed a strategy for embedding ribs into porous materials (Fig. 6j), achieving an average absorption coefficient of 0.937 in the 0–10 kHz range for the composite metamaterial. Later, Gao et al. [125] further optimized side panels (Fig. 6k), achieving significantly higher average absorption coefficients in the 0–6.4 kHz range, reaching a peak of 0.8126. From this, it can be found that the widening of the bandgap is accompanied by a decrease in the peak absorption rate, which once again reflects the importance of on-demand design.

In general, although meta-porous AMMs can achieve great acoustic absorption, porous AMM has high requirements for design optimization and is prone to degradation in wet or polluted environments, thus, its application is limited. Future research should focus on their applications in complex structures and extreme environments while further optimizing structural designs to enhance tolerance to complex environments. The comparison of typical meta porous study is shown in Table 6.

2.6. Active control

The noisy environment in real life is often complex and dynamic. Once fabricated, passive acoustic metamaterials have fixed properties that are difficult to adjust, making them severely limited in handling complex and evolving acoustic environments. In contrast, active acoustic metamaterials can dynamically regulate and control acoustic parameters through external stimuli such as piezoelectric effects, mechanical pressure, fluid infusion, or temperature adjustment. In the field of noise control, active acoustic metamaterials hold significant potential for development.

The concept of active acoustic metamaterials was first proposed by Akl and Baz [132] in 2009, who designed a multi-layer liquid cavity structure separated by piezoelectric membranes. By applying voltage to regulate the vibration state of the piezoelectric membrane, he achieved active control of the effective mass density without altering the physical structure, effectively tuning sound wave transmission. This study laid the foundation for active acoustic metamaterials and guided subsequent explorations of different active control mechanisms. Xiao et al. [133] further advanced this direction by proposing a vibration regulation method based on electromagnetic control (Fig. 7a). By fixing magnets on a membrane and using electromagnets to regulate its motion, they achieved tunability of the characteristic frequency and transmission phase of the metamaterial at 70 Hz. Chen et al. [134] designed a magnetic-mechanical tunable AMM that employed elastic membranes and magnetic core masses (Fig. 7b). By altering the magnetic force distribution without changing the physical structure, they achieved wave phenomena such as sound redirection, focusing, and bending. In the same year, Chen et al. [135] developed an adaptive phononic crystal that combined the extreme bending stiffness tunability (softening, hardening, and negative stiffness) provided by shunted piezoelectric patches with the negative mass density mechanism of passive metamaterials (Fig. 7c). By integrating these two wave control mechanisms into one system, they achieved real-time tunable wave manipulation and control. Meanwhile, Yu et al. [136] proposed a metamaterial composed of composite resonators on the sidewalls of rigid tubes (Fig. 7d). By using pre-stretched dielectric elastomer membranes to regulate the acoustic characteristics of the resonators, they achieved tunability of up to 14 % in the attenuation band frequency.

The application of nanocomposite materials in active acoustic metamaterials has also attracted increasing attention. In 2019, Li et al. [142] developed a membrane-type acoustic metamaterial using polyvinyl alcohol/graphene nanocomposite membranes, achieving active tuning of the first anti-resonance frequency within the 369.2–420 Hz range,

Table 6
The literature comparison of typical Meta porous AMMs has been presented.

Approach	Stopband Range (Hz)	Average Transmission loss (dB)	Strengths	Limitations	Study/year
Micro-helical AMM	About 10 dB peak transmission loss rate and about 50 Hz span stopband in 200–1600 Hz,		Light weight	Narrow bandgap	Gao and Hou [121] (2018)
Dual-resonant porous structure	700–6000	About 7	Wide bandgap	Relatively weak transmission loss	Kim and Park [123] (2018)
Periodic AMM embedded porous layer	180–10,000	About 7	Ultra-wide bandgap	Relatively weak transmission loss	Zhu et al. [129] (2019)
Meta porous structure	500–6400	About 12.2	Wide bandgap, relatively high transmission loss	Large size	Gao et al. [124] (2021)

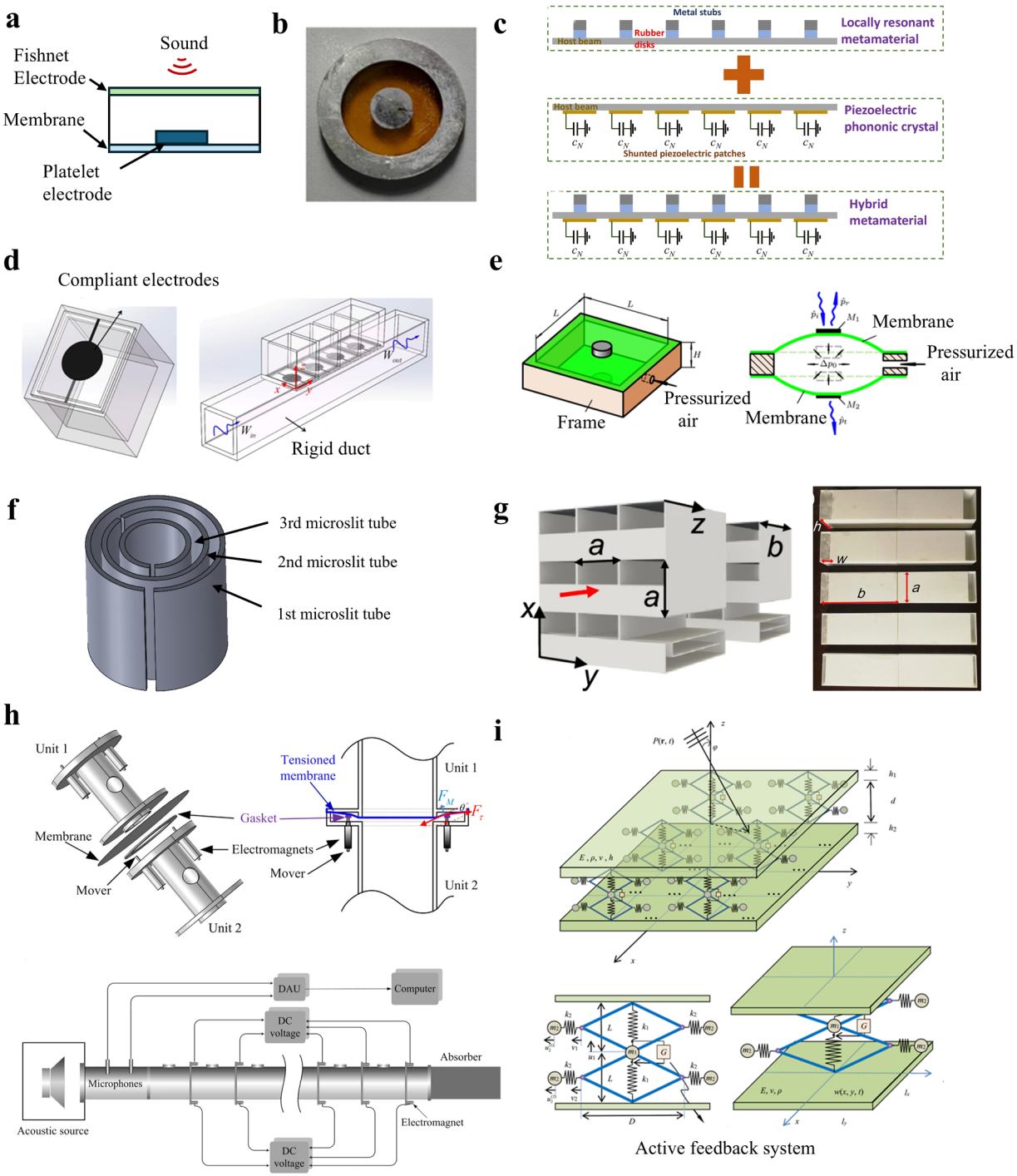


Fig. 7. Schematic diagram of active AMM structures: (a) Electric field control AMM. Figure redrawn based on [133]. (b) A magnetic-mechanical tunable AMM. Reproduced from [134], under the terms of the Creative Commons CC BY license. (c) Shunted piezoelectric patches AMM. Reprinted from [135], Copyright 2017, with permission from Elsevier. (d) A metamaterial composed of composite resonators. Reprinted from [136], Copyright 2017, with permission from Elsevier. (e) Air pressure control AMM. Reprinted from [137], Copyright 2016, with permission from Elsevier. (f) Multi-layer annular micro-slit tubes AMM. Figure redrawn based on [138]. (g) A dual-layer labyrinthine AMM. Reproduced from [139], under the terms of the Creative Commons CC BY license. (h) A tunable acoustic metamaterial composed of periodic membranes with side holes. Reproduced from [140], under the terms of the Creative Commons CC BY license. (i) Active feedback control system. Reprinted from [141], Copyright 2021, with permission from Elsevier.

demonstrating excellent noise suppression performance. Additionally, the noise reduction frequency could be actively modulated by direct current voltage. In the same year, Zhou et al. [143] developed a tunable beam-type metamaterial composed of an elastic substrate beam and periodic active beam resonators. Each resonator employed a piezoelectric parallel array, allowing for active control of the system's frequency bands. Due to the element damping effect induced by the shunt resistance, they achieved an ultra-wide low-frequency bandgap in the 30–470 Hz range. Akl and Baz [144] further demonstrated the ability to actively control sound propagation by embedding piezoelectric elements into materials to regulate effective density.

Beyond piezoelectric control methods, other mechanisms have been explored to achieve tunability in acoustic metamaterials. Chen et al. [140] reported a tunable acoustic metamaterial composed of periodic

membranes with side holes (Fig. 7h). The tension and stiffness of the periodically arranged membranes were actively controlled by electromagnets, generating additional stress. Results showed that a small direct current voltage of 6 V could shift the double-negative passband by 40 % in bandwidth. In 2016, Xia et al. [145] studied the effect of water temperature on the LR bandgap and equivalent acoustic parameters of acoustic metamaterials with Helmholtz resonators. When the water temperature varied between 0 °C and 75 °C, the LR bandgap and negative effective bulk modulus were tunable by approximately 11 %. That same year, Langfeldt et al. [137] developed a membrane-based acoustic metamaterial that used external air pressure regulation (Fig. 7e). The metamaterial consisted of two stacked membranes with attached masses, where external air pressure was used to control membrane stiffness, thereby influencing transmission modes and transmission loss. He et al. [141] employed an active feedback control system in wave metamaterials, where vertical local resonators were coupled to the top and bottom plates via two four-bar linkages (Fig. 7i), enabling changes in effective mass density and sound transmission under incident acoustic pressure.

Active control has also achieved notable progress in sound absorption applications. Xu et al. [138] developed a low-frequency absorber using multi-layer annular micro-slit tubes with deep subwavelength thickness (Fig. 7f). By adjusting the angle of the micro-slit tubes, they altered the absorber's absorption bandwidth, achieving high-efficiency absorption (absorption coefficient greater than 0.9) in the 280–572 Hz range. Du et al. [139] proposed a dual-layer labyrinthine AMM that allowed for tunability of the relative absorption bandwidth from 12 % to 80 % by adjusting the structure's open area ratio (Fig. 7*g*). For normally incident sound waves, near-perfect absorption (98.6 %) was achieved at the resonance frequency. Gardiner et al. [146] utilized stereolithography to design a functional ultramagnetic membrane, enabling the fabrication of tunable magnetic acoustic metamaterials at ultra-subwavelength scales ($\leq\lambda/77.5$), with tunable resonance frequencies ranging from 88.73 Hz to 86.63 Hz.

Active architecture is suitable for reliability assurance systems that require dynamic frequency adjustment or environment adaptation. Currently, research on active acoustic metamaterials remains in its early stages, spanning multiple disciplines including acoustics, mechanics, materials science, and control science. Among various approaches, piezoelectric control has dominated due to its relatively high maturity. However, the high cost of piezoelectric materials and their accelerated aging in extreme environments present challenges for practical applications. Future research should explore more stable and efficient active tuning methods, such as smart materials, temperature control, and air pressure regulation, to enhance the adaptability of active acoustic metamaterials and drive their commercialization. Table 7 compares typical control approaches and list parameters in detail. Table 8 analyzes each type of AMMs and list suitable application cases, aiming to features of different types and provide available ROD toolbox for engineering design.

3. Multifunction acoustic metamaterials (MFAMs)

In real-world applications, electronic device failures are often induced by multiple interacting stressors such as vibration, thermal cycling, impact, EMI etc. These stressors do not act in isolation but couple to exacerbate damage. From the ROD perspective, addressing such complex failure scenarios requires acoustic metamaterials capable of simultaneously regulating multiple physical fields. This chapter introduces recent developments in multifunctional acoustic metamaterials that integrate structural, thermal, acoustic, and electromagnetic functions. These MFAMs are designed to mitigate compound failure modes through synergistic control, providing robust solutions for electronic reliability enhancement.

3.1. Acousto-mechanical metamaterials

Given the widespread issues of vibration and noise in various environments, metamaterials that simultaneously achieve noise reduction and impact suppression have emerged as a crucial solution. In recent years, researchers have proposed various MFAM designs capable of absorbing low-frequency noise while mitigating impact. Li et al. [147] reported a novel paradigm for acoustic-mechanical multifunctional metamaterials using a decoupling approach. By embedding customized pillars controlling mechanical responses within HR (Fig. 8a), they achieved outstanding broadband low-frequency (<1.0 kHz) sound absorption with high deformation recoverability (up to 98 %) and impact resistance. This innovative approach broadens the design scope of MFAMs, offering new strategies for low-frequency vibration and impact control.

This design approach follows a decoupled design concept. In subsequent studies, Li et al. [154] further defined this configuration—where the acoustic and mechanical units are designed independently—as a weakly coupled design, and additionally proposed a biomimetic strategy that integrates heterogeneous multilayered resonators with cambered cell walls. Compared with previous design proposed by Li et al. [147], this study achieved substantial multifunctional enhancements. By introducing limited structural interaction between heterogeneous resonators and cambered load-bearing walls, the new design expanded the absorption bandwidth from < 1 kHz to 1–6 kHz while reducing thickness by around 40 %. More strikingly, the specific energy absorption increased to 50.7 J g^{-1} and the yield strength reached 211 MPa. Such weak coupling enables synergistic energy dissipation and efficient stress redistribution without sacrificing tunability, marking a transition from mechanically soft absorbers to compact load-bearing multifunctional metamaterials. Although the weakly coupled design offers advantages such as structural simplicity and independent tunability, practical engineering applications demand higher levels of miniaturization. To address this, Li et al. [155] subsequently developed an all-in-one fully coupled acoustic–mechanical metamaterial structure. In this configuration, the acoustic and mechanical subsystems share identical geometries, forming multi-level neck–cavity resonators embedded within a

Table 7
The literature comparison of typical Active AMMs has been presented.

Approach	Frequency Range	Peak Transmission loss (dB)	Strengths	Limitations	Study/year
Electric field control	About 10 Hz span in 100–170 Hz	21.3	Real time control, low-frequency tuning	Narrow bandgap	Xiao et al. [133] (2015)
Water temperature control	About 200 Hz span in 3000–3300 Hz	10	Underwater application	Limited tunable range	Xia et al. [145] (2016)
ir pressure control	About 5 Hz span in 180-230 Hz	70	Effective transmission loss	Limited tunable range, narrow bandgap	Langfeldt et al. [137] (2016)
Multi-layer annular micro-slit tubes AMM	About 20 Hz span in 280–572 Hz	>40	Effective transmission loss, light weight	Limited tunable range	Xu et al. [138] (2021)
Functional ultramagnetic membrane	86.63–88.74	About 40	Low-frequency tuning, effective transmission loss	Narrow bandgap	Gardiner et al. [146] (2024)

Table 8
The comparison of different types of AMMs.

AMM Type	Typical Frequency Range (Hz)	Typical Transmission loss (dB)	Strengths	Limitations	Typical Use Case
MAM	100–2000	20	Lightweight, compact, tunable	Sensitive to prestress, fragile, narrow bandgap	MEMS, PCB vibration
Mechanical local resonator	100–5000	>50	Effective transmission loss	Manufacturing difficult for wide bandgap design	Vehicle panels
Phononic Crystals	1000–10,000, MHz, GHz	>50	Wide bandgap, large bandgap coverage rate, Effective transmission loss, supportive structure integration available,	Bulky and heavy at low frequency	Device housing, chassis, ultra-high frequency damping
Cavity types	500–5000 Hz	30	Ventilation-friendly, supportive structure integration available	Bulky, geometry-sensitive, relatively weaker transmission loss	Data center fans, device housing
Acoustic Black Holes	1000–20,000	30	Strong energy localization, wide bandgap	Poor low frequency transmission loss,	Structural fatigue zones
Porous AMMs	500–10,000	10	Broadband transmission loss	Degrades in wet/polluted environment, relatively weaker transmission loss	Sensors, soft packaging
Active AMMs	50–4000 Hz (tunable)	>40	Programmable response	Costly, power needed, narrow bandgap	Adaptive filters, smart casings

load-bearing microlattice. The interlaced phases establish strong modal coupling, enabling an over-damped broadband absorption (about 2.7 kHz) together with high stiffness and elastic isotropy. Compared with the weakly coupled counterparts, the fully coupled design maximizes functional synergy, minimizes structural volume, and provides a data-driven optimization framework integrating machine learning and multi-objective evolution. This paradigm represents the most compact and comprehensive solution for next-generation multifunctional acoustic metamaterials.

Other studies have explored different structures. Wang et al. [148] introduced a hierarchical multifunctional chiral metamaterial (HMCM) with damage resistance and broadband low-frequency sound absorption capabilities (Fig. 8b). Utilizing Helmholtz resonators with hierarchically extended internal tubes as the primary unit, this metamaterial exhibited near-perfect broadband absorption between 425 Hz and 553 Hz, with an average absorption coefficient exceeding 0.9. Additionally, it demonstrated excellent impact resistance, making it highly suitable for applications such as sound barriers in the transportation and construction industries, effectively reducing low-frequency noise while enhancing crash resistance. Further advancing compact multifunctional designs, Ren et al. [149] developed a novel multifunctional metastructure for broadband low-frequency absorption and superior impact energy dissipation (Fig. 8c). Cavity resonators with internally extended tubes (CRIET), arranged in a hexagonal honeycomb configuration, were selected as unit components. This structure achieved broadband absorption (SAC $>$ 0.9) in the 600–1000 Hz range. Compression tests revealed that the CRIET metastructure exhibited exceptional load-bearing and impact energy dissipation properties comparable to complete honeycomb structures, providing insights into compact and multifunctional broadband absorption structures. Additionally, Hosseinkhani et al. [150] proposed embedding local resonators into auxetic honeycomb metamaterials to enhance the vibroacoustic performance of anti-chiral auxetic sandwich panels, significantly improving sound attenuation (Fig. 8d). Fan et al. [152] introduced an acoustic absorption-bearing metamaterial (AABM) that simultaneously provides low-frequency sound absorption and excellent load-bearing capacity (Fig. 8f). These studies clearly demonstrate that AMMs possess excellent compatibility with mechanical functions. By incorporating load-bearing capabilities into AMMs, they can directly replace conventional structural components, thereby enhancing the overall integration of the device. This combination significantly expands the design toolbox of the ROD framework, greatly enhancing its capability to address structural vibrations in supporting components using AMMs.

3.2. Acousto-thermal metamaterials

Thermal dimensional stability is a crucial parameter for many space structures. One of the key technical requirements for large-scale precision structures in astrophysical and optical imaging satellites is the development of materials that provide stable mechanical performance while maintaining a lightweight structure [156]. The design of MFAMs offers insights into maintaining stability in electronic devices exposed to coupled vibration and thermal loads, especially for automotive, aerospace, and other electronic systems operating in harsh environments [157]. Zhang et al. [153] proposed a three-dimensional metamaterial with tunable thermal expansion and phononic bandgaps (Fig. 8*g*). The coefficient of thermal expansion (CTE) could be adjusted from $-1 \times 10^{-5}/\,^{\circ}C$ to $2.5 \times 10^{-5}/\,^{\circ}C$, while the bandgap coverage ratio could be tuned from 0 to 0.5. This study demonstrated the enormous potential of optimized metamaterials for controlling thermal deformation and phonon transport. In this study, the combination of topological optimization and proxy model is systematically proposed for the first time to design three-dimensional multi-functional metamaterials with dual functions (thermal expansion and band gap regulation). In the field of MFAMs aimed at controlling thermal resistance, Lmekalli et al. [158] conducted relevant studies. They developed a clay metaBrick integrating Helmholtz resonators into conventional hollow bricks, achieving a 20 dB enhancement in sound transmission loss across a broad frequency range from 500 to 2500, and an 8 % improvement in thermal resistance. Such passive designs reveal how resonant cavities can serve as both acoustic energy traps and heat-flow barriers, offering lightweight and low-cost solutions for thermal–acoustic protection in large structures and enclosures. Beyond building applications, the acoustic-thermal coupling strategy provides valuable design inspiration for next-generation electronic housings, EV battery pack and high voltage electronic control system where minimizing thermal deformation and acoustic vibration concurrently is essential to ensure reliability under harsh coupled environments.

3.3. Acousto-electromagnetic metamaterials

For EMI shielding function, Li et al. [142] investigated MFAMs by incorporating polyvinyl alcohol/graphene (PVA/GR) nanocomposite films into acoustic metamaterials (Fig. 8h). The high electrical conductivity of graphene enabled multiple reflections and scattering of electromagnetic waves within the graphene layer, enhancing energy dissipation and achieving EMI shielding effectiveness exceeding 22 dB in the 8–12 GHz range. This study provides valuable insights into the development of acoustoelectric multifunctional materials, especially

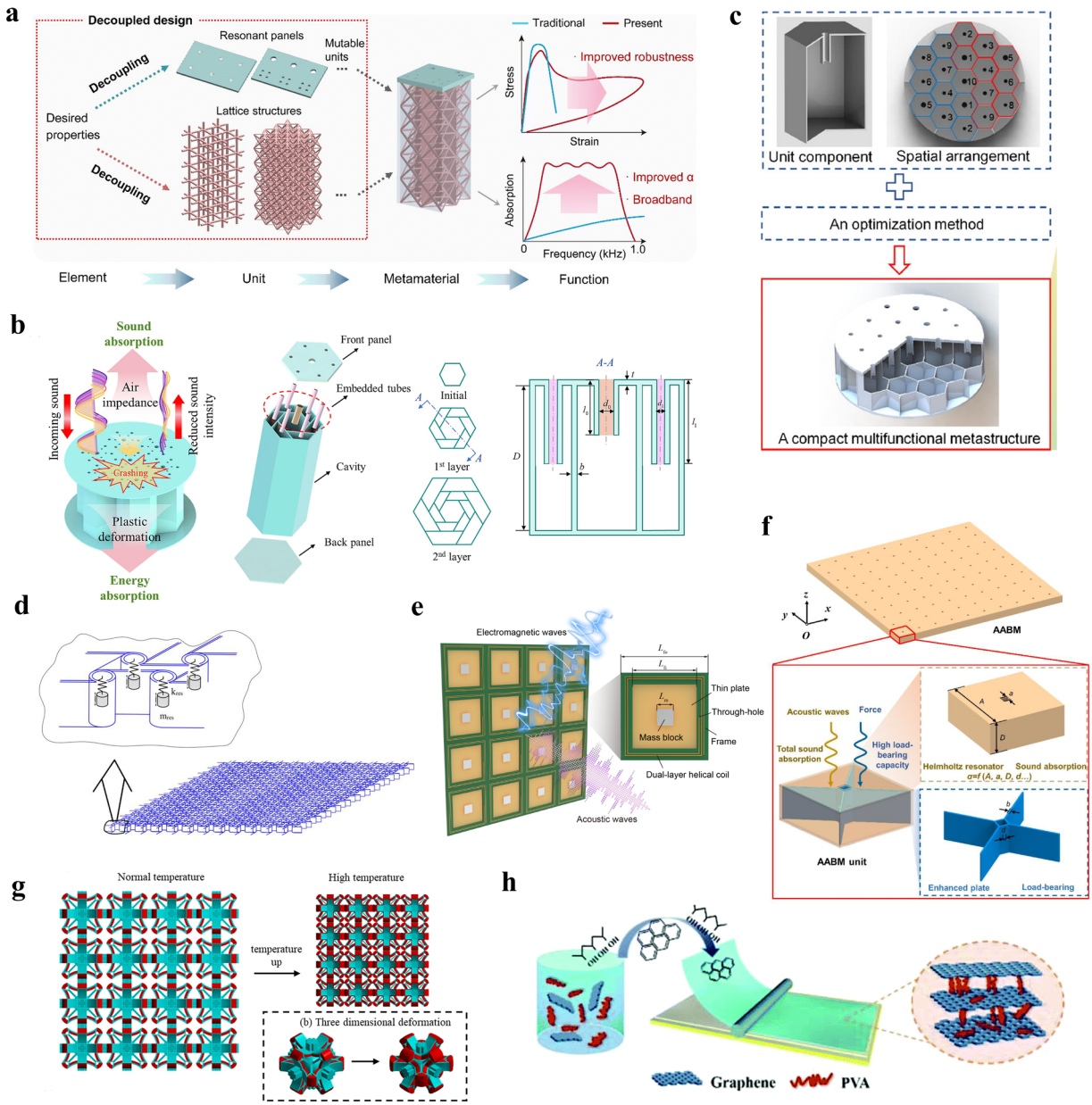


Fig. 8. Schematic diagram of MFAMs structures: (a) Pillars embedded acoustic-mechanical MFAMs. Reproduced with permission from [147]. © Royal Society of Chemistry. (b) HMCM. Reproduced from [148], under the terms of the Creative Commons CC-BY-NC—ND license. (c) Compact MFAMs. Reproduced from [149], under the terms of the Creative Commons CC-BY-NC—ND license. (d) LR embedded anti-chiral auxetic sandwich panels. Reprinted from [150], Copyright 2021, with permission from Elsevier. (e) Dual-resonant hybrid metamaterial. Reprinted from [151], Copyright 2025, with permission from Elsevier. (f) AABM. Reprinted from [152], Copyright 2023, with permission from Elsevier. (g) Thermal expansion MFAMs. Reproduced from [153], under the terms of the Creative Commons CC-BY-NC—ND license. (h) EMI shielding and MFAMs. Reproduced with permission from [142] © Royal Society of Chemistry.

highlighting that such integration can be achieved without altering the original structure—simply by adding a shielding layer. For decoupling design, Li et al. [159] adopted a decoupled multifunctional design strategy by integrating broadband electromagnetic absorption, based on dielectric loss, into an acoustically resonant honeycomb structure. By introducing a carbon fiber/carbon nanotube-reinforced composite into the cell walls, polarization and conductive loss–dominated electromagnetic energy dissipation was achieved. The gradient-thickness configuration ensured impedance matching and low reflection, with reflection coefficients below −10 dB across the 2–40 GHz range. This non-resonant, material-based EMI shielding mechanism enabled efficient electromagnetic attenuation without compromising the acoustic resonance characteristics, further demonstrating the feasibility of decoupled acoustoelectric multifunctional metamaterials. In contrast, Song et al. [160] realized simultaneous microwave absorption and sound reduction through a coupled-membrane metamaterial coated with indium-tin-oxide (ITO) films. The ultrathin ITO layers generated surface electric resonances that dissipated electromagnetic energy (> 80 % absorption between 9 and 14 GHz) while preserving the low-frequency acoustic insulation (> 10 dB transmission loss in 400–900 Hz). Owing to the sub-micron thickness and high optical transparency of the ITO coating, this design achieved independent control of sound and electromagnetic waves without affecting optical transmittance, providing a lightweight, transparent, and low-cost solution for electromagnetic and acoustic pollution mitigation. Such membrane-type MFAMs bridge the gap between acoustic and electromagnetic domains and offer new possibilities for transparent electronic enclosures, smart windows, and packaging of sensitive electronic

modules.

In addition to EMI shielding, there have also been studies on acoustoelectric metamaterials related to electromagnetic wave amplification. Xu et al. [151] introduced a fully-structured hybrid metamaterial enabling decoupled control of electromagnetic and acoustic waves through dual-resonant mechanisms—electromagnetic resonance in a dual-layer helical coil and acoustic resonance between a thin plate and mass block (Fig. 8e). The structural parameters for each field can be tuned independently, achieving a 6 % improvement in wireless-power-transfer efficiency and 7.5 dB noise suppression in 200–400 Hz simultaneously. This work pioneers the structural decoupling of cross-physics wave manipulation and establishes a promising route for co-located acoustic-electromagnetic systems. It is particularly inspiring for applications that require the integration of wireless transmission and vibration mitigation, such as electric vehicle chassis, power-supplying systems for industrial robots, and wireless sensing devices.

3.4. Other MFAMs

Beyond the aforementioned multifunctional couplings in this chapter, other coupling modes have also been explored. For instance, acousto-optic coupling leverages both acoustic functionalities and the acousto-optic effect, enabling the use of acousto-optic metamaterials to manipulate light propagation and thereby enhance optical signal controllability [161–163]. Moreover, Some MFAMs also integrate functions such as energy harvesting and impact resistance [164–166]. However, as these are less directly related to electronic reliability, they are not further discussed here.

At present, research on MFAMs primarily focuses on mechanical function integration, while studies addressing thermal and electrical properties remain relatively limited. Existing works have demonstrated significant progress from weakly coupled and fully coupled designs, achieving improved structural compactness, tunability, and multifunctional synergy. Emerging acousto-thermal and acousto-electromagnetic metamaterials further broaden the functional landscape, enabling combined regulation of sound, heat, and electromagnetic waves within lightweight architectures. These developments highlight the growing potential of MFAMs as key materials for ROD, especially in complex environments where vibration, heat, and EMI coexist. As future research increasingly leverages data-driven optimization and intelligent manufacturing, AMMs are expected to evolve into highly integrated, adaptive multifunctional materials, providing robust and efficient solutions for next-generation electronic reliability. The MFAMs comparation is shown in Table 9.

4. Linking acoustic performance metrics to electrical devices reliability

The reliability enhancement contributed by acoustic performance metrics can be categorized into two types. The first involves extending the operational lifetime of electronic devices under unchanged environmental conditions, while the second refers to maintaining the same service life but ensuring stable operation under more severe or harsh environments. The most direct and effective way to validate reliability is through full-scale testing under realistic operating environments. However, such reliability tests require long verification periods and are highly case-specific, resulting in limited publicly available data and necessitating customized experimental setups for each application scenario. In this section, a simplified yet broadly applicable approach for estimating electronic reliability is introduced. By employing the S–N (stress–number of cycles) curve to predict fatigue life, this method establishes a link between acoustic performance metrics and electronic reliability, providing a practical tool for early-stage reliability-oriented design assessments.

The S–N curve is generally divided into three regimes: low-cycle fatigue, mid-cycle fatigue, and high-cycle fatigue. Low-cycle fatigue typically occurs under conditions involving repeated plastic deformation, such as solder joint degradation during thermal cycling, and can be predicted using the Coffin–Manson equation [167]. Mid-cycle fatigue applies to cases where both plastic and elastic deformations play non-negligible roles [168]. High-cycle fatigue, by contrast, is relevant when external loading consists primarily of small-amplitude vibrations and material deformation remains predominantly elastic [169]. Because fatigue models incorporating plastic strain require detailed material-dependent parameters, which limits their general applicability, this study adopts a predictive approach based solely on the high-cycle fatigue regime, where elastic deformation is dominant.

Under high-cycle-fatigue operating conditions, the fatigue life can be predicted using the Basquin equation as [168].

$$\sigma = \sigma_f' \left(2N_f\right)^b \tag{1}$$

where σ is the stress amplitude, σ_f' is the fatigue strength coefficient, b is

Table 9
The literature comparison of typical MFAMs.

Function	MFAM approach	Characters	Potential Use Case	Study/year
Acoustic absorption, impact resistance, load-bearing	Pillars embedded acoustic-mechanical MFAMs, a bioinspired architecture, interwoven design strategy	Light weight, human body friendly, compact	Vehicle chair, device housing or supporter	Li et al. [147] (2023), Li et al. [154] (2024), Li et al. [155] (2024)
	HMCM, CRIET, AABM	Load-bearing, low-frequency absorption	Device housing or supporter	Wang et al. [148] (2024), Ren et al. [149] (2024), Fan et al. [152] (2023)
	LR embedded anti-chiral auxetic sandwich panels	Light weight, supportive structure	Vehicle panel, device housing	Hosseinkhani et al. [150] (2021)
Tunable thermal expansion, phononic bandgaps, Thermal resistance	Three-dimensional metamaterial microstructure with negative thermal expansion, metaBrick	Tunable thermal expansion coefficient, Higher thermal resistance	MEMS package, Device housing	Zhang et al. [153] (2021), Lmekalli et al. [158] (2025)
EMI shielding, acoustic absorption, Wireless transmission enhancement	Incorporate PVA/GR nanocomposite films into AMM, Embedding Loss-driven composite into AMM, embedding dual-layer helical coils	Effective EMI shielding, Improved wireless power transfer	MEMS package, device housing, wire coating, wireless charging, body sensors	Li et al. [142] (2019), Li et al. [159] (2025), Song et al. [160] (2018), Xu et al. [151] (2025)

the fatigue strength exponent and $2N_f$ is the reversals to failure.

When transmissibility is known, the corresponding increase in fatigue life N_f can be estimated by deriving the stress ratio from the displacement transmissibility equation in combination with Hooke's law:

$$T = 20log_{10}\frac{u_{test}}{u_{ref}} \tag{2}$$

where T is Transmissibility, u_{test} is the displacement of test point, u_{ref} is the displacement of reference point.

$$\sigma = E\varepsilon \tag{3}$$

where E is Young's Modulus, ε is the axial strain, defined by

$$\varepsilon = \frac{\partial u}{\partial x} \tag{4}$$

where u represents the displacement of a material point from its equilibrium position, and x denotes the spatial coordinate along the deformation direction.

Therefore, the life change rate R_L is:

$$R_L = \frac{N_{new}}{N_{old}} = \left(\frac{\sigma_{new}}{\sigma_{old}}\right)^{\frac{-1}{b}} = 10^{\frac{-T}{20*b}} \tag{5}$$

where N_{new} is the new device reversals to failure, N_{old} is the old device reversals to failure, σ_{new} is the new device stress amplitude, σ_{old} is the old device stress amplitude.

Meanwhile, based on Eq. (2), the vibration amplitude ratio r can also be derived as:

$$r = \frac{u_{test}}{u_{ref}} = 10^{\frac{-T}{20}} \tag{6}$$

Eq. (5) provides an intuitive representation of the lifetime extension achieved through AMM-induced vibration attenuation, while Eq. (6) further refines the estimation of precision enhancement ratios across different applications by introducing the vibration amplitude ratio. Together, these equations establish a simplified framework linking acoustic performance indices to electronic reliability in ROD.

It should be emphasized that, to simplify the prediction and highlight the influence of acoustic performance on device lifetime, this approach is applicable only to failure modes dominated by elastic deformation. Within the high-cycle fatigue regime, only the stress contribution from acoustic vibration is considered, without accounting for other environmental stressors present in real engineering scenarios. As a result, the predicted lifetime values may be overestimated and should be regarded as preliminary design references. For more accurate lifetime predictions, the fatigue exponent b should be corrected based on the influence of additional stressors.

In addition to cycle life, other parameters—such as the quality factor, Duffing coefficient, and detection resolution—can also serve as indicators of reliability [170–172]. However, these parameters tend to be application-specific and lack broad generality. The following section presents how AMMs can be effectively applied to enhance the reliability of electronic systems.

5. Electrical devices reliability applications

In the context of ROD, the effective application of AMMs requires clear linkage between the stress environment, failure mechanisms, and material response functions. This section introduces several representative application scenarios of AMMs in electronic systems. Moreover, systematic analysis from the ROD framework's view is made in each case including how AMMs are selected or customized based on the dominant environmental stressors and the failure modes they induce and evaluate how the metamaterial mechanisms contribute to mitigating those failures and improve reliability.

5.1. Micro-electromechanical systems (MEMS) noise insulation

Microelectromechanical systems (MEMS) are miniature devices that integrate both electronic and mechanical components. Typically ranging in size from 1 to 100 μm , MEMS consist of a central processing unit—often an integrated circuit (IC) chip such as a microprocessor—along with several components that interact with the surrounding environment, such as microsensors. A wide range of MEMS devices—including gyroscopes, accelerometers, micromirrors, micropumps, mass sensors, and timing devices such as micro clocks—operate based on resonant elements that are excited at their intrinsic natural frequencies [173]. Among these, MEMS gyroscopes are sensors that detect angular velocity by utilizing vibrating proof masses rather than rotating ones. Due to their high mechanical quality factor, MEMS gyroscopes are particularly susceptible to environmental disturbances, especially high-frequency and high-power acoustic noise, which can result in signal distortion or even unreliable output [174]. The reliability of such devices is typically characterized by the Angle Random Walk (ARW), which quantifies the random fluctuation in the measured angular velocity [175]. Previous studies have demonstrated that high acoustic pressure can induce additional vibration of the proof mass in MEMS gyroscopes, thereby coupling acoustic noise into the output signal and significantly degrading the noise performance [176]. Since the ARW fundamentally corresponds to the square root of the white-noise power in the rate output, its total value in this gyroscope can be decomposed into two components: the intrinsic noise and the acoustic-pressure-induced noise [177]. In practice, the relative contribution of the acoustic-induced component varies across different gyroscopes depending on their operating environments. To simplify the model and to highlight the performance gain provided by vibration-attenuating materials, the intrinsic noise is idealized to be negligible in the present case. Under this assumption, the ARW can be approximated as being proportional to the applied acoustic pressure. Several methods have been reported to mitigate vibrations in MEMS devices, such as employing tuning fork gyroscopes, adjusting the device's resonant frequency to avoid overlapping with dominant vibration bands, and integrating low-pass filters to suppress acoustically induced interference [178]. However, these strategies often come at the cost of reduced sensitivity or the introduction of additional forms of signal distortion. Other studies have explored the use of micromechanical isolators based on squeeze-film or shear-mode damping mechanisms to reduce vibrational effects but implementing these solutions at the wafer-level packaging stage remains technically challenging.

From ROD view, high-frequency vibration is the main stressor in this case, which directly damages the quality of gyroscope system. Therefore, after clarifying the failure mode, it is necessary to apply suitable AMMs solution. Yunker et al. [179] were the first to apply AMMs for vibration isolation in MEMS gyroscopes. They proposed a Helmholtz array-based design that combined excellent isolation performance with relatively simple fabrication (Fig. 9a), forming a compact cubic structure with a side length of only 25.4 mm. Using Deep Reactive Ion Etching (DRIE), they patterned a two-dimensional array of microscale Helmholtz resonant cavities into a silicon substrate, which was then sealed with glass to form an enclosed structure. Multiple 1-inch square resonator arrays were assembled into a box with the opening oriented toward the MEMS gyroscope. The design was tested in an anechoic chamber, demonstrating up to 18 dB attenuation within a 700 Hz bandwidth centered at 14.5 kHz. Correspondingly, the derived vibration amplitude ratio (r) is approximately 0.126, indicating a sound pressure reduction of about 87 %. Therefore, within this frequency range, the ARW can theoretically be reduced to 12.6 % of its original value. This pioneering work showcased the potential of AMMs for miniature-scale noise isolation and offered valuable insights for AMM miniaturization. Using cavity type AMMs to design the vibration damping housing for

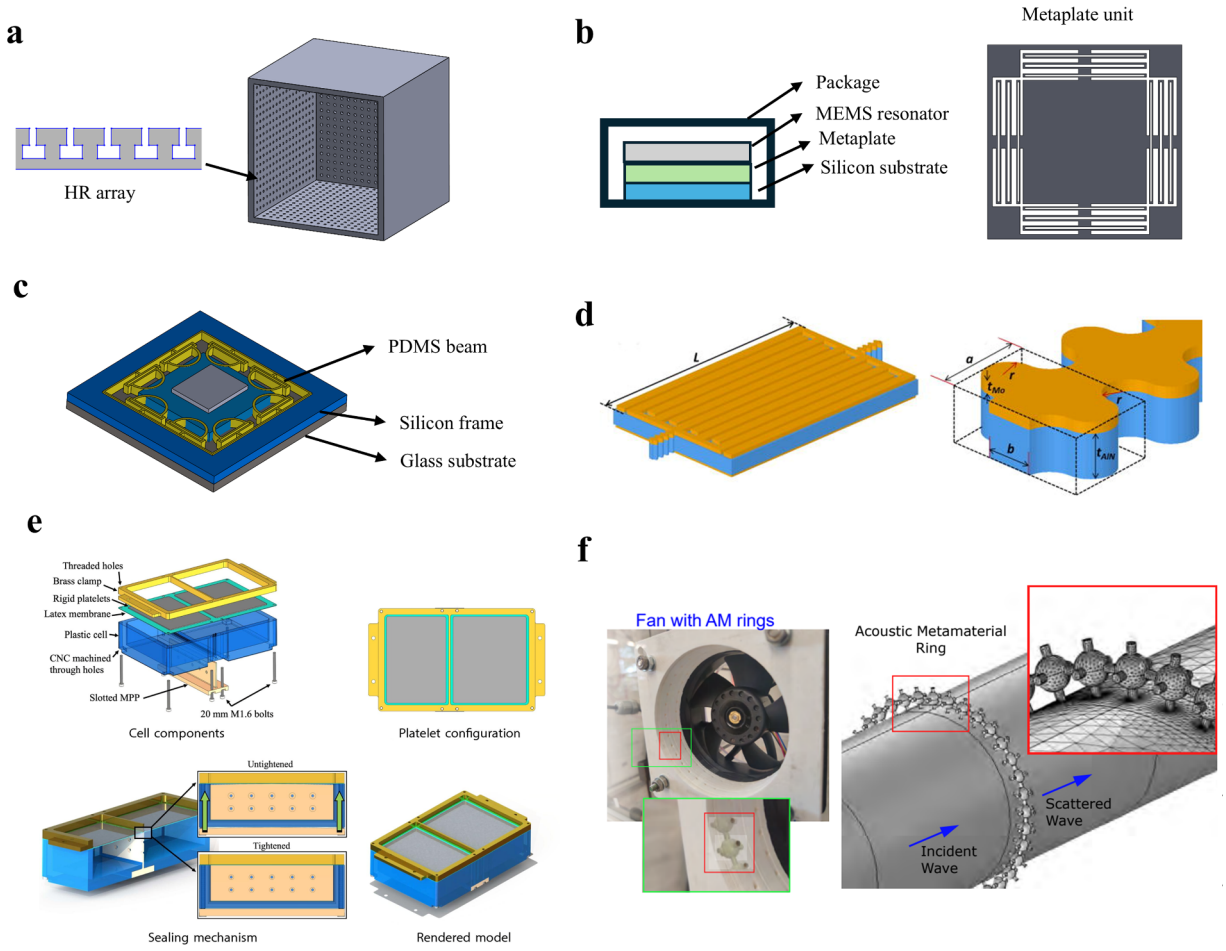


Fig. 9. Schematic diagram of AMM applications (Part I): (a) MEMS gyroscopes vibration isolation box. Figure redrawn based on [179]. (b) Metasurface vibration isolation structure in MEMS package. Figure redrawn based on [173]. (c) MEMS thermal-vibration isolator. Figure redrawn based on [174] (d) AlN-based PnCs resonator structure. Reprinted from [170], with the permission of AIP Publishing. (e) SeMSA. Reproduced from [180], under the terms of the Creative Commons CC BY license. (f) HR ring structure for fans. Reproduced from [181], with the permission of INCE-USA.

gyroscopes is in line with ROD's method selection. However, the design lacked customized integration with specific MEMS devices, which may lead to performance degradation in real-world applications. To overcome these shortcomings, Yao et al. [173] developed a metasurface-based vibration isolation structure integrated directly within the MEMS package (Fig. 9b). This design employed a membrane-type configuration, in which the masses were represented by square blocks and the membrane by folded beam, The unit cell size is reduced to 1400 μm, with an overall device dimension of only 20 mm × 20 mm × 0.2 mm. By constructing a periodic unit cell arrangement, the system achieved a complete three-dimensional bandgap within the target frequency range. The metaplate was positioned between the MEMS resonator and the substrate, anchored at four corners and fixing the MEMS resonator at the center. External vibrations were transmitted through the anchors, but effectively blocked from reaching the resonator, achieving vibration isolation. Experimental results showed vibration attenuation of up to −30 dB, corresponding to a theoretical reduction of the ARW to approximately 3.16 % of its original value, in the 14–17 kHz range. This performance is comparable to that of traditional active control systems, while occupying significantly less volume. This design demonstrated a successful integration of AMMs with electronic packaging. By using a structure like MAM, precise integration in the compact space was achieved, and an efficient vibration reduction effect was obtained, which is consistent with the characteristics of MAM in the ROD framework.

Another noteworthy design is the MEMS thermal-vibration isolator developed by Xu et al. [174]. For solving vibration and thermal insulation stressors in MEMS component, a PDMS beam array (MAM type) based insulator is proposed (Fig. 9c). While also based on a frame–spring–mass concept like Yao et al.'s metasurface approach [173], this design does not adopt a periodic array or integrate into the MEMS package. Instead, a freestanding isolation platform was fabricated to shift the resonance frequency from 9000 Hz to 300 Hz and reduce average shock displacement by approximately 40 %. The overall dimensions of the device is approximately 8 mm × 8 mm × 5 mm. A particularly innovative feature of this design is the use of PDMS, with its extremely low thermal conductivity, in conjunction with a suspended structure to significantly enhance thermal insulation from the substrate. This is especially effective in protecting MEMS devices against transient thermal shocks by maintaining a more stable initial temperature. Furthermore, this approach closely resembles the design philosophy of tunable multifunctional thermal metamaterials [182]. By alternating high thermal conductivity silicon and low thermal conductivity PDMS in an interleaved pattern, the structure guides heat flow and improves thermal management. In this study, the compact structure of MAM was still utilized as the main vibration damping design. On this basis, the heat insulation performance was added according to the stressor requirements of ROD, and theoretically, the control of vibration and heat was achieved.

Although these studies did not directly verify the impact of the proposed designs on device reliability, we applied the predictive approach described earlier to roughly estimate the mapping relationship

between acoustic performance and reliability. These studies collectively demonstrate the accuracy and efficiency of the ROD framework in addressing MEMS-related challenges. By leveraging the compact nature of MAMs and the supportive characteristics of cavity-type structures within the toolbox, appropriate design strategies can be selected based on the failure modes and failure ranges under different working conditions. This significantly enhances the capability of AMMs to solve practical problems and accelerates their transition from laboratory research to industrial application. These findings highlight the guiding role of the ROD framework in AMM research.

5.2. Radio frequency (RF) resonator

Due to the significantly lower propagation speed of sound compared to electromagnetic waves—by approximately five orders of magnitude—acoustic resonators can be much smaller than their electromagnetic counterparts at the same frequency. Moreover, acoustic components are passive and energy-efficient, making them ideal candidates for compact, high-performance, and highly integrated RF filters and frequency control devices.

Scandium-doped aluminum nitride (AlScN)–based RF micro-acoustic resonators have gained increasing popularity as the use of AlScN enables wider bandwidths compared to conventional AlN-based RF filters [171]. However, the lower power-handling capability of AlScN devices, relative to AlN counterparts, leads to increased phase noise levels in oscillators, thereby significantly reducing the achievable minimum detection limit [171]. Consequently, mitigating noise interference has become a critical challenge. At the same time, the advent of fifth generation (5 G) communication standards has introduced more stringent demands on device architectures, requiring not only enhanced noise suppression and thermal regulation, but also multifunctional resilience against multiple coupled stressors such as mechanical vibration and thermal fluctuation.

Compared with traditional vibration reduction approaches that rely primarily on the intrinsic damping properties of materials, AMMs offer several distinct advantages — including superior noise attenuation, multi-band suppression capability, enhanced miniaturization and potential for multifunctional integration. These characteristics make AMMs a promising research direction for the development of next-generation RF communication technologies.

One of the important components in RF communication is resonators, which selectively amplify or suppress signals of specific frequencies. However, the anchor loss, where acoustic energy leaks through support tethers into the substrate, degrading the quality factor in GHz-frequency resonators. Moreover, the thermal stability of the resonator is particularly critical, and the temperature will cause a change in the elastic modulus of the material, which will cause a change in the resonant frequency and reduce the performance of the resonator. Conventional approaches such as material mismatch, mesa isolation, and suspended structures offer partial mitigation but face limitations in mechanical stability, precision, and material compatibility. To address energy leaking, Wu et al. [170] incorporated AlN-based PnCs into Lamb wave resonators (LWRs), proposing a GHz-range resonator with one-dimensional gourd-shaped PnC tethers that effectively suppressed spurious modes (Fig. 9d). By exploiting BG and acoustic impedance mismatch, a complete bandgap was created around the operating frequency, blocking acoustic leakage through the tethers. The resulting device achieved a loaded quality factor of 1893 at 1.02 GHz, representing a 45.2 % improvement compared to conventional beam-tethered LWRs—demonstrating the clear advantage of AMM-based anchoring. More recently, Zhao et al. [171] proposed an AMM-based anchor structure using SiO_2/AlScN multilayers to enhance thermal and mechanical performance without sacrificing quality factor or footprint. The design features unetched, high thermal conductivity AlScN combined with periodic low-thermal-resistance pathways to form an anchor that provides both phononic bandgap isolation and efficient heat conduction. The research results demonstrated that the quality factor of the resonator employing the AMM-based structure was significantly higher than that of conventional designs. Compared with traditional fully etched configurations, its Duffing coefficient was reduced by approximately 60 %, and the thermal resistance was nearly halved. This structure significantly reduces the thermal resistance of RF resonators, enabling better temperature stability, linearity, and power handling—critical for high-frequency, high-power applications. Moreover, the use of unetched films simplifies fabrication and enhances manufacturability for large-scale production.

From the perspective of the ROD framework, the primary objective in RF resonator research is to mitigate acoustic energy leakage into the substrate via structural vibrations, while the secondary goal is to minimize thermal interference caused by temperature fluctuations. Both Wu and Zhao employed PnCs as vibration-suppression solutions. The fundamental rationale behind this choice lies in the structural simplicity of PnCs and their relatively larger feature size compared to other types of AMMs operating at the same frequency. At MHz and GHz scales, this significantly reduces fabrication complexity. On-device validations further demonstrated the superior reliability enhancement provided by AMMs over conventional approaches. To address thermal interference, Zhao extended the vibration mitigation strategy by modifying the PnC structure to create additional thermal pathways, thereby lowering thermal resistance without compromising the vibration isolation performance. This not only improved the overall device reliability but also further validated the feasibility of applying the ROD framework to solve targeted reliability issues.

5.3. Wave control of acoustoelectric equipment

High-precision acousto-electric devices are often limited by persistent interference noise, which can compromise performance or even render devices inoperative in noisy environments. Traditional acoustic absorbing / filtering materials struggle to precisely control such interference [183], whereas AMMs—due to their unique capabilities in wave manipulation, frequency selectivity, and energy management—are emerging as key materials for the design of advanced filtering and signal processing systems. In applications such as structural health monitoring, nonlinear ultrasonic testing, ultrasonic flow meters, parametric loudspeakers, and medical imaging, AMMs offer superior frequency control and integration potential. Phononic crystals based on BG or LR mechanisms have been extensively employed to suppress background noise, harmonic distortion, and structural crosstalk, thereby improving signal-to-noise ratio (SNR) and detection sensitivity. In SHM, AMM structures can be designed to block specific noise bands—such as frictional vibrations or fixture-induced signals—enhancing early detection of microcracks or fatigue damage [184]. In ultrasonic applications, particularly in industrial and medical imaging, AMM-based filters effectively suppress back-propagating waves, spurious harmonics, and echo noise, improving image clarity and measurement accuracy [185]. In parametric loudspeakers, AMMs help isolate the desired modulation signal by filtering out the primary carrier wave, thus enhancing sound reconstruction quality. Embedded AMMs in ultrasonic flow meter housings reduce structural cross-talk, leading to more stable and reliable flow measurements in complex industrial environments [186]. Recent studies also demonstrate that gradient AMMs with strong anisotropy can induce wave compression and localized pressure field enhancement, significantly improving acoustic sensing precision [187]. That means AMMs can amplify and extract weak signals buried below the noise floor, significantly improving device accuracy and robustness beyond noise suppression.

AMMs have also brought innovation to ultrasonic transducers, particularly in optimizing the backing layer—a critical component. Conventional piezoelectric transducers radiate both forward and backward sound waves; insufficient absorption by the backing layer results in reflections that cause reverberations and false signals. Hence, the backing must exhibit both impedance matching and high energy

absorption. Traditionally, soft materials such as epoxy—sometimes mixed with metal powders—are used, but AMMs offer a more flexible, design-oriented alternative. For instance, Stoakes et al. [188] developed an AMM-based backing structure using triangular scatterers in a diode-like configuration. Fabricated via 3D printing, the introduction of the AMM structure produced a 14.58 dB increase in reflection absorption in the MHz range compared with a homogeneous material. According to the proportional relationship between acoustic power and echo intensity [172], this corresponds to an approximately 96.5 % reduction in echo strength, thereby significantly enhancing the SNR. Li et al. [189] further advanced this by integrating active gradient metamaterials into the piezoelectric element and fabricated an ultrasonic transducer with AGM. A non-periodic axisymmetric groove array enabled broadband self-focusing across 4–20 MHz, enhancing both focal pressure and bandwidth. This approach simplifies conventional phased-array structures, reduces electrical complexity, and improves focusing on water and biological media—highlighting AMMs' potential for adaptive waveguiding and acoustic field shaping.

5.4. Data center cooling fan noise reduction

In the past decade, the demand for cloud-based memory storage has surged dramatically. According to IDC, global data generation reached over 59 zettabytes (ZB) in 2020 and is expected to more than triple to 175 ZB by 2025 [181]. Currently, >95 % of data centers rely on air cooling, where noise has become a critical concern [190]. Beyond posing health risks to workers, excessive noise can interfere with electronic components, particularly sensitive storage devices.

Hard disk drives (HDDs), due to their low cost and high storage capacity, remain widely used in data centers. However, their nanometer-scale tracks and precision servo systems are highly sensitive to acoustic and vibrational disturbances, particularly at certain frequencies [191]. These disturbances often originate from cooling fans [181]. Although adding soundproofing around the HDD enclosure can reduce noise exposure, conventional sound insulator also impede airflow [192], compromising heat dissipation and increasing the risk of overheating. Therefore, effective sound insulation for HDDs must achieve both acoustic damping and low airflow resistance—requirements that traditional soundproof materials struggle to meet.

To address this challenge, researchers have turned to AMMs. Killeen et al. [180] embedded an array of Segmented Membrane Sound Absorber (SeMSA) cells into a deflector plate and compared its performance to that of traditional hard-wall enclosures and PU foam (Fig. 9e). The SeMSA-integrated design achieved a 43.9 % reduction in total acoustic emission. Each SeMSA cell comprises three main components: segmented air chambers, a micro-perforated plate, and a decorative membrane. Incident sound excites the membrane into resonance, converting acoustic energy into kinetic and subsequently thermal energy. The asymmetric design of dual chambers causes out-of-phase membrane motion at different frequencies, creating pressure differentials that drive airflow through the micro-perforations—enabling simultaneous noise absorption and thermal exchange. The study showed that this design achieved an airborne noise attenuation of 2.5–3 dB while preserving ventilation capability, with no significant degradation observed in airflow or thermal performance. This represents a successful innovation in ventilated noise-control technology. Although this approach offers a novel balance between acoustic insulation and heat dissipation, the resulting noise reduction remains insufficient for high-noise servers (>80 dB), indicating the need for further optimization.

An alternative AMM-based design was proposed by Wasala et al. [191], who developed a Helmholtz resonator structure consisting of spherical internal cavities with interconnected cylindrical openings along each axis (Fig. 9f). These units were arranged in a ring and embedded at the fan inlet or outlet. The optimized configuration achieved a notable 10.8 dB noise reduction without causing any detrimental impact on ventilation or cooling performance. Unlike Killeen's design, which targeted noise around 600 Hz, Wasala's system focused on higher-frequency noise at approximately 4000 Hz. Since lower-frequency noise is generally harder to attenuate, both studies offer valuable and complementary insights.

It is important to note that, in practical HDD applications, the relationship between sound pressure level (SPL) and device performance is not linear. The performance of HDDs tends to deteriorate sharply once a specific SPL threshold is exceeded, eventually leading to failure. Therefore, in real-world implementations, AMM designs should be carefully optimized according to the failure baseline and operational environment of the HDD to ensure reliable performance. They highlight the need for AMM designs to be customized based on specific device parameters and noise characteristics in future ventilation and noise-isolation applications. It is worth noting that if we review this problem using the ROD framework, we can see that the design of the metamaterial with ventilation and noise reduction mentioned in chapter 2.3, such as Kim [101] and Shen et al. [102], is very suitable for data center applications. Their design not only allows for multi-directional airflow, heat dissipation, efficient noise reduction within broadband, but more importantly, it is also excellent and supportive, perfectly fitting the needs of the case housing. Although this design may require a redesign of the chassis structure due to the large occupancy volume, it is still an ideal solution.

5.5. Vibration reduction for in-vehicle devices

Designing structural components for space applications requires balancing mechanical robustness and weight reduction. While structures must endure severe launch loads and operate reliably for years, minimizing mass is crucial to reduce launch costs. However, lightweight designs often degrade vibration performance, making it difficult to achieve both low mass and effective vibration control. Micro vibrations from components like reaction wheels and cryocoolers can disturb optical instruments such as telescopes, leading to line-of-sight jitter. As pointing accuracy requirements grow, micro vibration becomes a more critical issue. Active isolation systems can suppress such disturbances but increase system complexity and are typically used only when passive methods—such as viscoelastic materials or damping platforms—are inadequate. Common passive approaches involve viscoelastic damping materials or isolation platforms, but these often lack sufficient stiffness. To endure launch loads, additional fixtures are usually required to secure sensitive instruments, adding further design constraints [193].

AMMs offer a promising approach for reducing micro vibrations affecting optical instruments in space. Manushyna et al. [193] investigated the use of AMMs in space-based optical systems by attaching an array of cylindrical local resonators to a breadboard-mounted test instrument (Fig. 10a) Under random excitation, the system achieved 72 %–95 % amplitude attenuation at target frequencies. Notably, the vibration attenuation did not scale linearly with the number of resonators. In fact, configurations with fewer resonators demonstrated higher damping efficiency per unit mass, which is particularly advantageous for mass-sensitive space applications. This highlights the importance of optimizing the trade-off between added mass and damping performance. The study also explored the application of resonators on satellite sandwich panels, which serve as mounting surfaces for components such as fuel tanks, electronic boxes, and scientific instruments (Fig. 10c) [193]. These components are highly sensitive to dynamic loads, necessitating structural designs that minimize interface-level excitation. Beam-type resonators were mounted on the panel surface to attenuate vibrations within a specific stopband. Since the dominant panel modes primarily excite shaping loads, a wide bandgap is not required, making local resonators ideal for narrowband, high-efficiency vibration suppression.

Similar applications of AMMs have also emerged in the automotive field. Vehicle-mounted devices also require appropriate vibration protection to prevent premature failure. In 2019, Jung et al. [194] were the

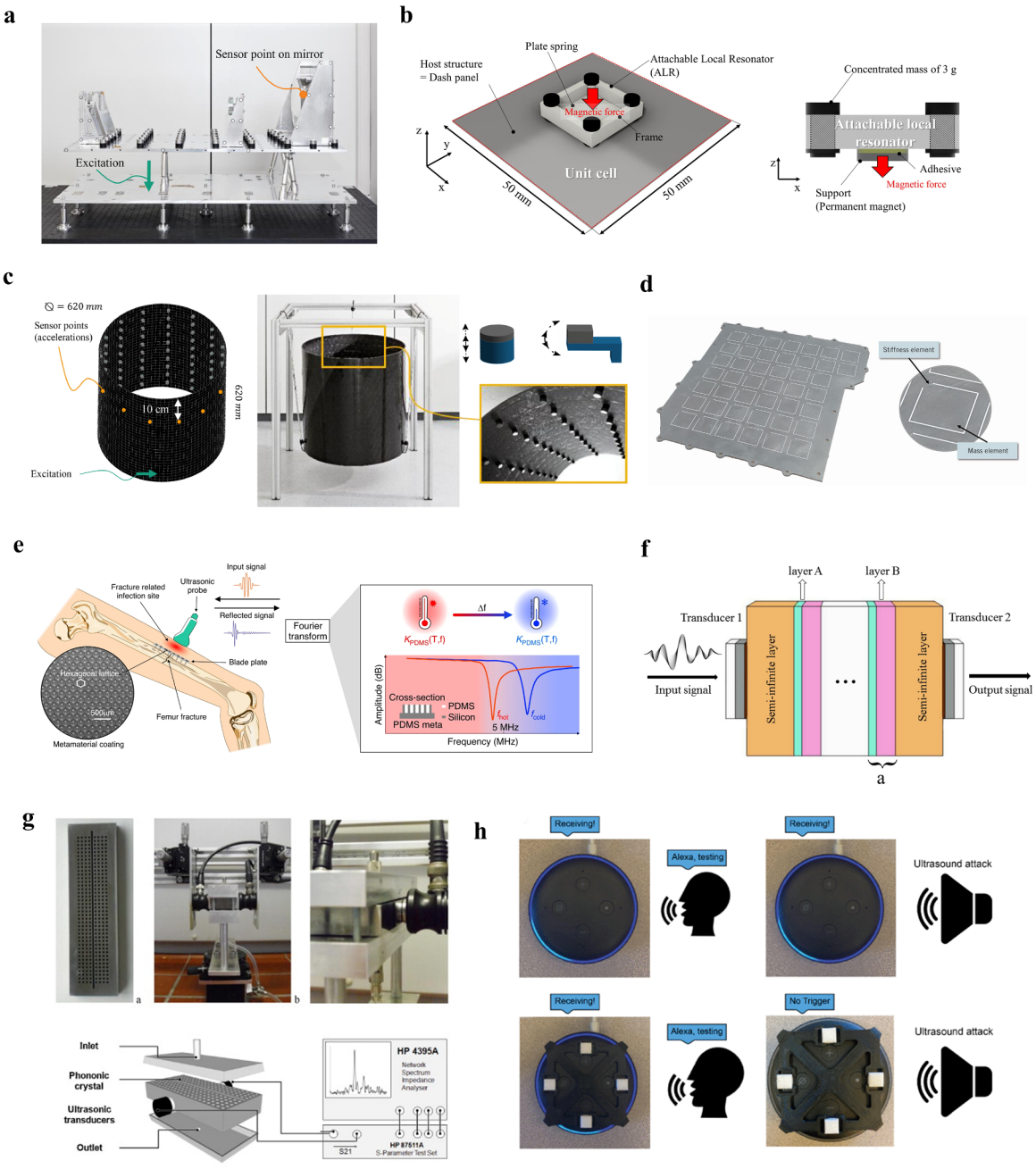


Fig. 10. Schematic diagram of AMM applications (Part II): (a) AMMs applied optical system. Reproduced from [193], under the terms of the Creative Commons CC BY license. (b) ALR system. Reprinted from [194], Copyright 2019, with permission from Elsevier. (c) Resonators on satellite sandwich panels. Reproduced from [193], under the terms of the Creative Commons CC BY license. (d) A cover integrated AMM. Reprinted from [195], copyright 2023,with permission from Springer Nature. (e) AMM temperature sensor. Reproduced from [196], under the terms of the Creative Commons CC BY license. (f) AMM based gas sensor. Reprinted from [197], Copyright 2019, with permission from Elsevier. (g) AMM based-gasoline sensor. Reprinted from [198], Copyright 2013, with permission from Elsevier. (h) Acoustic filter for voice assistant. Reproduced from [199], under the terms of the Creative Commons CC BY license.

first to apply LR theory to complex industrial structures, proposing an attachable local resonator (ALR) system for noise and vibration reduction in vehicle dashboards (Fig. 10b). The ALR consists of a frame plate spring, a concentrated mass, and a permanent magnet for attachment. Frequency tuning is achieved by adjusting the spring stiffness and mass. The magnetic attachment enables easy, non-permanent installation on complex dashboard surfaces without altering the original structure. Significant bandgaps were formed at 150, 750, and 1200 Hz, resulting in a 5–16 dB reduction in structural noise and vibration. Taking the mid-range fatigue strength exponent of metals ($b = -0.1$) as a reference [200,201], Eq. (5) indicates that the corresponding fatigue lifetime, solely attributed to vibration reduction by acoustic means, could increase by approximately 316 to 31,600,000 times. A key advantage of this design is its reusability and adaptability across different operating environments. However, due to magnetic components, care must be taken to position the ALRs away from sensitive parts such as GPS antennas and electronic compasses to avoid magnetic interference. Another approach, proposed by Droste et al. [195], integrated AMMs into the cover of the power electronics housing in electric drivetrains (Fig. 10d). Using waterjet cutting, resonators were formed directly from the cover material as flexible flaps. This fully integrated design achieved an average SPL reduction of 8 dB within a one-third octave stopband and

even reduced the component's weight by 3 %, offering a promising solution for weight-sensitive automotive applications. Nonetheless, the impact of this modification on the structural stiffness of the cover requires further evaluation.

Additional studies by Liao et al. [200], and others have also advanced AMM integration in vehicles. These works confirm the significant potential of AMMs in achieving precise, efficient vibration and noise suppression, while also contributing to lightweight design. Although challenges such as miniaturization and system integration remain, particularly for LR-based AMMs, the technology holds great promise. Continued research is expected to unlock broader applications and practical implementations in the near future.

5.6. Sensing

In the field of sensing, AMMs contribute indirectly to electronic device reliability by enabling advanced monitoring of key parameters such as temperature, magnetic fields, and mechanical integrity. By leveraging AMM-based sensor technologies, it is possible to perform rapid, non-invasive, and high-precision assessments of device health—allowing for timely fault localization, failure mitigation, and even predictive maintenance before critical malfunction occurs.

Aly et al. [201] employed the transfer matrix method to investigate a one-dimensional phononic crystal (PnC) with a piezoelectric defect layer, demonstrating that temperature variations could modulate the bandgap width, thereby enabling temperature-sensing functionality. More recently, Maini et al. [196] introduced a novel AMM-based temperature sensor composed of silicon inclusions embedded in a polydimethylsiloxane (PDMS) matrix (Fig. 10e). An ultrasonic probe is used to detect a sensor located on the surface of the implant. The temperature change alters the bulk modulus of the associated materials (PDMS and Si), resulting in a shift in the resonance frequency of the acoustic mode proportional to the temperature change. Using a standard ultrasonic transducer to excite and detect reflected signals, the system achieved resonance near 5 MHz with a high-quality factor, resulting in a temperature resolution of 30 mK. Unlike conventional sensors, this approach requires no external power supply, making it well-suited for harsh environments. AMMs also show potential for magnetic field sensing. Nagaty et al. [202] proposed a one-dimensional PnC incorporating a magnetostrictive material as a defect layer. When the defect thickness approached half the acoustic wavelength, a resonance mode appeared within the bandgap. The study revealed that applying an external magnetic field could shift the resonance frequency, providing a theoretical basis for PnC-based magnetic field sensors. In addition, AMMs have been demonstrated as effective sensing elements in gas (Fig. 10f) and liquid (Fig. 10g) environments without relying on electronic components, making them ideal for extreme operating conditions [196,197]. For PnC-based sensors, improving sensitivity requires optimizing the relationship between frequency shift, bandwidth, and resonance amplitude. Under ideal conditions, detection frequency resolution should reach levels on the order of 10^{-6} the probing frequency [203]. Nonetheless, dimensional constraints remain a challenge. For instance, the lateral size of electromechanical transducers may limit the excitation of pure longitudinal modes, while thermal field control imposes strict requirements on panel geometry. Despite these limitations, AMMs and PnCs offer significant promise across a wide range of sensing applications. Continued research into multi-dimensional optimization and experimental validation is essential to unlock their full potential.

5.7. Emerging applications

Beyond traditional applications in PCBs, MEMS, and packaging systems, several emerging directions are extending the functional scope of AMMs toward new reliability-driven applications.

An emerging and intriguing application of AMMs lies in enhancing the security of voice-controlled devices. Modern voice assistants (e.g., Alexa, Siri) have become ubiquitous in smart homes and device control systems. However, they are vulnerable to a form of attack known as ultrasound attack, in which commands are transmitted using ultrasonic frequencies beyond the range of human hearing. Due to the shadow effect, built-in microphones can still detect these signals, allowing attackers to issue unauthorized commands without user awareness [199]. To address this security vulnerability, Lloyd et al. [199] developed a composite AMM-based acoustic filter composed of a rigid panel perforated with multiple holes, each acting as a Helmholtz resonator (Fig. 10h). This design targets and passively absorbs ultrasonic signals in the 20–40 kHz range, effectively suppressing ultrasound-based attacks. The structure is simple, does not require modifications to existing firmware, and can be integrated into various smart speaker devices—offering a practical and low-cost enhancement to user security. However, the filter's passive nature and fixed frequency range impose limitations. Ultrasonic signals outside the designed band may not be effectively attenuated. If we review ROD toolbox, we may find a more suitable solution for this application-active control AMM. These AMMs such as tunable piezoelectric AMM can dynamically adapt to varying ultrasonic threats and accordingly offset the waves in different frequencies. That greatly enhances the safety of voice-controlled devices.

In addition, several promising future research directions can be identified. In flexible and wearable electronics, soft and deformable AMMs constructed from elastomers, hydrogels, or auxetic lattices can serve as mechanically compliant vibration-damping layers, protecting stretchable conductors and thin-film interconnects from fatigue and delamination while maintaining acoustic sensing and comfort [204]. Furthermore, AMMs with electromagnetic wave amplification capabilities can simultaneously achieve vibration suppression and signal enhancement, enabling applications such as sensor systems that require both vibration isolation and wireless charging or near-field communication signal gain. Similar multifunctional architecture can also be applied to industrial robotic systems to realize more stable signal exchange and energy replenishment. In battery and energy-storage modules, AMMs can simultaneously mitigate vibration-induced degradation and guide heat flow, improving the coupled thermo-mechanical reliability of high-power systems, particularly in electric vehicles. For underwater acoustic communication, metamaterial-inspired structures provide precise control of sound propagation, reflection, and impedance matching, enhancing signal stability and transducer efficiency under dynamic pressure conditions [40,56,205]. Meanwhile, the use of AMMs for vibration and acoustic energy harvesting is gaining attention: locally resonant metastructures can concentrate and convert ambient mechanical energy into electricity, enabling self-sustained sensor nodes and adaptive monitoring platforms [48,164,166,206,207].

Although these technologies remain at an early research stage, they highlight the expanding multifunctional potential of AMMs for reliability enhancement across next-generation electronic and electromechanical systems.

The applications in each field of this section are summarized in Table 10 with the ROD framework.

6. Discussion and future perspectives

The previous sections have clearly demonstrated the advantages of AMMs in electronic and electrical applications, as well as the efficiency and precision offered by the ROD framework in AMM design. AMMs designed under the ROD framework exhibit strong application-oriented characteristics, avoiding the pitfalls of over-design driven by excessive pursuit of singular material properties. This approach significantly strengthens the connection between academic research and engineering practice, facilitating the commercialization of research outcomes and the broader societal adoption of metamaterials. However, AMM design under the ROD framework still faces several challenges. In this section, several representative challenges and future development trends in ROD-guided AMM design will be discussed in detail.

Table 10
Comparison of AMM applications based on the ROD framework.

Application Scenarios	Stressors	Failure Modes	AMM Structure	ROD Solutions
MEMS gyroscopes	Vibration	Mechanical interference around gyroscope resonant frequency may distort the measurement results	Local resonator	Create an accurate stopband cover the frequency of gyroscope resonant
RF resonator tethers	Vibration/ Temperature	Acoustic energy leaks through tethers may degrade Q value, and temperature will interfere with resonator properties	Local resonator with thermal dissipation	Create a stopband cover resonator frequency and implement thermal dissipation function
Acousto-electric equipment housing or backing	Vibration	Background noise or crosstalk may lower the SNR.	PnC or LR	Create stopbands cover all interference frequency needed in application environment
Data center Cooling Fan Noise	Vibration/ Temperature	Noise may interfere with magnetic head in HDD leading to read/ write errors, and overheating may damage devices.	HR or Space coiling with thermal dissipation	Stopband frequencies depend on fan rotation speeds and structure layouts. Design needs keep airflow
In-Vehicle devices	Vibration/ Temperature/	Vibration from vehicle body may interfere with the accuracy of device or accelerate failure of welding spot. Near engine devices need thermal protection.	Depends on specific devices	It depends on the specific device's working environment
Voice controlled security	Vibration	Sounds above 20 kHz may bypass human ear and send commands to voice controlled devices	Active AMMs	Shielding is performed by active adjustment according to the received ultrasonic signal

6.1. *Multifunctional coupling*

One of the most persistent challenges in MFAMs research lies in achieving multifunctional coupling—the seamless integration of different physical-field responses (e.g., mechanical, thermal, and electromagnetic) within a single structure. Due to the inherent mismatch of working frequencies, energy transport mechanisms, and characteristic scales across wave types, achieving coherent multifunctionality remains a formidable task. This section will focus on two critical aspects: size compatibility and performance trade-offs.

First, considering acoustoelectric metamaterials, it is essential to note that both acoustic and electromagnetic metamaterials rely on the precise manipulation of wave propagation. Consequently, the characteristic size of their unit cells must be on the same order of magnitude as the corresponding wavelength [195]. However, due to the substantial difference between the speed of sound and the speed of light, the wave speed equation implies that, at the same frequency, the wavelengths of acoustic and electromagnetic waves differ by several orders of magnitude. This disparity makes simultaneous control of multiple wave types within a single structure extremely challenging and severely limits structural compactness.

Two primary strategies have been proposed to address this challenge.

(1). Decoupled structural–material design: In this approach, the acoustic metamaterial is designed at a scale corresponding to the target acoustic wavelength, while electromagnetic control is achieved through the intrinsic properties of the base material, such as using high-dielectric-loss materials for EMI shielding. Previous studies have shown that the acoustic performance of AMMs is predominantly governed by their topological geometry rather than the matrix material, meaning that modulating the electromagnetic properties through the base material has minimal influence on the acoustic response [208]. By decoupling the structure and the material, this method enables independent yet coordinated control across distinct wavelength regimes, realizing effective multifunctionality.

(2). Wavelength-matched functional integration: Another strategy is to focus on applications where the wavelengths of acoustic and electromagnetic waves are of comparable magnitudes. For example, acoustic waves in the 10–30 kHz range correspond to wavelengths of approximately 1–3 cm in air, which are comparable to microwave wavelengths (10–30 GHz). —as demonstrated in the design proposed by Xu et al. [151] discussed earlier in Section 3.3. This allows for functional coupling designs that maximize spatial efficiency, promote structural compactness, and facilitate integrated fabrication, making them particularly attractive for engineering applications.

Beyond wavelength compatibility, performance interference between the acoustic and electromagnetic domains must also be considered. The introduction of conductive layers into AMMs may distort the propagation of acoustic waves, particularly when there is a large impedance mismatch or when the layer dimensions are comparable to the target acoustic wavelength. Such effects can cause undesirable reflections, preventing efficient acoustic energy dissipation, reducing AMM efficiency, or even introducing spurious resonances that compromise device reliability. Conversely, for electromagnetic amplification materials, the inclusion of additional acoustic layers may attenuate EM signals—especially when high-dielectric-loss materials are employed [209]. Similarly, in AMMs designed for acoustic amplification, excessive vibration amplitudes may alter electromagnetic resonant features, such as capacitor spacing, thereby disturbing the EM performance [210].

To overcome these challenges, fully coupled acousto-electromagnetic metamaterials are often more suitable when the matrix material primarily governs the electromagnetic properties. Embedding conductive particles within existing AMM matrices can enable EM functionality with minimal disruption to the original acoustic behavior. In contrast, when the electromagnetic response relies on resonant structures, a layered configuration or integration with membrane-type AMMs offers a more practical and fabrication-friendly solution. Although the inclusion of acoustic layers may introduce some attenuation, properly engineered resonant architectures can retain substantial electromagnetic control, achieving efficient multifunctional coupling.

In contrast to acousto-electromagnetic metamaterials, which focus on wave manipulation and are thus constrained by wavelength-scale unit dimensions, mechanical metamaterials are not limited by the propagation wavelength, allowing greater freedom in geometric design. Although some studies have reported that the ratio between the unit-cell size and the overall structure influences the effective homogenized behavior—where, ideally, the characteristic size of the unit cell should be sufficiently small (overall size/unit size $>$ 50) to ensure reliable continuum performance [211] —this condition is not always critical in practical engineering applications. In designs dominated by buckling, nonlinearity, or LR, the functionality often depends on localized deformation and nonuniform stress fields, where homogenization loses its practical significance and the global performance is instead governed by local responses [155,212]. Therefore, in acousto-mechanical metamaterial coupling, attention should be directed primarily toward overall structural compatibility rather than strict unit-scale proportionality.

From a functional perspective, the core conflict between AMMs and

mechanical metamaterials arises from their contrasting structural requirements. AMMs typically rely on resonance, reflection, and dissipation mechanisms, which favor open or porous architectures to enhance acoustic performance. In contrast, mechanical metamaterials depend on continuous or densely connected frameworks to provide structural integrity and load-bearing capacity. These opposing design requirements make fully coupled acousto-mechanical systems challenging to realize.

A feasible optimization strategy involves adopting a decoupled, layered architecture, where the supporting layer and the acoustic layer are separated—such as through a sandwich panel configuration—to minimize mutual interference and achieve balanced performance. Alternatively, employing artificial intelligence (AI) or machine-learning (ML) – based topology optimization can facilitate the design of fully coupled architectures, iteratively improving both acoustic and mechanical responses to identify optimal structural configurations that reconcile these competing demands.

Similarly, the compatibility conflict between acoustic and thermal metamaterials primarily arises from their contradictory structural requirements. Thermal metamaterials typically rely on continuous conductive pathways to guide and regulate heat flow [182], which conflicts with the open or porous architectures commonly adopted in AMMs. The presence of these open structures complicates the formation of effective thermal conduction routes, thereby diminishing the overall heat-transfer control capability. An ideal acousto-thermal metamaterial should therefore be designed with both the thermal conduction pathways and the acoustic bandgap structure considered simultaneously, allowing the two functionalities to reach an optimal balance suited to the target application environment. However, this co-design process is often complex and challenging to implement in practice. As a result, most existing acousto-thermal metamaterials still adopt a decoupled, layered architecture, in which the thermal and acoustic functions are realized separately. Other feasible compatibility strategies include exploiting acousto-thermal anisotropy, where the structure is designed to achieve acoustic impedance matching and sound absorption in one direction (e.g., normal to the surface), while establishing high thermal conductivity channels in another direction (e.g., in-plane), thus enabling bidirectional regulation of sound blocking and heat conduction. Another promising approach involves the use of phase-change materials or thermo-responsive polymers, which can maintain the acoustic structural integrity at low temperatures while activating thermal conduction channels at elevated temperatures, thereby achieving environmentally adaptive acousto-thermal regulation.

Although there are many studies on multifunctional materials of thermoelectric combination, only a few scholars have studied multifunctional metamaterials combined with acoustic heat and acoustic electricity, which may be due to complex reasons such as asymmetric development of theoretical basis and difficulty of mechanical wave and electromagnetic wave coupling. However, with the development of metamaterials, the difficulty of coupling control between different physical fields is greatly reduced, and different physical fields can be controlled through different material structure designs. And as industrial applications gradually move towards more complex application environments and higher precision requirements, such as thermal power increase and EMI increase caused by high-performance chips, more and more on-vehicle electronic equipment, radar ultrasonic and even cameras and other on-vehicle equipment detection accuracy requirements are getting higher and higher, these needs will inevitably promote the emergence of materials that integrate more functions. As a metamaterial with natural advantages for multi-physical field coupling control, it will certainly play a key role in the subsequent development. Especially under the guidance of the ROD framework, the free integration ability of multiple functional materials can make the solution of engineering problems more accurate and efficient, effectively play the material properties, and solve practical problems with the highest efficiency.

6.2. Integration and manufacturing

Another significant challenge lies in the integration of AMMs into practical applications, especially in precision electronic components such as PCBs, semiconductor packaging, and microsystems, where the compatibility between material dimensions and device scales must be carefully engineered.

The scale mismatch between low frequency targeted AMM structures and these systems is a major constraint. AMMs typically require periodic structures with unit sizes ranging from one-tenth to one-half of the target wavelength [195]. For ultra-high-frequency (MHz–GHz) filtering, the physical size of AMMs is not a major concern — acoustic wavelength is only micron scale and AMMs are around this scale. However, for low- to mid-frequency vibration control (10 Hz–20,000 Hz), the required structural dimensions typically fall within the millimeter to meter scale. The available installation space, however, varies greatly across applications, particularly in miniaturized electronic systems. In such cases, the available volume within electronic packaging, PCB interlayers, or MEMS devices is often limited to the micrometer or sub-millimeter range, making direct AMM integration highly challenging. To address these issues, AMM design within the ROD framework should consider the following strategies. For devices requiring narrowband vibration suppression, a transition toward planar architectures—such as membrane- or thin-plate-based AMMs—can effectively alleviate integration constraints. As discussed in Section 5.1, Yao et al. [173] proposed a metasurface design based on MAMs, and Xu et al. [174] developed a PDMS beam-array–based insulator. Such designs substantially reduce the structural footprint and enhance dimensional compatibility, though at the expense of a narrower bandgap (about 1000 Hz) and higher operating frequencies (10–20 kHz), limiting their applicability for broadband or low-frequency isolation. To achieve broader bandgaps or effective control in the low-frequency regime (<100 Hz), alternative AMM configurations are required—typically with centimeter-scale geometries. In these cases, placing the AMM structure externally, such as on the device housing or supporting base, can enhance dimensional compatibility and enable practical implementation without compromising the internal electronic layout.

Secondly, the periodic architecture of AMMs may disrupt the original heat conduction pathways, leading to thermal stress concentration within the structure. To address this issue, two feasible approaches can be considered. The first approach is to account for heat-path interference during AMM design, incorporating thermal management functionality that compensates for the disturbance caused by the embedded metamaterial structure. The second approach involves enhancing thermal conduction within the AMM itself, for instance, by integrating through-thickness thermal channels within the unit cells and filling them with high–thermal-conductivity materials such as Cu, Al, AlN, or graphite/graphene sheets. This design not only improves heat-transfer efficiency but also helps prevent localized heat accumulation, thereby maintaining the thermal reliability of the overall system.

Furthermore, precision electronic devices impose stricter requirements on the fabrication accuracy and integration compatibility of AMMs. Achieving direct co-fabrication of AMM structures with electronic components is therefore of critical importance; however, several mismatches between AMM materials and electronic manufacturing processes currently hinder this goal. Many AMM designs rely on the interaction between elastomeric and rigid materials, necessitating multi-material fabrication. Yet, introducing such multi-material AMM components into CMOS or MEMS process chains may introduce contamination risks and compromise device yield. In addition, there exists a fundamental dimensional and process-level mismatch between AMM fabrication methods and conventional electronic manufacturing. AMMs are typically produced via 3D printing, laser cutting, or CNC machining, whereas PCBs and MEMS rely on planar microfabrication techniques such as lithography, deposition, and etching, which are inherently incompatible with embedding complex 3D AMM geometries [179,

213–215]. These factors collectively limit the applicability and scalability of AMMs in precision electronic systems.

To address the mismatch between AMM materials and electronic fabrication processes, one feasible approach is to adopt AMM architectures composed of single rigid metallic materials, such as PnCs, cavity-type, or ABH structures. By employing MEMS fabrication techniques such as ultraviolet lithography, dry etching, and atomic layer deposition, it is possible to achieve two-dimensional or quasi-two-dimensional AMM arrays with micron-scale precision [216–218]. This enables direct monolithic integration with miniature components such as wafers or AlN-based devices, embedding the AMM array structure directly within electronic parts and thereby substantially enhancing integration density, structural stability, and functional reliability. Regarding the dimensional mismatch in fabrication, several strategies can be employed. First, within the required performance range, 2D AMM configurations such as PnCs and space-coiling structures should be prioritized, as they are more manufacturing-friendly. Second, layered manufacturing can be applied to construct three-dimensional cavity structures through multilayer stacking, balancing performance and process compatibility. Moreover, the rapid emergence of 3D electronic manufacturing technologies provides new opportunities for AMM–electronics co-integration. In contrast to conventional planar lithography, next-generation 3D microfabrication techniques—such as focused ion beam (FIB) machining, additive microfabrication, and laser-assisted selective etching—enable true volumetric structuring at the microscale. Among them, FIB offers the highest precision but suffers from limited throughput, additive methods provide geometric flexibility though constrained by resolution and material compatibility, and laser-assisted etching allows internal 3D patterning within non-silicon substrates [213,214]. While these technologies are still in their early developmental stages, they are expected to complement mature techniques such as DRIE, paving the way for next-generation 3D integration of electronic and acoustic metamaterial systems.

For large-scale industrial deployment, high-performance AMM structures are often too intricate to manufacture. This is especially true for designs like Helmholtz resonators, where performance is highly sensitive to manufacturing precision, or for complex 3D cavity structures. Reducing fabrication complexity is thus crucial. One key approach is to consider manufacturability during the initial design phase, for example, replacing intricate cavities with beam or slot arrays, or designing modular, easy-to-assemble units. Although such strategies may sacrifice some performance, they can significantly improve economic feasibility and accelerate widespread adoption of AMMs.

6.3. Emerging and less-explored AMMs

At present, numerous AMMs have been applied in the field of electronic reliability, particularly those based on mechanical LR, PnCs, and cavity-type structures. However, the application of ABH, meta-porous, and active-control–type AMMs in reliability enhancement remains relatively limited. The possible reasons for this limitation are as follows.

The ABH concept relies on a continuous power-law thickness profile to trap and dissipate flexural waves, which imposes stringent geometric precision requirements. Moreover, the fabrication of curved or small-scale tapered geometries presents significant manufacturing challenges and high costs, making ABH structures more suitable for large-scale designs [219]. These factors collectively limit the application of ABH-based AMMs in electronic systems. Future development directions may include integrating ABH designs with precision microfabrication technologies to improve geometric accuracy and thereby enhance acoustic absorption efficiency. Additionally, adopting design strategies similar to Yunker et al.'s concept [179]—such as creating acoustically absorptive enclosures—could further exploit the broadband absorption potential of ABH structures for compact and multifunctional electronic applications.

The design limitations of meta-porous AMMs also primarily stem from manufacturing challenges. Due to their sandwich-like porous architecture, fabrication typically relies on methods such as 3D printing [220] and chemical foaming [221] often followed by post-assembly of the constraining plates. Compared with other AMM fabrication approaches, the production of porous materials generally involves higher costs and stricter material constraints, such as the need for customized viscoelastic damping matrices. Furthermore, the introduction of porous layers can impede heat dissipation, which is particularly undesirable in high–energy-density electronic applications. Potential improvement strategies include adopting a modular design framework to enhance tunability and adaptability. For instance, by maintaining a fixed plate geometry while allowing interchangeable porous interlayers, the system can be easily reconfigured to meet different reliability requirements under varying operating conditions. Moreover, functional integration with other features—such as mechanical support or EMI shielding—offers additional opportunities. Coupling multifunctional capabilities with the porous interlayer can preserve the modular advantages while expanding design versatility. Such approaches could lead to the development of a new class of modular, reconfigurable AMMs that differ fundamentally from conventional metamaterial architectures.

Active-control AMMs face a distinct set of challenges. Because their operation relies on external stimuli to dynamically modulate material responses in real time, such interventions may inadvertently interfere with the intrinsic performance of electronic devices. For example, magnetic-field–based control of membrane tension necessitates careful evaluation of potential side effects of introducing magnetic field, including local hot-spot generation, signal instability, and electrochemical degradation within nearby electronic components [222,223]. Furthermore, the requirement for auxiliary control systems adds to the complexity of integration and increases overall design constraints. Possible optimization strategies include using non-intrusive external stimuli that do not interfere with the device's primary function—for instance, employing acousto-optic control in electronic systems or electromagnetic tuning in optical devices—to minimize undesired cross-coupling effects. Another promising approach is to locate the control unit externally, avoiding occupation of the limited internal space within the regulated electronic device and thereby improving spatial efficiency and system-level integration.

6.4. Prediction and validation

Within the ROD framework, performing early-stage reliability prediction for the designed AMMs is also a crucial step. However, due to the diversity of environmental stressors, operating loads, material parameters, and reliability evaluation criteria across different application scenarios, it is challenging to establish a universal predictive model capable of accurately estimating the reliability of AMMs under all conditions. Although the predictive method introduced in Section 4 serves only as a preliminary reference for early-stage AMM design, it nonetheless provides a conceptual bridge linking acoustic performance to reliability. In recent years, many researchers have developed more scenario-specific reliability models, such as those tailored for solder joint degradation in electronic boards [224–226]. Within the ROD framework, such models can be readily substituted to suit different application environments, enhancing predictive accuracy. Furthermore, extending the current model to incorporate multi-physics coupling effects—for example, by considering the influence of humidity, EMI, and thermal cycling as interacting stressors—would allow the establishment of more comprehensive and precise reliability prediction frameworks for AMM-enabled systems.

In another side, experimental validation should also focus on the "integrated state" that is, testing AMMs under realistic working conditions. Currently, most AMM validations are conducted in idealized settings, such as acoustic tubes, which can lead to discrepancies between lab performance and practical outcomes. Future testing should adopt more rigorous conditions to better align research with real-world

applications.

6.5. Artificial intelligence

Looking ahead, the integration of AI and ML techniques into AMM design holds transformative potential. Traditional AMM design relies heavily on parameter sweeps and designer intuition, resulting in low efficiency and limited exploration of the design space. AI-based approaches, such as topology optimization combined with deep learning surrogate models, can rapidly predict performance and discover non-intuitive, highly efficient structures [155]. For multifunctional coupling and balance design in MFAMs, AI can iteratively optimize the topology to identify the optimal trade-off among multiple functionalities, enabling application-specific designs with enhanced performance integration. Incorporating AI technologies within the ROD framework is expected to significantly shorten the cycle from design to prototyping, enhance manufacturability, and intelligently account for various practical fabrication constraints. In the future, with the assistance of AI, AMM design guided by the ROD framework is expected to experience a significant reduction in development cycle time and achieve widespread application across various fields.

7. Conclusion

Ensuring the long-term reliability of electronic systems under complex environmental stressors remains a pressing challenge. This review highlights AMMs as a promising solution for mitigating reliability-critical issues such as vibration, thermal cycling, and EMI. We reviewed the structure types, mechanisms, and application scenarios of both single-function and multifunctional AMMs. To guide the deployment of AMMs in real-world systems, we proposed the ROD framework, which maps stress sources to failure modes and aligns them with tailored metamaterial functions. This approach bridges fundamental material design with system-level reliability requirements. Looking forward, future research should focus on miniaturized, integrable, and multifunctional AMMs, along with scalable fabrication methods and system-level verification. Under the ROD framework, AMMs can evolve from experimental structures into embedded reliability modules for next-generation electronics.

Declaration of generative AI and AI-assisted technologies in the writing process

During the preparation of this work, the authors used ChatGPT to assist with language refinement and editorial polishing. After using this tool, the author reviewed and edited the content as needed and takes full responsibility for the content of the publication

CRediT authorship contribution statement

Lingfeng Huang: Writing – review & editing, Writing – original draft, Visualization, Resources, Project administration, Investigation, Conceptualization. **Mostafa Ranjbar:** Writing – review & editing, Supervision, Conceptualization. **Mohammad Samie:** Writing – review & editing, Supervision, Conceptualization.

Declaration of competing interest

The authors declare that they have no known competing financial interests or personal relationships that could have appeared to influence the work reported in this paper.

Acknowledgments

This research did not receive any specific grant from funding agencies in the public, commercial, or not-for-profit sectors.

Data availability

Data will be made available on request.

References

[1] M. Samie, A. Sheikh-Akbari, K.K. Singh, E. Ofoegbu, Experimental results of an intermittency fault detection and isolation test rig for low power no-fault-found applications, in: 2023 12th Mediterr. Conf. Embed. Comput. MECO, 2023, pp. 1–5, https://doi.org/10.1109/MECO58584.2023.10155104.
[2] A.J. Braaksma, W. Klingenberg, J. Veldman, Failure mode and effect analysis in asset maintenance: a multiple case study in the process industry, Int. J. Prod. Res. 51 (2013) 1055–1071, https://doi.org/10.1080/00207543.2012.674648.
[3] H. Cui, W. Tian, H. Xu, H. Wang, J. Huang, C. Peng, et al., The reliability of the complex components under temperature cycling, random vibration, and combined loading for airborne applications, Crystals 13 (2023) 473, https://doi.org/10.3390/cryst13030473.
[4] K.T. Kloch, P. Kozak, A. Mlyniec, A review and perspectives on predicting the performance and durability of electrical contacts in automotive applications, Eng. Fail. Anal. 121 (2021) 105143, https://doi.org/10.1016/j.engfailanal.2020.105143.
[5] R. Bakhshi, S. Kunche, M. Pecht, Intermittent Failures in Hardware and Software, J. Electron. Packag. 136 (2014) 011014, https://doi.org/10.1115/1.4026639.
[6] S. Söderberg, U. Bryggman, T. McCullough, Frequency effects in fretting wear, Wear 110 (1986) 19–34, https://doi.org/10.1016/0043-1648(86)90149-3.
[7] K. Lyu, L. Wu, X. Wu, Q. Li, J. Qiu, G. Liu, Study on intermittent fault mechanism of electrical connector with corrosion degradation under the vibration stress, IEEE Trans. Compon. Packag. Manuf. Technol. 12 (2022) 627–637, https://doi.org/10.1109/TCPMT.2022.3161652.
[8] L. Yang, Y. Chen, Z. Yuan, L. Chen, Effect of vibration transmissibility on fatigue lifetime of electronic devices, in: M. Gen, K.J. Kim, X. Huang, Y. Hiroshi (Eds.), Industrial Engineering, Management Science and Applications, Springer, Berlin, Heidelberg, 2015, pp. 1031–1039, https://doi.org/10.1007/978-3-662-47200-2_107.
[9] J. Ahmet Erkoyuncu, S. Khan, S.M.F. Hussain, R. Roy, A framework to estimate the cost of No-Fault Found events, Int. J. Prod. Econ. 173 (2016) 207–222, https://doi.org/10.1016/j.ijpe.2015.12.013.
[10] I. Beniaminy, D. Joseph, Reducing the "No Fault Found" problem: contributions from expert-system methods, Proc. IEEE Aerosp. Conf. 6 (2002) 6, https://doi.org/10.1109/AERO.2002.1036138.
[11] W. Debra, A maddening, costly problem, Aerosp. Am. (2015). https://web.archive.org/web/20170510083521/http://www.aerospaceamerica.org/Documents/Aerospace%20America%20PDFs%202015/February2015/Feature1_AA_Feb2015.pdf (Accessed 31 January 2025).
[12] X. Zhang, Z. Qu, H. Wang, Engineering acoustic metamaterials for sound absorption: from uniform to gradient structures, iScience 23 (2020) 101110, https://doi.org/10.1016/j.isci.2020.101110.
[13] L. Chang, A. Jiang, M. Rao, F. Ma, H. Huang, Z. Zhu, et al., Progress of low-frequency sound absorption research utilizing intelligent materials and acoustic metamaterials, RSC. Adv. 11 (2021) 37784–37800, https://doi.org/10.1039/D1RA06493B.
[14] H. Chen, C.T. Chan, Acoustic cloaking in three dimensions using acoustic metamaterials, Appl. Phys. Lett. 91 (2007) 183518, https://doi.org/10.1063/1.2803315.
[15] X. Wu, K.Y. Au-Yeung, X. Li, R.C. Roberts, J. Tian, C. Hu, et al., High-efficiency ventilated metamaterial absorber at low frequency, Appl. Phys. Lett. 112 (2018) 103505, https://doi.org/10.1063/1.5025114.
[16] M. Yang, P. Sheng, Sound absorption structures: from porous media to acoustic metamaterials, Annu Rev. Mater. Res. 47 (2017) 83–114, https://doi.org/10.1146/annurev-matsci-070616-124032.
[17] S. Peng, Z. He, H. Jia, A. Zhang, C. Qiu, M. Ke, et al., Acoustic far-field focusing effect for two-dimensional graded negative refractive-index sonic crystals, Appl. Phys. Lett. 96 (2010) 263502, https://doi.org/10.1063/1.3457447.
[18] Z. Jacob, L.V. Alekseyev, E. Narimanov, Optical Hyperlens: far-field imaging beyond the diffraction limit, Opt. Express. 14 (2006) 8247–8256, https://doi.org/10.1364/OE.14.008247.
[19] N. Kaina, F. Lemoult, M. Fink, G. Lerosey, Negative refractive index and acoustic superlens from multiple scattering in single negative metamaterials, Nature 525 (2015) 77–81, https://doi.org/10.1038/nature14678.
[20] S. Zhang, C. Xia, N. Fang, Broadband acoustic cloak for ultrasound waves, Phys. Rev. Lett. 106 (2011) 024301, https://doi.org/10.1103/PhysRevLett.106.024301.
[21] C. Han, S. Park, H. Lee, Intermittent failure in electrical interconnection of avionics system, Reliab. Eng. Syst. Saf. 185 (2019) 61–71, https://doi.org/10.1016/j.ress.2018.12.016.
[22] L. Raghavan, A.S. Phani, Local resonance bandgaps in periodic media: theory and experiment, J. Acoust. Soc. Am. 134 (2013) 1950–1959, https://doi.org/10.1121/1.4817894.
[23] G. Ma, P. Sheng, Acoustic metamaterials: from local resonances to broad horizons, Sci. Adv. 2 (2016) e1501595, https://doi.org/10.1126/sciadv.1501595.
[24] Z. Yang, J. Mei, M. Yang, N.H. Chan, P. Sheng, Membrane-type acoustic metamaterial with negative dynamic mass, Phys. Rev. Lett. 101 (2008) 204301, https://doi.org/10.1103/PhysRevLett.101.204301.

[25] J. Liu, H. Guo, T. Wang, A review of acoustic metamaterials and phononic crystals, Crystals 10 (2020) 305, https://doi.org/10.3390/cryst10040305.
[26] N. Hashimoto, M. Katsura, M. Yasuoka, H. Fujii, Sound insulation of a rectangular thin membrane with additional weights, Appl. Acoust. 33 (1991) 21–43, https://doi.org/10.1016/0003-682X(91)90063-K.
[27] C.J. Naify, C.-M. Chang, G. McKnight, S. Nutt, Transmission loss and dynamic response of membrane-type locally resonant acoustic metamaterials, J. Appl. Phys. 108 (2010) 114905, https://doi.org/10.1063/1.3514082.
[28] H. Nguyen, Q. Wu, J. Chen, Y. Yu, H. Chen, S. Tracy, et al., A broadband acoustic panel based on double-layer membrane-type metamaterials, Appl. Phys. Lett. 118 (2021) 184101, https://doi.org/10.1063/5.0042584.
[29] N. Gao, H. Hou, Y. Mu, Low frequency acoustic properties of bilayer membrane acoustic metamaterial with magnetic oscillator, Theor. Appl. Mech. Lett. 7 (2017) 252–257, https://doi.org/10.1016/j.taml.2017.06.001.
[30] H.-Z. Li, X.-C. Liu, Q. Liu, S. Li, J.-S. Yang, L-L Tong, et al., Sound insulation performance of double membrane-type acoustic metamaterials combined with a Helmholtz resonator, Appl. Acoust. 205 (2023) 109297, https://doi.org/10.1016/j.apacoust.2023.109297.
[31] X. Li, J. Zhao, W. Wang, T. Xing, L. Zhu, Y. Liu, et al., Tunable acoustic insulation characteristics of membrane-type acoustic metamaterials array with compact magnets, Appl. Acoust. 187 (2022) 108514, https://doi.org/10.1016/j.apacoust.2021.108514.
[32] Y. Li, Y. Zhang, S. Xie, A lightweight multilayer honeycomb membrane-type acoustic metamaterial, Appl. Acoust. 168 (2020) 107427, https://doi.org/10.1016/j.apacoust.2020.107427.
[33] S. Varanasi, J.S. Bolton, T.H. Siegmund, R.J. Cipra, The low frequency performance of metamaterial barriers based on cellular structures, Appl. Acoust. 74 (2013) 485–495, https://doi.org/10.1016/j.apacoust.2012.09.008.
[34] L.Y.M. Sampaio, P.C.M. Cerântola, L.P.R. de Oliveira, Lightweight decorated membranes as an aesthetic solution for sound insulation panels, J. Sound. Vib. 532 (2022) 116971, https://doi.org/10.1016/j.jsv.2022.116971.
[35] F. Bucciarelli, O. Iervolino, M. Meo, A new membrane-type metamaterial for multiple peaks absorption at low frequencies, in: Health Monitoring of Structural and Biological Systems XII 10600, SPIE, 2018, pp. 310–317, https://doi.org/10.1117/12.2297670.
[36] Z. He, J. Zhao, H. Yao, X. Chen, Sound insulation performance of Helmholtz cavity with thin film bottom, Acta Phys. Sin. 68 (2019) 214302–214312, https://doi.org/10.7498/aps.68.20191131.
[37] G. Zhou, J.H. Wu, K. Lu, X. Tian, W. Huang, K. Zhu, Broadband low-frequency membrane-type acoustic metamaterials with multi-state anti-resonances, Appl. Acoust. 159 (2020) 107078, https://doi.org/10.1016/j.apacoust.2019.107078.
[38] K. Lu, J.H. Wu, D. Guan, N. Gao, L. Jing, A lightweight low-frequency sound insulation membrane-type acoustic metamaterial, AIP Adv. 6 (2016) 025116, https://doi.org/10.1063/1.4942513.
[39] N. Gao, H. Hou, J.H. Wu, A composite and deformable honeycomb acoustic metamaterial, Int. J. Mod. Phys. B 32 (2018) 1850204, https://doi.org/10.1142/S0217979218502041.
[40] H. Zhong, Y. Tian, N. Gao, K. Lu, J. Wu, Ultra-thin composite underwater honeycomb-type acoustic metamaterial with broadband sound insulation and high hydrostatic pressure resistance, Compos. Struct. 277 (2021) 114603, https://doi.org/10.1016/j.compstruct.2021.114603.
[41] F. Ma, M. Huang, J.H. Wu, Ultrathin lightweight plate-type acoustic metamaterials with positive lumped coupling resonant, J. Appl. Phys. 121 (2017) 015102, https://doi.org/10.1063/1.4972839.
[42] X. Wang, Y. Chen, G. Zhou, T. Chen, F. Ma, Synergetic coupling large-scale plate-type acoustic metamaterial panel for broadband sound insulation, J. Sound. Vib. 459 (2019) 114867, https://doi.org/10.1016/j.jsv.2019.114867.
[43] X. Wang, X. Guo, T. Chen, G. Yao, Plate-type metamaterials for extremely broadband low-frequency sound insulation, Int. J. Mod. Phys. B (2018), https://doi.org/10.1142/S0217979218500194.
[44] L. Van Belle, C. Claeys, E. Deckers, W. Desmet, The impact of damping on the sound transmission loss of locally resonant metamaterial plates, J. Sound. Vib. 461 (2019) 114909, https://doi.org/10.1016/j.jsv.2019.114909.
[45] N.G.R. de Melo Filho, L. Van Belle, C. Claeys, E. Deckers, W. Desmet, Dynamic mass based sound transmission loss prediction of vibro-acoustic metamaterial double panels applied to the mass-air-mass resonance, J. Sound. Vib. 442 (2019) 28–44, https://doi.org/10.1016/j.jsv.2018.10.047.
[46] F. Langfeldt, W. Gleine, Membrane- and plate-type acoustic metamaterials with elastic unit cell edges, J. Sound. Vib. 453 (2019) 65–86, https://doi.org/10.1016/j.jsv.2019.04.018.
[47] J. Zhao, Analysis of a geometrical-stiffening membrane acoustic metamaterial with individually tunable multi-frequencies, Arch. Acoust. (2021), https://doi.org/10.24425/aoa.2021.136563.
[48] F. Mir, D. Mandal, S. Banerjee, Metamaterials for acoustic noise filtering and energy harvesting, Sensors 23 (2023) 4227, https://doi.org/10.3390/s23094227.
[49] J.-C. Hsu, Local resonances-induced low-frequency band gaps in two-dimensional phononic crystal slabs with periodic stepped resonators, J. Phys. Appl. Phys. 44 (2011) 055401, https://doi.org/10.1088/0022-3727/44/5/055401.
[50] E. Coffy, T. Lavergne, M. Addouche, S. Euphrasie, P. Vairac, A. Khelif, Ultra-wide acoustic band gaps in pillar-based phononic crystal strips, J. Appl. Phys. 118 (2015) 214902, https://doi.org/10.1063/1.4936836.
[51] J. Liu, T. Zeng, H. Ni, Y. Hou, G. Pan, A new local resonance metamaterial for flat and cylindrical structures depended on elastic chiral spiral beams, Sci. China Technol. Sci. 67 (2024) 3597–3611, https://doi.org/10.1007/s11431-024-2739-x.
[52] Z. Zhang, X.K. Han, A new hybrid phononic crystal in low frequencies, Phys. Lett. A 380 (2016) 3766–3772, https://doi.org/10.1016/j.physleta.2016.09.019.
[53] Y. Dong, H. Yao, J. Du, J. Zhao, C. Ding, Research on bandgap property of a novel small size multi-band phononic crystal, Phys. Lett. A 383 (2019) 283–288, https://doi.org/10.1016/j.physleta.2018.10.042.
[54] G.-G. Xu, X.-W. Sun, R.-S. Li, Z.-R. Zhang, T. Song, Z.-J Liu, The low-frequency bandgap characteristics of a new three-dimensional multihole phononic crystal, Appl. Phys. A 127 (2021) 812, https://doi.org/10.1007/s00339-021-04958-z.
[55] R. Tang, T. Lu, W. Zheng, Low-frequency ultrawide band gap study of symmetric conical scatterer phononic crystal, J. Vib. Eng. Technol. 12 (2024) 3667–3676, https://doi.org/10.1007/s42417-023-01077-2.
[56] M. Ranjbar, M.U. Bayer, Design of acoustic coating for underwater stealth in low-frequency ranges, J. Braz. Soc. Mech. Sci. Eng. 46 (2024) 140, https://doi.org/10.1007/s40430-024-04720-5.
[57] S. Ning, F. Yang, C. Luo, Z. Liu, Z. Zhuang, Low-frequency tunable locally resonant band gaps in acoustic metamaterials through large deformation, Extreme Mech. Lett. 35 (2020) 100623, https://doi.org/10.1016/j.eml.2019.100623.
[58] P. Wang, F. Casadei, S. Shan, J.C. Weaver, K. Bertoldi, Harnessing buckling to design tunable locally resonant acoustic metamaterials, Phys. Rev. Lett. 113 (2014) 014301, https://doi.org/10.1103/PhysRevLett.113.014301.
[59] S. Wen, Y. Xiong, S. Hao, F. Li, C. Zhang, Enhanced band-gap properties of an acoustic metamaterial beam with periodically variable cross-sections, Int. J. Mech. Sci. 166 (2020) 105229, https://doi.org/10.1016/j.ijmecsci.2019.105229.
[60] J. Yu, C. Nerse, K. Chang, S. Wang, A framework of flexible locally resonant metamaterials for attachment to curved structures, Int. J. Mech. Sci. 204 (2021) 106533, https://doi.org/10.1016/j.ijmecsci.2021.106533.
[61] M.-H. Lu, L. Feng, Y.-F. Chen, Phononic crystals and acoustic metamaterials, Mater. Today 12 (2009) 34–42, https://doi.org/10.1016/S1369-7021(09)70315-3.
[62] N.-K. Kuo, G. Piazza, Ultra high frequency resonant cavity in aluminum nitride phononic crystals, in: 2012 IEEE Int. Ultrason. Symp., 2012, pp. 1236–1239, https://doi.org/10.1109/ULTSYM.2012.0308.
[63] M.S. Kushwaha, B. Djafari-Rouhani, Giant sonic stop bands in two-dimensional periodic system of fluids, J. Appl. Phys. 84 (1998) 4677–4683, https://doi.org/10.1063/1.368710.
[64] Y. Lai, Z.-Q. Zhang, Large band gaps in elastic phononic crystals with air inclusions, Appl. Phys. Lett. 83 (2003) 3900–3902, https://doi.org/10.1063/1.1625998.
[65] N. Susa, Large absolute and polarization-independent photonic band gaps for various lattice structures and rod shapes, J. Appl. Phys. 91 (2002) 3501–3510, https://doi.org/10.1063/1.1450022.
[66] Y. Li, J. Chen, X. Han, K. Huang, J. Peng, Large complete band gap in two-dimensional phononic crystal slabs with elliptic inclusions, Phys. B 407 (2012) 1191–1195, https://doi.org/10.1016/j.physb.2012.01.089.
[67] Z.Y. Cui, T.N. Chen, H.L. Chen, Y.P. Su, Experimental and calculated research on a large band gap constituting of tubes with periodic narrow slits, Appl. Acoust. 70 (2009) 1087–1093, https://doi.org/10.1016/j.apacoust.2009.02.005.
[68] K. Yu, T. Chen, X. Wang, Large band gaps in two-dimensional phononic crystals with neck structures, J. Appl. Phys. 113 (2013) 134901, https://doi.org/10.1063/1.4798968.
[69] T. Wang, H. Wang, M.-P. Sheng, Q.-H. Qin, Complete low-frequency bandgap in a two-dimensional phononic crystal with spindle-shaped inclusions*, Chin. Phys. B 25 (2016) 046301, https://doi.org/10.1088/1674-1056/25/4/046301.
[70] M. Ranjbar, L. Boldrin, F. Scarpa, S. Neild, S. Patsias, Vibroacoustic optimization of anti-tetrachiral and auxetic hexagonal sandwich panels with gradient geometry, Smart Mater. Struct. 25 (2016) 054012, https://doi.org/10.1088/0964-1726/25/5/054012.
[71] D. Mousanezhad, S. Babaee, R. Ghosh, E. Mahdi, K. Bertoldi, A. Vaziri, Honeycomb phononic crystals with self-similar hierarchy, Phys. Rev. B 92 (2015) 104304, https://doi.org/10.1103/PhysRevB.92.104304.
[72] G. Wen, H. Ou, J. Liu, Ultra-wide band gap in a two-dimensional phononic crystal with hexagonal lattices, Mater. Today Commun. 24 (2020) 100977, https://doi.org/10.1016/j.mtcomm.2020.100977.
[73] Y. Li, T. Chen, X. Wang, K. Yu, R. Song, Band structures in two-dimensional phononic crystals with periodic Jerusalem cross slot, Phys. B 456 (2015) 261–266, https://doi.org/10.1016/j.physb.2014.08.035.
[74] S. Jiang, H. Hu, V. Laude, Ultra-wide band gap in two-dimensional phononic crystal with combined convex and concave holes, Phys. Status Solidi 12 (2018) 1700317, https://doi.org/10.1002/pssr.201700317.
[75] Y. Sun, Y. Yu, Y. Zuo, L. Qiu, M. Dong, J. Ye, et al., Band gap and experimental study in phononic crystals with super-cell structure, Results Phys. 13 (2019) 102200, https://doi.org/10.1016/j.rinp.2019.102200.
[76] K. Wang, Y. Liu, T. Liang, B. Wang, Band structures in fractal grading porous phononic crystals, J. Phys. Chem. Solids. 116 (2018) 367–374, https://doi.org/10.1016/j.jpcs.2018.01.048.
[77] J. Liu, L. Li, B. Xia, X. Man, Fractal labyrinthine acoustic metamaterial in planar lattices, Int. J. Solids. Struct. 132–133 (2018) 20–30, https://doi.org/10.1016/j.ijsolstr.2017.06.019.
[78] E. Panahi, A. Hosseinkhani, M.F. Khansanami, D. Younesian, M. Ranjbar, Novel cross shape phononic crystals with broadband vibration wave attenuation characteristic: design, modeling and testing, Thin-Walled Struct. 163 (2021) 107665, https://doi.org/10.1016/j.tws.2021.107665.
[79] N. Kumar, S. Pal, Low frequency and wide band gap metamaterial with divergent shaped star units: numerical and experimental investigations, Appl. Phys. Lett. 115 (2019) 254101, https://doi.org/10.1063/1.5119754.

[80] S.-Y. Chang, C.-D. Chen, J.-Y. Yeh, L-W. Chen, Elastic wave propagation of two-dimensional metamaterials composed of auxetic star-shaped honeycomb structures, Crystals 9 (2019) 121, https://doi.org/10.3390/cryst9030121.
[81] M. Ranjbar, H.-J. Hardtke, D. Fritze, S. Marburg, Finding the best design within limited time: a comparative case study on methods for optimization in structural acoustics, J. Comput. Acoust. (2011), https://doi.org/10.1142/S0218396X10004139.
[82] M. Ranjbar, S. Marburg, H.-J. Hardtke, Structural-acoustic optimization of a rectangular plate: a tabu search approach, Finite Elem. Anal. Des. 50 (2012) 142–146, https://doi.org/10.1016/j.finel.2011.09.005.
[83] M. Ranjbar, S. Marburg, Fast vibroacoustic optimization of mechanical structures using artificial neural networks, Int. J. Mech. Eng. Appl. 1 (2013) 64–68, https://doi.org/10.11648/j.ijmea.20130103.11.
[84] H.-W. Dong, X.-X. Su, Y.-S. Wang, Multi-objective optimization of two-dimensional porous phononic crystals, J. Phys. Appl. Phys. 47 (2014) 155301, https://doi.org/10.1088/0022-3727/47/15/155301.
[85] M. Wormser, F. Wein, M. Stingl, C. Körner, Design and additive manufacturing of 3D phononic band gap structures based on gradient based optimization, Materials 10 (2017) 1125, https://doi.org/10.3390/ma10101125.
[86] X.K. Han, Z. Zhang, Bandgap design of three-phase phononic crystal by topological optimization, Wave Motion 93 (2020) 102496, https://doi.org/10.1016/j.wavemoti.2019.102496.
[87] X.K. Han, Z. Zhang, Topological optimization of phononic crystal thin plate by a genetic algorithm, Sci. Rep. 9 (2019) 8331, https://doi.org/10.1038/s41598-019-44850-8.
[88] H.-W. Dong, X.-X. Su, Y.-S. Wang, C. Zhang, Topological optimization of two-dimensional phononic crystals based on the finite element method and genetic algorithm, Struct. Multidiscip. Optim. 50 (2014) 593–604, https://doi.org/10.1007/s00158-014-1070-6.
[89] S. Timorian, G. Petrone, S. De Rosa, F. Franco, M. Ouisse, N. Bouhaddi, Spectral analysis and structural response of periodic and quasi-periodic beams, Proc. Inst. Mech. Eng. Part C 233 (2019) 7498–7512, https://doi.org/10.1177/0954406219888948.
[90] L. Wang, K. Bertoldi, Mechanically tunable phononic band gaps in three-dimensional periodic elastomeric structures, Int. J. Solids Struct. 49 (2012) 2881–2885, https://doi.org/10.1016/j.ijsolstr.2012.05.008.
[91] W. Cheng, J. Wang, U. Jonas, G. Fytas, N. Stefanou, Observation and tuning of hypersonic bandgaps in colloidal crystals, Nat. Mater. 5 (2006) 830–836, https://doi.org/10.1038/nmat1727.
[92] M. Gorisse, S. Benchabane, G. Teissier, C. Billard, A. Reinhardt, V. Laude, et al., Observation of band gaps in the gigahertz range and deaf bands in a hypersonic aluminum nitride phononic crystal slab, Appl. Phys. Lett. 98 (2011) 234103, https://doi.org/10.1063/1.3598425.
[93] M. Ghasemi Baboly, S. Alaie, C.M. Reinke, I. El-Kady, Z.C Leseman, Ultra-high frequency, high Q/volume micromechanical resonators in a planar AlN phononic crystal, J. Appl. Phys. 120 (2016) 034502, https://doi.org/10.1063/1.4958671.
[94] R. Dehghannasiri, A.A. Eftekhar, A. Adibi, Hypersonic surface phononic bandgap demonstration in a CMOS-compatible pillar-based piezoelectric structure on silicon, Phys. Rev. Appl. 10 (2018) 064019, https://doi.org/10.1103/PhysRevApplied.10.064019.
[95] G. Aydın, S.E. San, Breaking the limits of acoustic science: a review of acoustic metamaterials, Mater. Sci. Eng. B 305 (2024) 117384, https://doi.org/10.1016/j.mseb.2024.117384.
[96] L. Xiang, G. Wang, C. Zhu, Controlling sound transmission by space-coiling fractal acoustic metamaterials with broadband on the subwavelength scale, Appl. Acoust. 188 (2022) 108585, https://doi.org/10.1016/j.apacoust.2021.108585.
[97] N. Fang, D. Xi, J. Xu, M. Ambati, W. Srituravanich, C. Sun, et al., Ultrasonic metamaterials with negative modulus, Nat. Mater. 5 (2006) 452–456, https://doi.org/10.1038/nmat1644.
[98] C.-L. Ding, X.-P. Zhao, Multi-band and broadband acoustic metamaterial with resonant structures, J. Phys. Appl. Phys. 44 (2011) 215402, https://doi.org/10.1088/0022-3727/44/21/215402.
[99] Z. Xiao, P. Gao, D. Wang, X. He, L. Wu, Ventilated metamaterials for broadband sound insulation and tunable transmission at low frequency, Extreme Mech. Lett. 46 (2021) 101348, https://doi.org/10.1016/j.eml.2021.101348.
[100] J. Yang, J.S. Lee, H.R. Lee, Y.J. Kang, Y.Y. Kim, Slow-wave metamaterial open panels for efficient reduction of low-frequency sound transmission, Appl. Phys. Lett. 112 (2018) 091901, https://doi.org/10.1063/1.5003455.
[101] S.-H. Kim, S.-H. Lee, Air transparent soundproof window, AIP. Adv. 4 (2014) 117123, https://doi.org/10.1063/1.4902155.
[102] C. Shen, Y. Xie, J. Li, S.A. Cummer, Y. Jing, Acoustic metacages for sound shielding with steady air flow, J. Appl. Phys. 123 (2018) 124501, https://doi.org/10.1063/1.5009441.
[103] Y. Tang, S. Ren, H. Meng, F. Xin, L. Huang, T. Chen, et al., Hybrid acoustic metamaterial as super absorber for broadband low-frequency sound, Sci. Rep. 7 (2017) 43340, https://doi.org/10.1038/srep43340.
[104] V. Romero-García, G. Theocharis, O. Richoux, A. Merkel, V. Tournat, V. Pagneux, Perfect and broadband acoustic absorption by critically coupled sub-wavelength resonators, Sci. Rep. 6 (2016) 19519, https://doi.org/10.1038/srep19519.
[105] S. Huang, X. Fang, X. Wang, B. Assouar, Q. Cheng, Y. Li, Acoustic perfect absorbers via Helmholtz resonators with embedded apertures, J. Acoust. Soc. Am. 145 (2019) 254–262, https://doi.org/10.1121/1.5087128.
[106] H. Nguyen, Q. Wu, X. Xu, H. Chen, S. Tracy, G. Huang, Broadband acoustic silencer with ventilation based on slit-type Helmholtz resonators, Appl. Phys. Lett. 117 (2020) 134103, https://doi.org/10.1063/5.0024018.
[107] S. Kumar, T.B. Xiang, H.P. Lee, Ventilated acoustic metamaterial window panels for simultaneous noise shielding and air circulation, Appl. Acoust. 159 (2020) 107088, https://doi.org/10.1016/j.apacoust.2019.107088.
[108] M. Sun, X. Fang, D. Mao, X. Wang, Y. Li, Broadband acoustic ventilation barriers, Phys. Rev. Appl. 13 (2020) 044028, https://doi.org/10.1103/PhysRevApplied.13.044028.
[109] R. Ghaffarivardavagh, J. Nikolajczyk, S. Anderson, X. Zhang, Ultra-open acoustic metamaterial silencer based on Fano-like interference, Phys. Rev. B 99 (2019) 024302, https://doi.org/10.1103/PhysRevB.99.024302.
[110] X. Cai, Q. Guo, G. Hu, J. Yang, Ultrathin low-frequency sound absorbing panels based on coplanar spiral tubes or coplanar Helmholtz resonators, Appl. Phys. Lett. 105 (2014) 121901, https://doi.org/10.1063/1.4895617.
[111] S. Huang, Z. Zhou, D. Li, T. Liu, X. Wang, J. Zhu, et al., Compact broadband acoustic sink with coherently coupled weak resonances, Sci. Bull. 65 (2020) 373–379, https://doi.org/10.1016/j.scib.2019.11.008.
[112] V.V. Krylov, F.J.B.S. Tilman, Acoustic 'black holes' for flexural waves as effective vibration dampers, J. Sound. Vib. 274 (2004) 605–619, https://doi.org/10.1016/j.jsv.2003.05.010.
[113] L. Tang, L. Cheng, Ultrawide band gaps in beams with double-leaf acoustic black hole indentations, J. Acoust. Soc. Am. 142 (2017) 2802–2807, https://doi.org/10.1121/1.5009582.
[114] V. Krylov, Laminated Plates of Variable Thickness as Effective Absorbers For Flexural Vibrations, 2001.
[115] S.C. Conlon, F. Semperlotti, J.B. Fahnline, Passive control of vibration and sound transmission for vehicle structures via embedded Acoustic Black Holes, in: INTER-NOISE and NOISE-CON Congress and Conference Proceedings 246, 2013, pp. 176–184.
[116] L. Tang, L. Cheng, Impaired sound radiation in plates with periodic tunneled Acoustic Black Holes, Mech. Syst. Signal. Process. 135 (2020) 106410, https://doi.org/10.1016/j.ymssp.2019.106410.
[117] N. Gao, X. Guo, J. Deng, B. Cheng, H. Hou, Elastic wave modulation of double-leaf ABH beam embedded mass oscillator, Appl. Acoust. 173 (2021) 107694, https://doi.org/10.1016/j.apacoust.2020.107694.
[118] L. Zhao, Low-frequency vibration reduction using a sandwich plate with periodically embedded acoustic black holes, J. Sound. Vib. 441 (2019) 165–171, https://doi.org/10.1016/j.jsv.2018.10.046.
[119] X. Du, D. Huang, Q. Fu, J. Zhang, Effects of acoustic black hole parameters and damping layer on sound insulation performance of ABH circular plate, Appl. Sci. 9 (2019) 5366, https://doi.org/10.3390/app9245366.
[120] J. Deng, O. Guasch, L. Maxit, L. Zheng, Annular acoustic black holes to reduce sound radiation from cylindrical shells, Mech. Syst. Signal. Process. 158 (2021) 107722, https://doi.org/10.1016/j.ymssp.2021.107722.
[121] N. Gao, H. Hou, Sound absorption characteristic of micro-helix metamaterial by 3D printing, Theor. Appl. Mech. Lett. 8 (2018) 63–67, https://doi.org/10.1016/j.taml.2018.02.001.
[122] Y. Fang, X. Zhang, J. Zhou, J. Guo, X. Huang, Acoustic metaporous layer with composite structures for perfect and quasi-omnidirectional sound absorption, Compos. Struct. 223 (2019) 110948, https://doi.org/10.1016/j.compstruct.2019.110948.
[123] B.-S. Kim, J. Park, Double resonant porous structure backed by air cavity for low frequency sound absorption improvement, Compos. Struct. 183 (2018) 545–549, https://doi.org/10.1016/j.compstruct.2017.06.027.
[124] N. Gao, D. Luo, B. Cheng, H. Hou, Teaching-learning-based optimization of a composite metastructure in the 0–10 kHz broadband sound absorption range, J. Acoust. Soc. Am. 148 (2020) EL125–EL129, https://doi.org/10.1121/10.0001678.
[125] N. Gao, J. Wu, K. Lu, H. Zhong, Hybrid composite meta-porous structure for improving and broadening sound absorption, Mech. Syst. Signal. Process. 154 (2021) 107504, https://doi.org/10.1016/j.ymssp.2020.107504.
[126] E.P. Bowyer, V.V. Krylov, Acoustic Black Hole Manufacturing For Practical Applications and the Effect of Geometrical and Material Imperfections, Loughborough University, 2016.
[127] N. Gao, Z. Zhang, J. Deng, X. Guo, B. Cheng, H. Hou, Acoustic metamaterials for noise reduction: a review, Adv. Mater. Technol. 7 (2022) 2100698, https://doi.org/10.1002/admt.202100698.
[128] C. Lagarrigue, J.P. Groby, V. Tournat, O. Dazel, O. Umnova, Absorption of sound by porous layers with embedded periodic arrays of resonant inclusions, J. Acoust. Soc. Am. 134 (2013) 4670–4680, https://doi.org/10.1121/1.4824843.
[129] X.-F. Zhu, S.-K. Lau, Z. Lu, W. Jeon, Broadband low-frequency sound absorption by periodic metamaterial resonators embedded in a porous layer, J. Sound. Vib. 461 (2019) 114922, https://doi.org/10.1016/j.jsv.2019.114922.
[130] L. Feng, Enhancement of low frequency sound absorption by placing thin plates on surface or between layers of porous materials, J. Acoust. Soc. Am. 146 (2019) EL141–EL144, https://doi.org/10.1121/1.5121571.
[131] J. Yang, J.S. Lee, Y.Y. Kim, Metaporous layer to overcome the thickness constraint for broadband sound absorption, J. Appl. Phys. 117 (2015) 174903, https://doi.org/10.1063/1.4919844.
[132] W. Akl, A. Baz, Multi-cell active acoustic metamaterial with programmable bulk modulus, J. Intell. Mater. Syst. Struct. (2010), https://doi.org/10.1177/1045389X09359434.
[133] S. Xiao, G. Ma, Y. Li, Z. Yang, P. Sheng, Active control of membrane-type acoustic metamaterial by electric field, Appl. Phys. Lett. 106 (2015) 091904, https://doi.org/10.1063/1.4913999.
[134] X. Chen, P. Liu, Z. Hou, Y. Pei, Magnetic-control multifunctional acoustic metasurface for reflected wave manipulation at deep subwavelength scale, Sci. Rep. 7 (2017) 9050, https://doi.org/10.1038/s41598-017-09652-w.

[135] Y. Chen, G. Hu, G. Huang, A hybrid elastic metamaterial with negative mass density and tunable bending stiffness, J. Mech. Phys. Solids. 105 (2017) 179–198, https://doi.org/10.1016/j.jmps.2017.05.009.
[136] X. Yu, Z. Lu, F. Cui, L. Cheng, Y. Cui, Tunable acoustic metamaterial with an array of resonators actuated by dielectric elastomer, Extreme Mech. Lett. 12 (2017) 37–40, https://doi.org/10.1016/j.eml.2016.07.003.
[137] F. Langfeldt, J. Riecken, W. Gleine, O. von Estorff, A membrane-type acoustic metamaterial with adjustable acoustic properties, J. Sound. Vib. 373 (2016) 1–18, https://doi.org/10.1016/j.jsv.2016.03.025.
[138] Z. Xu, H. Meng, A. Chen, J. Yang, B. Liang, J. Cheng, Tunable low-frequency and broadband acoustic metamaterial absorber, J. Appl. Phys. 129 (2021) 094502, https://doi.org/10.1063/5.0038940.
[139] J. Du, Y. Luo, X. Zhao, X. Sun, Y. Song, X. Hu, Bilayer ventilated labyrinthine metasurfaces with high sound absorption and tunable bandwidth, Sci. Rep. 11 (2021) 5829, https://doi.org/10.1038/s41598-021-84986-0.
[140] Z. Chen, C. Xue, L. Fan, S. Zhang, X. Li, H. Zhang, et al., A tunable acoustic metamaterial with double-negativity driven by electromagnets, Sci. Rep. 6 (2016) 30254, https://doi.org/10.1038/srep30254.
[141] Z.-H. He, Y.-Z. Wang, Y.-S. Wang, Active feedback control of effective mass density and sound transmission on elastic wave metamaterials, Int. J. Mech. Sci. 195 (2021) 106221, https://doi.org/10.1016/j.ijmecsci.2020.106221.
[142] Y. Li, S. Wang, Q. Peng, Z. Zhou, Z. Yang, X. He, et al., Active control of graphene-based membrane-type acoustic metamaterials using a low voltage, Nanoscale 11 (2019) 16384–16392, https://doi.org/10.1039/C9NR04931B.
[143] W. Zhou, C.W. Muhammad, Z. Chen, C.W. Lim, Actively controllable flexural wave band gaps in beam-type acoustic metamaterials with shunted piezoelectric patches, Eur. J. Mech. A 77 (2019) 103807, https://doi.org/10.1016/j.euromechsol.2019.103807.
[144] W. Akl, A. Baz, Active control of the dynamic density of acoustic metamaterials, Appl. Acoust. 178 (2021) 108001, https://doi.org/10.1016/j.apacoust.2021.108001.
[145] B. Xia, N. Chen, L. Xie, Y. Qin, D. Yu, Temperature-controlled tunable acoustic metamaterial with active band gap and negative bulk modulus, Appl. Acoust. 112 (2016) 1–9, https://doi.org/10.1016/j.apacoust.2016.05.005.
[146] A. Gardiner, R. Domingo-Roca, J.F.C. Windmill, A. Feeney, An adjustable acoustic metamaterial cell using a magnetic membrane for tunable resonance, Sci. Rep. 14 (2024) 15044, https://doi.org/10.1038/s41598-024-65819-2.
[147] Z. Li, X. Li, Z. Wang, W. Zhai, Multifunctional sound-absorbing and mechanical metamaterials via a decoupled mechanism design approach, Mater. Horiz. 10 (2023) 75–87, https://doi.org/10.1039/D2MH00977C.
[148] X. Wang, R. Qin, J. Lu, M. Huang, X. Zhang, B. Chen, Laser additive manufacturing of hierarchical multifunctional chiral metamaterial with distinguished damage-resistance and low-frequency broadband sound-absorption capabilities, Mater. Des. 238 (2024) 112659, https://doi.org/10.1016/j.matdes.2024.112659.
[149] Z. Ren, Y. Cheng, M. Chen, X. Yuan, D. Fang, A compact multifunctional metastructure for Low-frequency broadband sound absorption and crash energy dissipation, Mater. Des. 215 (2022) 110462, https://doi.org/10.1016/j.matdes.2022.110462.
[150] A. Hosseinkhani, D. Younesian, M. Ranjbar, F. Scarpa, Enhancement of the vibro-acoustic performance of anti-tetra-chiral auxetic sandwich panels using topologically optimized local resonators, Appl. Acoust. 177 (2021) 107930, https://doi.org/10.1016/j.apacoust.2021.107930.
[151] S. Xu, X. Wang, Z. Yu, H. Wu, L. Ma, X. Luo, et al., Decoupled manipulation of electromagnetic and acoustic waves via fully-structural-designed hybrid metamaterials, Thin-Walled Struct. 216 (2025) 113652, https://doi.org/10.1016/j.tws.2025.113652.
[152] J. Fan, B. Song, L. Zhang, X. Wang, Z. Zhang, S. Wei, et al., Structural design and additive manufacturing of multifunctional metamaterials with low-frequency sound absorption and load-bearing performances, Int. J. Mech. Sci. 238 (2023) 107848, https://doi.org/10.1016/j.ijmecsci.2022.107848.
[153] X. Zhang, H. Ye, N. Wei, R. Tao, Z. Luo, Design optimization of multifunctional metamaterials with tunable thermal expansion and phononic bandgap, Mater. Des. 209 (2021) 109990, https://doi.org/10.1016/j.matdes.2021.109990.
[154] Z. Li, X. Wang, K. Zeng, Z. Guo, C. Li, X. Yu, et al., Unprecedented mechanical wave energy absorption observed in multifunctional bioinspired architected metamaterials, NPG Asia Mater. 16 (2024) 45, https://doi.org/10.1038/s41427-024-00565-5.
[155] Z. Li, K. Zeng, Z. Guo, Z. Wang, X. Yu, X. Li, et al., All-in-one: an interwoven dual-phase strategy for acousto-mechanical multifunctionality in microlattice metamaterials, Adv. Funct. Mater. 35 (2025) 2420207, https://doi.org/10.1002/adfm.202420207.
[156] D. Zhengchun, Z. Mengrui, W. Zhiguo, Y. Jianguo, Design and application of composite platform with extreme low thermal deformation for satellite, Compos. Struct. 152 (2016) 693–703, https://doi.org/10.1016/j.compstruct.2016.05.073.
[157] K. Meier, K. Bock, M. Roellig, Developments for highly reliable electronics - experiments on combined thermal and vibration loading, in: 2018 IEEE 68th Electron. Compon. Technol. Conf. ECTC, 2018, pp. 1050–1053, https://doi.org/10.1109/ECTC.2018.00161.
[158] B. Lemkalli, S. Bensallam, M. Kadic, S. Guenneau, H. Jakjoud, A. Mir, et al., Clay metaBrick-based motif to enhance thermal and acoustic insulation, J. Acoust. Soc. Am. 158 (2025) 28–37, https://doi.org/10.1121/10.0037086.
[159] Z. Li, Z. Ren, H. Dong, J. Li, Y. Huang, M. Chen, Optimization design of lightweight multi-functional non-local metastructure for broadband sound absorption and electromagnetic dissipation, Thin-Walled Struct. 211 (2025) 112925, https://doi.org/10.1016/j.tws.2025.112925.
[160] G. Song, C. Zhang, Q. Cheng, Y. Jing, C. Qiu, T. Cui, Transparent coupled membrane metamaterials with simultaneous microwave absorption and sound reduction, Opt. Express 26 (2018) 22916–22925, https://doi.org/10.1364/OE.26.022916.
[161] M. Tianxue, S. Xiaoxing, D. Haowen, W. Yuesheng, Z. Chuanzeng, Review of bandgap characteristics and acousto-optical coupling in phoxonic crystals, 力学学报 49 (2017) 743–757, https://doi.org/10.6052/0459-1879-17-130.
[162] H. Imanian, M. Noori, Study of acousto-optic interaction in 1D Thue-Morse phoxonic quasicrystal, Heliyon 11 (2025) e43442, https://doi.org/10.1016/j.heliyon.2025.e43442.
[163] J. An, S. Park, W. Jeon, Enhancement of acousto-optic interaction using a phoxonic cavity with structural hierarchy, Sci. Rep. 14 (2024) 8764, https://doi.org/10.1038/s41598-024-57816-2.
[164] X. Xu, Q. Wu, Y. Pang, Y. Cao, Y. Fang, G. Huang, et al., Multifunctional Metamaterials for Energy Harvesting and Vibration Control, 2021, https://doi.org/10.1002/adfm.202107896.
[165] W. Jiang, G. Yin, L. Xie, M. Yin, Multifunctional 3D lattice metamaterials for vibration mitigation and energy absorption, Int. J. Mech. Sci. 233 (2022) 107678, https://doi.org/10.1016/j.ijmecsci.2022.107678.
[166] Z. Xiao, P. Gao, X. He, Y. Qu, L. Wu, Lightweight cellular multifunctional metamaterials with superior low-frequency sound absorption, broadband energy harvesting and high load-bearing capacity, Mater. Des. 241 (2024) 112912, https://doi.org/10.1016/j.matdes.2024.112912.
[167] C. Hillman, N. Blattau, M. Lacy, Predicting fatigue of solder joints subjected to high number of power cycles, in: IPC APEX EXPO 2014, 2014.
[168] S. Kwofie, An exponential stress function for predicting fatigue strength and life due to mean stresses, Int. J. Fatigue 23 (2001) 829–836, https://doi.org/10.1016/S0142-1123(01)00044-5.
[169] D. Yu, A. Al-Yafawi, T.T. Nguyen, S. Park, S. Chung, High-cycle fatigue life prediction for Pb-free BGA under random vibration loading, Microelectron. Reliab. 51 (2011) 649–656, https://doi.org/10.1016/j.microrel.2010.10.003.
[170] G. Wu, Y. Zhu, S. Merugu, N. Wang, C. Sun, Y. Gu, GHz spurious mode free AlN lamb wave resonator with high figure of merit using one dimensional phononic crystal tethers, Appl. Phys. Lett. 109 (2016) 013506, https://doi.org/10.1063/1.4955410.
[171] X. Zhao, O. Kaya, T. Maggioli, C. Cassella, Multipurpose acoustic metamaterial anchors for aluminum scandium nitride contour mode resonators, J. Microelectromech. Syst. 33 (2024) 473–481, https://doi.org/10.1109/JMEMS.2024.3399593.
[172] T.L. Szabo, Chapter 12 - Nonlinear acoustics and imaging, in: T.L. Szabo (Ed.), Diagnostic Ultrasound Imaging Second Ed., Academic Press, Boston, 2014, pp. 501–563, https://doi.org/10.1016/B978-0-12-396487-8.00012-4.
[173] Z. Yao, V. Zega, Y. Su, Y. Zhou, J. Ren, J. Zhang, et al., Design, fabrication and experimental validation of a metaplate for vibration isolation in MEMS, J. Microelectromech. Syst. 29 (2020) 1401–1410, https://doi.org/10.1109/JMEMS.2020.3016179.
[174] K. Xu, N. Zhu, S. Cao, W. Su, W. Zhang, Y. Hao, Design and simulation of MEMS thermal and vibration isolator based on PDMS beam arrays, in: 2016 IEEE 11th Annu. Int. Conf. NanoMicro Eng. Mol. Syst. NEMS, 2016, pp. 213–216, https://doi.org/10.1109/NEMS.2016.7758235.
[175] W. Gao, Z. Wang, G. Wang, W. Miao, Angular random walk improvement of resonator fiber optic gyro by optimizing modulation frequency, IEEE Photonics J. 11 (2019) 1–13, https://doi.org/10.1109/JPHOT.2019.2928458.
[176] S. Castro, R. Dean, G. Roth, G.T. Flowers, B. Grantham, Influence of acoustic noise on the dynamic performance of MEMS gyroscopes, Am. Soc. Mech. Eng. Dig. Collect. (2009) 1825–1831, https://doi.org/10.1115/IMECE2007-42108.
[177] Inertial Sensor Noise Analysis Using Allan Variance - MATLAB & Simulink n.d. https://www.mathworks.com/help/fusion/ug/inertial-sensor-noise-analysis-using-allan-variance.html (Accessed 18 November 2025).
[178] A. Walther, C. Le Blanc, N. Delorme, Y. Deimerly, R. Anciant, J. Willemin, Bias contributions in a MEMS tuning fork gyroscope, J. Microelectromech. Syst. 22 (2013) 303–308, https://doi.org/10.1109/JMEMS.2012.2221158.
[179] W.N. Yunker, C.B. Stevens, G.T. Flowers, R.N. Dean, Sound attenuation using microelectromechanical systems fabricated acoustic metamaterials, J. Appl. Phys. 113 (2013) 024906, https://doi.org/10.1063/1.4774021.
[180] J. Killeen, I. Davis, J. Wang, G.J. Bennett, Fan-noise reduction of data centre telecommunications' server racks, with an acoustic metamaterial broadband, low-frequency sound-absorbing liner, Appl. Acoust. 203 (2023) 109229, https://doi.org/10.1016/j.apacoust.2023.109229.
[181] S. Wasala, Y. Xue, T. Wiegandt, L. Stevens, T. Persoons, Aeroacoustic Noise Prediction from a Contra-Rotating Cooling Fan Used in Data Center Cooling systems. AIAA Aviat, American Institute of Aeronautics and Astronautics, 2021, https://doi.org/10.2514/6.2021-2313. FORUMn.d.
[182] G. Park, S. Kang, H. Lee, W. Choi, Tunable multifunctional thermal metamaterials: manipulation of local heat flux via assembly of unit-cell thermal shifters, Sci. Rep. 7 (2017) 41000, https://doi.org/10.1038/srep41000.
[183] M.A. Kuczmarski, J.C. Johnston, Acoustic Absorption in Porous Materials, NASA Glenn Research Center, Cleveland, 2011.
[184] M. Kabir, A. Mostavi, D. Ozevin, Noise isolation with phononic crystals to enhance fatigue crack growth detection using acoustic emission, J. Civ. Struct. Health Monit. 8 (2018) 529–542, https://doi.org/10.1007/s13349-018-0291-6.
[185] G.R. Sherwood, D. Chronopoulos, A. Marini, F. Ciampa, 3D-printed phononic crystal waveguide transducers for nonlinear ultrasonic damage detection, NDT e Int. 121 (2021) 102456, https://doi.org/10.1016/j.ndteint.2021.102456.

[186] S.V. Valappil, J.F.L. Goosen, A.M. Aragón, Phononic crystals for suppressing crosstalk in ultrasonic flowmeters, IEEE Trans. Instrum. Meas. 72 (2023) 1–11, https://doi.org/10.1109/TIM.2023.3284960.
[187] Y. Chen, H. Liu, M. Reilly, H. Bae, M. Yu, Enhanced acoustic sensing through wave compression and pressure amplification in anisotropic metamaterials, Nat. Commun. 5 (2014) 5247, https://doi.org/10.1038/ncomms6247.
[188] R. Stoakes, R. Domingo-Roca, A. Feeney, J.F.C. Windmill, Acoustic metamaterial optimization for megahertz frequencies, in: 2024 IEEE Ultrason. Ferroelectr. Freq. Control Jt. Symp. UFFC-JS, 2024, pp. 1–5, https://doi.org/10.1109/UFFC-JS60046.2024.10794061.
[189] Z. Li, J. Zhao, C. Hou, C. Fei, C. Zheng, L. Lou, et al., High-frequency self-focusing ultrasonic transducer with piezoelectric metamaterial, IEEE Electron. Device Lett. 43 (2022) 946–949, https://doi.org/10.1109/LED.2022.3170613.
[190] S.V. Garimella, T. Persoons, J. Weibel, L-T. Yeh, Technological drivers in data centers and telecom systems: multiscale thermal, electrical, and energy management, Appl. Energy 107 (2013) 66–80, https://doi.org/10.1016/j.apenergy.2013.02.047.
[191] S. Wasala, W. Zhao, O. Ogun, L. Stevens, R. Sosseh, J. Kennedy, et al., Acoustic Metamaterials for Electronics Cooling Fan Noise Reduction, 2023, https://doi.org/10.3397/IN_2023_0454.
[192] V. Hongisto, P. Saarinen, R. Alakoivu, J. Hakala, Acoustic properties of commercially available thermal insulators – an experimental study, J. Build. Eng. 54 (2022) 104588, https://doi.org/10.1016/j.jobe.2022.104588.
[193] D. Manushyna, M. Hülsebrock, A. Kuisl, A.D. Vivo, P. Heloret, H. Atzrodt, et al., Application of vibroacoustic metamaterials for structural vibration reduction in space structures, Mech. Res. Commun. 129 (2023) 104090, https://doi.org/10.1016/j.mechrescom.2023.104090.
[194] J. Jung, H.-G. Kim, S. Goo, K.-J. Chang, S. Wang, Realisation of a locally resonant metamaterial on the automobile panel structure to reduce noise radiation, Mech. Syst. Signal. Process. 122 (2019) 206–231, https://doi.org/10.1016/j.ymssp.2018.11.050.
[195] M. Droste, S. Rieß, J.G. Cóndor López, A. Erraji, Vibroacoustic metamaterials for reduced sound radiation of an electric powertrain, MTZ Worldw 84 (2023) 44–47, https://doi.org/10.1007/s38313-023-1436-5.
[196] L. Maini, V. Genovés, R. Furrer, N. Cesarovic, C. Hierold, C. Roman, An in vitro demonstration of a passive, acoustic metamaterial as a temperature sensor with mK resolution for implantable applications, Microsyst. Nanoeng. 10 (2024) 1–14, https://doi.org/10.1038/s41378-023-00632-x.
[197] H. Imanian, M. Noori, A. Abbasiyan, Highly efficient gas sensor based on quasi-periodic phononic crystals, Sens. Actuat. B 345 (2021) 130418, https://doi.org/10.1016/j.snb.2021.130418.
[198] A. Oseev, M. Zubtsov, R. Lucklum, Gasoline properties determination with phononic crystal cavity sensor, Sens. Actuat. B 189 (2013) 208–212, https://doi.org/10.1016/j.snb.2013.03.072.
[199] J.S. Lloyd, C.G. Ludwikowski, C. Malik, C. Shen, Mitigating inaudible ultrasound attacks on voice assistants with acoustic metamaterials, IEEE Access 11 (2023) 36464–36470, https://doi.org/10.1109/ACCESS.2023.3266722.
[200] Y. Liao, H. Huang, G. Chang, D. Luo, C. Xu, Y. Wu, et al., Research on low-frequency noise control of automobiles based on acoustic metamaterial, Mater 15 (2022) 3261, https://doi.org/10.3390/ma15093261.
[201] A.H. Aly, A. Nagaty, A. Mehaney, Thermal properties of one-dimensional piezoelectric phononic crystal, Eur. Phys. J. B 91 (2018) 251, https://doi.org/10.1140/epjb/e2018-90297-y.
[202] A. Nagaty, A. Mehaney, A.H. Aly, Acoustic wave sensor based on piezomagnetic phononic crystal, J. Supercond. Nov. Magn. 31 (2018) 4173–4177, https://doi.org/10.1007/s10948-018-4702-z.
[203] R. Lucklum, N. Mukhin, B. Djafari Rouhani, Y. Pennec, Phononic crystal sensors: a new class of resonant sensors—chances and challenges for the determination of liquid properties, Front. Mech. Eng. 7 (2021), https://doi.org/10.3389/fmech.2021.705194.
[204] S. Jiang, X. Liu, J. Liu, D. Ye, Y. Duan, K. Li, et al., Flexible metamaterial electronics, Adv. Mater. 34 (2022) 2200070, https://doi.org/10.1002/adma.202200070.
[205] E. Dong, P. Cao, J. Zhang, S. Zhang, N.X. Fang, Y. Zhang, Underwater acoustic metamaterials, Natl. Sci. Rev. 10 (2023) nwac246, https://doi.org/10.1093/nsr/nwac246.
[206] Y. Wang, X. Zhu, T. Zhang, S. Bano, H. Pan, L. Qi, et al., A renewable low-frequency acoustic energy harvesting noise barrier for high-speed railways using a Helmholtz resonator and a PVDF film, Appl. Energy 230 (2018) 52–61, https://doi.org/10.1016/j.apenergy.2018.08.080.
[207] D. Li, M. Hu, F. Wu, K. Liu, M. Gao, Z. Ju, et al., Design of tunable low-frequency acoustic energy harvesting barrier for subway tunnel based on an optimized Helmholtz resonator and a PZT circular plate, Energy Rep. 8 (2022) 8108–8123, https://doi.org/10.1016/j.egyr.2022.06.042.
[208] Z. Li, X. Wang, Z. Wang, X. Li, X. Yu, S. Ramakrishna, et al., Emerging acousto-mechanical metamaterials: from physics-guided design to coupling-driven performance, Mater. Today 89 (2025) 151–171, https://doi.org/10.1016/j.mattod.2025.06.029.
[209] S.J. Mostafavi Yazdi, A. Lisitski, S. Pack, H.R. Hiziroglu, J. Baqersad, Analysis of shielding effectiveness against electromagnetic interference (EMI) for metal-coated polymeric materials, Polymers 15 (2023) 1911, https://doi.org/10.3390/polym15081911.
[210] E. Ekmekci, Frequency tunable terahertz metamaterials using broadside coupled split-ring resonators, Phys. Rev. B 83 (2011), https://doi.org/10.1103/PhysRevB.83.193103.
[211] H. Yang, W.H. Müller, Size effects of mechanical metamaterials: a computational study based on a second-order asymptotic homogenization method, Arch. Appl. Mech. 91 (2021) 1037–1053, https://doi.org/10.1007/s00419-020-01808-x.
[212] M.M. Ameen, O. Rokoš, R.H.J. Peerlings, M.G.D. Geers, Size effects in nonlinear periodic materials exhibiting reversible pattern transformations, Mech. Mater. 124 (2018) 55–70, https://doi.org/10.1016/j.mechmat.2018.05.011.
[213] L. Zhao, Y. Cui, J. Li, Y. Xie, W. Li, J. Zhang, The 3D controllable fabrication of nanomaterials with FIB-SEM synchronization technology, Nanomaterials 13 (2023) 1839, https://doi.org/10.3390/nano13121839.
[214] N. Zhang, Z. Wang, Z. Zhao, D. Zhang, J. Feng, L. Yu, et al., 3D printing of micro-nano devices and their applications, Microsyst. Nanoeng. 11 (2025) 35, https://doi.org/10.1038/s41378-024-00812-3.
[215] D. Nwatu, D. Kip, K. Hasse, Femtosecond laser assisted selective etching of microchannels in lithium niobate, Opt. Express. 31 (2023) 37618–37629, https://doi.org/10.1364/OE.500439.
[216] R.R.A. Syms, D. Liu, M.M. Ahmad, Nanostructured 2D cellular materials in silicon by sidewall transfer lithography NEMS, J. Micromech. Microeng. 27 (2017) 075003, https://doi.org/10.1088/1361-6439/aa7167.
[217] S. Mohammadi, A.A. Eftekhar, A. Khelif, W.D. Hunt, A. Adibi, Proof of the existence of large complete band gaps in high frequency silicon phononic crystal plates, J. Acoust. Soc. Am. 123 (2008) 3039, https://doi.org/10.1121/1.2932715.
[218] T.-T. Wu, L-C Wu, Z.-G. Huang, Frequency band-gap measurement of two-dimensional air/silicon phononic crystals using layered slanted finger interdigital transducers, J. Appl. Phys. 97 (2005) 094916, https://doi.org/10.1063/1.1893209.
[219] A. Pelat, F. Gautier, S.C. Conlon, F. Semperlotti, The acoustic black hole: a review of theory and applications, J. Sound. Vib. 476 (2020) 115316, https://doi.org/10.1016/j.jsv.2020.115316.
[220] S.-M. Zaharia, M.A. Pop, M. Cosnita, C. Croitoru, S. Matei, C. Spîrchez, Sound absorption performance and mechanical properties of the 3D-printed bio-degradable panels, Polymers 15 (2023) 3695, https://doi.org/10.3390/polym15183695.
[221] N. Gao, L. Tang, J. Deng, K. Lu, H. Hou, K. Chen, Design, fabrication and sound absorption test of composite porous metamaterial with embedding I-plates into porous polyurethane sponge, Appl. Acoust. 175 (2021) 107845, https://doi.org/10.1016/j.apacoust.2020.107845.
[222] I. Limón, M. Multigner, C. Paternoster, M. Lieblich, B. Torres, D. Mantovani, et al., Study of the effect of magnetic fields on static degradation of Fe and Fe-12Mn-1.2C in balanced salts modified Hanks' solution, Bioact. Mater. 40 (2024) 524–540, https://doi.org/10.1016/j.bioactmat.2024.06.027.
[223] J. Prekodravac Filipovic, M. Milenkovic, D. Kepic, S. Dorontic, M. Yasir, B. Nardin, et al., Electromagnetic interference in the modern era: concerns, trends, and nanomaterial-based solutions, Nanomaterials 15 (2025) 1558, https://doi.org/10.3390/nano15201558.
[224] J. Gao, J.B. Kwak, Reliability and thermal fatigue life prediction of solder joints for advanced automotive microelectronics, J. Mech. Sci. Technol. 35 (2021) 3633–3641, https://doi.org/10.1007/s12206-021-0734-6.
[225] L. Li, X. Du, J. Chen, Y. Wu, Thermal fatigue failure of micro-solder joints in electronic packaging devices: a review, Materials 17 (2024) 2365, https://doi.org/10.3390/ma17102365.
[226] W. Xie, Modified Norris-Landzberg model for Pb-free solder joint reliability evaluation, Microelectron. Reliab. 135 (2022) 114590, https://doi.org/10.1016/j.microrel.2022.114590.



https://dspace.org/

A review of acoustic metamaterials for electrical devices reliability: a reliability-oriented design perspective

Huang, Lingfeng; Ranjbar, Mostafa; Samie, Mohammad

2026-02
Elsevier
https://doi.org/10.1016/j.apmt.2025.103030
Huang L, Ranjbar M, Samie M. (2026) A review of acoustic metamaterials for electrical devices reliability: a reliability-oriented design perspective. Applied Materials Today, Volume 48, February 2026, Article number 103030

Downloaded from a DSpace repository. https://dspace.org/